

**Guilin Liu**

Vom Fachbereich VI  
(Raum- und Umweltwissenschaften)  
der Universität Trier  
zur Erlangung des akademischen Grades  
Doktor der Naturwissenschaften  
(Dr. rer. nat.)  
genehmigte Dissertation

**Towards a spatially distributed concept for cotton growth  
modeling by coupling the APSIM model with optical remote  
sensing data**

Betreuer:

Univ.-Prof. Dr. Joachim Hill

Berichterstattende:

Univ.-Prof. Dr. Joachim Hill

apl. Prof. Dr. Christoph Emmerling

Dr. Marion Stellmes

Datum der wissenschaftlichen Aussprache:

17. February 2017

Trier, 2017

## Acknowledgements

How time flies! When I typed the last word in my dissertation, it has been more than 3 years. In the last three memorable years, I not only had the joy of success but also upset of difficulty. In short, three-year life in Germany proved my ability of learning and living. In the upcoming graduation day, scenes of the past emerged in my memory. I therefore would like to express my sincere thanks to all friends giving me help during these three years.

First, I am grateful for my supervisor, Univ.-Prof. Dr. Joachim Hill, head of the Department of Environmental Remote Sensing and Geo-informatics. An invitation from Prof. Hill three years ago let me have an opportunity to come to Germany for further study and research. Chinese have a saying, "teacher for one day, father forever". As this proverb, like a father, Prof. Hill was careful for guiding my dissertation, field campaigns, data collecting and processing. During researches in Germany, his rigorous attitude to research deeply affected me a lot.

Second, I am also grateful for Dr. Sebastian Mader in our team, one of my supervisors. Dr. Mader also paid a considerable amount of effort on my dissertation. In particular, he helped me revise the assimilation algorithm programming and other technical problems. Also I am grateful for Mr. Hendrik Bernert's atmospheric correction of Landsat 8 OLI remotely sensed images.

Also I say thanks to my office roommate Giovanni Buzzo for his help in my daily life and study and the happy field campaigns. Many thanks to respectable secretaries Anne Menkhaus and Tana Loch-Watts for helping me in the daily life in Germany and field campaigns. I am grateful for my colleagues in the Environmental Remote Sensing and Geographic Information Science for their helping and cares during last three years. I am also grateful for all Chinese and German colleagues in the SuMaRiO project. Especially, thanks for Mr. Hussein Othmanli from the University of Hohenheim, providing me the soil, observed yield, biomass data of cotton. And I am grateful for Mr. Liang He at Institute of Geographic Sciences and Natural Resources Research, Chinese Academy of Sciences (CAS) and Mr. Zhenhai Li for providing some advice on R script. I also thank Mr. Yanzhong Li (Institute of Geographic Sciences and Natural Resources Research, CAS) and Mr. Xiangyu Zhao (Ludwig-Maximilians-Universität München) for their advice and help on my dissertation.

Then thanks to my MSc supervisor associate Professor Alishir Kurban, taking me into the halls of scientific research. I am grateful for the help from associate Professor Chi Chunming

in the Tarim University, Prof. Zhao Chengyi and staffs at the Aksu Station and all people giving me help during my field campaigns. I am also grateful for United States Geological Survey (USGS) providing me the Landsat OLI, MODIS data (<http://earthexplorer.usgs.gov/>) within 2014. Meanwhile, I am also grateful for the Agricultural Production Systems Research Unit (APSRU) and the Queensland government providing the APSIM/OZCOT model. And I also thank my parents and sister giving me selflessly support on my studies. Special thanks to my wife, without her support I cannot have a firm determination to complete the dissertation. Whenever I have depressed mood of the occasion, she patiently encouraged me to keep a high morale!

Finally, thanks again for all my friends.

Guilin Liu  
Trier, Germany

## Abstract

This study aims to estimate the cotton yield at the field and regional level via the APSIM/OZCOT crop model, using an optimization-based recalibration approach based on the state variable of the cotton canopy—the leaf area index (LAI), derived from atmospherically corrected Landsat-8 OLI remote sensing images in 2014. First, a local sensitivity and global analysis approach was employed to test the sensitivity of cultivar, soil and agronomic parameters to the dynamics of the LAI. After sensitivity analyses, a series of sensitive parameters were obtained. Then, the APSIM/OZCOT crop model was calibrated by observations over a two-year span (2006–2007) at the Aksu station, combined with these sensitive cultivar parameters and the current understanding of cotton cultivar parameters. Third, the relationship between the observed in-situ LAI and synchronous perpendicular vegetation indices derived from six Landsat-8 OLI images covering the entire growth stage was modelled to generate LAI maps in time and space. Finally, the Particle Swarm Optimization (PSO) and general-purpose optimization approach (based on Nelder-Mead algorithm) were used to recalibrate four sensitive agronomic parameters (row spacing, sowing density per row, irrigation amount and total fertilization) according to the minimization of the root-mean-square deviation (RMSE) between the simulated LAI from the APSIM/OZCOT model and retrieved LAI from Landsat-8 OLI remote sensing images. After the recalibration, the best simulated results compared with observed cotton yield were obtained. The results showed that: (1) FRUDD, FLAI and DDISQ were the major cultivar parameters suitable for calibrating the cotton cultivar. (2) After the calibration, the simulated LAI performed well with an RMSE and mean absolute error (MAE) of 0.45 and 0.33, respectively, in 2006 and 0.46 and 0.41, respectively, in 2007. The coefficient of determination between the observed and simulated LAI was 0.83 and 0.97, respectively, in 2006 and 2007. The Pearson's correlation coefficient was 0.913 and 0.988 in 2006 and 2007, respectively, with a significant positive correlation between the simulated and observed LAI. The difference between the observed and simulated yield was 776.72 kg/ha and 259.98 kg/ha in 2006 and 2007, respectively. (3) Cotton cultivation in 2014 was obtained using three Landsat-8 OLI images—DOY136 (May), DOY 168 (June) and DOY 200 (July)—based on the phenological differences in cotton and other vegetation types. (4) The yield estimation after the assimilation closely approximated the field-observed values, and the coefficient of determination was as high as 0.82, after recalibration of the APSIM/OZCOT model for ten cotton fields. The difference between the observed and assimilated yields for the ten fields ranged from 18.2 to 939.7 kg/ha. The RMSE and MAE between the assimilated and observed yield was 417.5 and



303.1 kg/ha, respectively. These findings provide scientific evidence for the feasibility of coupled remote sensing and APSIM/OZCOT model at the field level. (5) Upscaling from field level to regional level, the assimilation algorithm and scheme are both especially important. Although the PSO method is very efficient, the computational efficiency is also the shortcoming of the assimilation strategy on a regional scale. Comparisons between the PSO and general-purpose optimization method (based on the Nelder-Mead algorithm) were implemented from the RSME, LAI curve and computational time. The general-purpose optimization method (based on the Nelder-Mead algorithm) was used for the regional assimilation between remote sensing and the APSIM/OZCOT model. Meanwhile, the basic unit for regional assimilation was also determined as cotton field rather than pixel. Moreover, the crop growth simulation was also divided into two phases (vegetative growth and reproductive growth) for regional assimilation. (6) The regional assimilation at the vegetative growth stage between the remote sensing derived and APSIM/OZCOT model-simulated LAI was implemented by adjusting two parameters: row spacing and sowing density per row. The results showed that the sowing density of cotton was higher in the southern part than in the northern part of the study area. The spatial pattern of cotton density was also consistent with the reclamation from 2001 to 2013. Cotton fields after early reclamation were mainly located in the southern part while the recent reclamation was located in the northern part. Poor soil quality, lack of irrigation facilities and woodland belts of cotton fields in the northern part caused the low density of cotton. Regarding the row spacing, the northern part was larger than the southern part due to the variation of two agronomic modes from military and private companies. (7) The irrigation and fertilization amount were both used as key parameters to be adjusted for regional assimilation during the reproductive growth period. The result showed that the irrigation per time ranged from 58.14 to 89.99 mm in the study area. The spatial distribution of the irrigation amount is higher in the northern part while lower in southern study area. The application of urea fertilization ranged from 500.35 to 1598.59 kg/ha in the study area. The spatial distribution of fertilization was lower in the northern part and higher in the southern part. More fertilization applied in the southern study area aims to increase the boll weight and number for pursuing higher yields of cotton. The frequency of the RSME during the second assimilation was mainly located in the range of 0.4–0.6 m<sup>2</sup>/m<sup>2</sup>. The estimated cotton yield ranged from 1489 to 8895 kg/ha. The spatial distribution of the estimated yield is also higher in the southern part than the northern study area.

# Contents

Acknowledgements .....	II
Abstract .....	IV
Contents.....	VI
List of Tables.....	VIII
List of Figures .....	IX
List of Abbreviations.....	XII
1 Introduction .....	1
1.1 Cotton production in the Tarim Basin: environmental sustainability.....	1
1.2 Introduction to crop growth models .....	2
1.3 Strategies for optimizing crop growth models.....	9
2 Objectives.....	18
3 Study Site .....	20
3.1 Characterisation of study site.....	20
3.2 Selection of test area .....	26
4 Data and Methods.....	27
4.1 Remote sensing images and pre-processing .....	27
4.2 Ground data collection.....	29
4.3 LAI retrieval from Landsat 8 OLI images .....	34
4.4 Mapping cotton cultivation pattern.....	35
4.5 APSIM/OZCOT model.....	38
4.5.1 Sensitivity analysis.....	38
4.5.2 Local calibration .....	41
4.5.3 Assimilation strategies .....	44
5 Results and Discussion.....	48
5.1 Cotton cultivation pattern .....	48
5.2 LAI maps derived from Landsat-8 OLI images .....	51
5.3 APSIM-based yield prediction .....	57

5.4 Regional assimilation results and discussions .....	71
6 Conclusions .....	89
References .....	92
Appendix .....	111
Appendix 1 PSO R script.....	111
Appendix 2 Sensitivity analysis R script.....	118
Appendix 3 General-purpose optimization algorithm in R script .....	121
Declaration .....	123
Curriculum Vitae.....	124

## List of Tables

Table 1.1 Descriptions of existing cotton simulation models (Thorp et al., 2014) .....	6
Table 1.2 Cotton growth and development processes simulated by OZCOT (Thorp et al., 2014) .....	6
Table 1.3 Cotton phenological development stages (Hearn, 1994; Hargreaves et al., 2013) ....	7
Table 1.4 Cotton growth stages in Alar (DAXUAR, 2001; Wang et al., 2002) .....	7
Table 1.5 Simulation of LAI within OZCOT model (Hearn, 1994) .....	8
Table 1.6 Previous researches on assimilation between remote sensing and crop models .....	16
Table 3.1 Description of study area used for the assimilation .....	26
Table 4.1 In situ observed cotton yield in 2014 (provided by University of Hohenheim) .....	31
Table 4.2 Description of parameters in OZCOT model (Hearn, 1994; McCarthy, 2010) .....	40
Table 4.3 Soil properties used in the APSIM/OZCOT model (provided by University of Hohenheim) .....	41
Table 4.4 Agronomic parameters used in the APSIM/OZCOT model .....	41
Table 5.1 Accuracy assessment of cotton cultivation mapping .....	50
Table 5.2 Comparison of individual soil line and average soil line .....	53
Table 5.3 Optimized cultivar parameters in the APSIM/OZCOT model .....	63
Table 5.4 Accuracy of the simulated and observed yield during 2006-2007 .....	64
Table 5.5 Initial parameters of OZCOT model calibration .....	65
Table 5.6 Initial value and ranges of parameters within APSIM model .....	66
Table 5.7 The comparison between computational time and RMSE at various fields .....	72
Table 5.8 Descriptions of cotton LAI growth .....	74
Table 5.9 The response of various combination of irrigation and urea fertilization to yield (kg/ha) (taking cotton field A04 as an example) .....	88

## List of Figures

Figure 1.1 The development process of APSIM model (Holzworth et al., 2014).....	5
Figure 1.2 Photos illustrating the major growth stages of cotton (from field works in 2014 and <a href="http://blog.sina.com.cn/s/blog_409096490101o5ps.html">http://blog.sina.com.cn/s/blog_409096490101o5ps.html</a> ) .....	8
Figure 1.3 Schematic diagram for the forcing strategy (Delécolle et al., 1992) .....	10
Figure 1.4 Schematic diagram for the recalibration strategy (Delécolle et al., 1992).....	11
Figure 1.5 Assimilation strategy by comparing simulated reflectance and satellite reflectance (Delécolle et al., 1992) .....	13
Figure 1.6 Schematic diagram for the sequence assimilation strategy (Delécolle et al., 1992).....	13
Figure 2.1 Flowchart of the assimilation between remote sensing and APSIM/OZCOT model .....	19
Figure 3.1 (a) Study area location in China; (b) LAI, yield and land cover samples in the study area .....	21
Figure 3.2 Cultivation and production of three major crops in 2014 .....	22
Figure 3.3 (a) Soil types map (FAO et al., 2012); (b) the digital elevation model (Jarvis et al., 2008).....	23
Figure 3.4 Inter and intra-annual changes of rainfall, radiation and temperature in Alar, 1959-2014 .....	25
Figure 4.1 The estimated atmospheric parameters based on an AtCPro software (Hill, 2013).....	28
Figure 4.2 Comparison of MODIS and corrected Landsat 8 OLI vegetation reflectance responses .....	29
Figure 4.3 Daily climate data within 2014 at the Alar State Station of Meteorology.....	30
Figure 4.4 LAI and height measurement during three major cotton growth stages.....	31
Figure 4.5 Sampling strategy for LAI-2000 over cotton field A01: (a) LAI was measured in a total of 12 plots, the size of each plot was about 5×5 meters and distance between them was > 30 meters (the pixel size of Landsat OLI image); (b) illustrate a detailed measurement about the first plot (A01-1) within field A01 .....	32
Figure 4.6 Field campaigns during three major cotton growth stages .....	33

Figure 4.7 Cultivation configuration of cotton using tracker sowing in study area.....	34
Figure 4.8 Temporal variations of vegetated signals between cotton and woodland, orchard	36
Figure 4.9 Crop cultivation and harvesting calendar in the study area .....	37
Figure 4.10 (a) Changes in NDVI of three crops, (b) NDVI changes of crops caused by hail disaster.....	38
Figure 4.11 Schematic diagram of the calibration process of the APSIM/OZCOT cotton model.....	43
Figure 4.12 The flowchart of PSO algorithm (Kennedy, 1997).....	47
Figure 4.13 (a) The response of particles; (b) iterations to PSO capacity.....	47
Figure 5.1 Flowchart of cotton cultivation extraction process .....	48
Figure 5.2 (a) Landsat 8 OLI images at DOY 232; (b) cotton cultivation pattern in 2014.....	49
Figure 5.3 (a) Cotton extraction of linear fields; (b) Google Earth image; (c) the location of linear field.....	50
Figure 5.4 Soil lines from Landsat 8 OLI images of 2014 (the green line is the individual soil line corresponding to each image, and the blue line is the average soil line) .....	52
Figure 5.5 The relationship between observed LAI and PVI derived from Landsat 8 OLI images.....	54
Figure 5.6 LAI maps derived from Landsat 8 OLI remotely sensed images within 2014.....	55
Figure 5.7 The error bar of 6 fields between remote sensing derived and in situ observed LAI (the red error bar is the RMSE between remote sensing derived LAI and in situ observed LAI) .....	57
Figure 5.8 Sensitivity of 10 major cultivar parameters to LAI dynamics .....	60
Figure 5.9 Sensitivity of two soil parameters to LAI dynamics.....	60
Figure 5.10 The sensitivity analysis of agronomic parameters to LAI dynamics .....	61
Figure 5.11 Error bar of global sensitivity of parameters at five plots to LAI dynamics .....	62
Figure 5.12 (a) Average global sensitivity; (b) and local sensitivity of parameters to LAI dynamics.....	63
Figure 5.13 The difference between simulated and observed LAI between 2006 and 2007 ...	64
Figure 5.14 Correlation analysis of simulated and observed cotton LAI during 2006-2007 ...	65
Figure 5.15 An illustration of the commonly used sowing mode in study area.....	67

Figure 5.16 The match between remote sensing derived LAI and initial LAI using APSIM/OZCOT model, simulated LAI after the PSO assimilation at the Aksu Station.....	68
Figure 5.17 (a) the relationship between the observed and simulated yield of 10 cotton fields using the mono APSIM/OZCOT model; (b) the relationship using PSO method .....	69
Figure 5.18 The relationship between observed and assimilated LAI using PSO method, simulated LAI using mono APSIM/OZCOT model at 9 cotton fields.....	71
Figure 5.19 The comparison between PSO and general-purpose optimization method (based on the Nelder-Mead algorithm) at Aksu station .....	72
Figure 5.20 The comparison between PSO and general-purpose optimization method (based on the Nelder-Mead algorithm) at other fields .....	73
Figure 5.21 Cotton LAI development stages simulated from the APSIM/OZCOT model.....	75
Figure 5.22 (a) Spatial distribution of row spacing; (b) Spatial distribution of density per row; (c) RMSE distribution of LAI adjusting APSIM to optimally match satellite observed LAI..	78
Figure 5.23 Frequency of LAI RMSE for each cotton field at early growth stage .....	79
Figure 5.24 (a) Spatial distribution of sowing density by adjusting APSIM to optimally match satellite observed LAI; (b) land use dynamics based on MODIS EVI (from Mader, 2013)....	80
Figure 5.25 (a) Landsat 8 OLI image at DOY 232; (b) High-standard Farmland Construction project in the southwestern study area overlaying on the Landsat image (yellow color is farmland) .....	81
Figure 5.26 Photos illustrating various factors influencing the emergence and survival rate of cotton seedling.....	82
Figure 5.27 Photos of (a) sandstorms; (b) cotton plants without disaster at the same day; (c) damaged cotton plants caused by sandstorms; (d) a dead cotton caused by the sandstorm.....	83
Figure 5.28 Cotton dry matter accumulation rate and its group genital dry matter accumulation rate in study area (Wang et al., 2002).....	84
Figure 5.29 (a) Spatial distribution of irrigation per time; (b) spatial distribution of total urea fertilization; (c) the RMSE of LAI between remote sensing observations and APSIM/OZCOT simulations.....	86
Figure 5.30 Frequency of RMSE of LAI for each cotton fields at mid-late growth stage.....	87
Figure 5.31 Spatial distribution of cotton yield at the end of growth season.....	87

## List of Abbreviations

PSO	Particle swarm optimization
APSIM	Agricultural Production Systems sIMulator
OAT	One-at-a-time
EFAST	Extended Fourier Amplitude Sensitivity Test
XLZ37	A cotton variety, named XLZ37
RMSE	Root mean squared error
MAE	Mean absolute error
UTM	Universal Transverse Mercator
HDF-EOS	Hierarchical Data Format-Earth Observing System
OLI	Operational Land Imager
NDVI	Normalized Difference Vegetation Index
PVI	Perpendicular Vegetation Index
GAI	Green Area Index
LAI	Leaf Area Index
SVATs	Soil-Vegetation-Atmosphere transfer models
ELCROS	Elementary Crop Simulator
BACROS	Basic Crop Growth Simulator
SUCROS	Simple and Universal Crop Growth Simulator
WOFOST	World Food Studies
CGMS	Crop Growth Monitoring System
CERES	Crop Environment Resource Synthesis
EPIC	Environmental Policy Integrated Climate Model
DSSAT	Decision Support System for Agro-technology Transfer
APSRU	Agricultural Production Systems Research Unit
GIS	Geographic information systems
LNA	Leaf nitrogen accumulation
ET	Evapotranspiration
CNY	Chinese Yuan
SuMaRiO	Sustainable management of river oases along the Tarim River
ACOTYL	Leaf area of cotyledons
RATE_EMERGENCE	Growth rate (mm per day) from sowing to emergence
RLAI	Base rate of leaf growth pre first square
DLDS_MAX	Maximum leaf area increase per site
FLAI	Varietal adjustment for rate of LAI gain per fruiting site
DDISQ	Thermal time between emergence and the appearance of the first square
SQCON	Squaring constant for generating sites per DD



FCUTOUT	Constant used to determine when site production stops due to boll load
TIPOUT	Day degrees delay caused by tipping out damage
FBURR	Proportional boll weight with Burr Fraction included
POPCON	Plant population constant for adjustment of daily site production
RESPCON	Respiration constant
FRUDD	Array of cumulative Day Degrees for each growth phase of fruit development
BLTME	Thermal time for fruit categories as a proportion of the total required to develop a complete boll
WT	Relative weight of each category relative to a mature green boll
SAT	Saturated water content
DUL	drained upper limit of soil water content
LL15	The 15 Bar lower limit of soil water content
BD	Bulk Density
Fert_amount	Fertilization amount
GDD	Growing degree-day
XPCC	Xinjiang Production and Construction Corps
HSWD	Harmonized World Soil Database
SWAP	Soil-Water-Atmosphere-Plant
WOFOST	WORld FOod STudies
DHP	Digital Hemispherical Photography
TRAC	Tracing Radiation and Architecture of Canopies
SEBAL	Surface Energy Balance Algorithm for Land
PEST	Parameters estimation software
EnKF	Ensemble Kalman Filter
GA	Genetic algorithm
SCE-UA	Shuffled Complex Evolution
EnSRF	Ensemble Square Root Filter
POD4DVar	Proper Orthogonal Decomposition Four-dimensional Variational
SA	Simulated annealing
VFSA	Very fast simulated annealing

# 1 Introduction

## 1.1 Cotton production in the Tarim Basin: environmental sustainability

As a famous cotton production region, the Tarim Basin is located in the northwest of China. The oasis area along the Tarim River, especially in the upper and middle reaches of Tarim River (**Figure 3.1a**), is the largest agricultural area in southern Xinjiang. Water in the Tarim River comes from the melting glacier and snow on the surrounding mountains. In recent decades, with the increase in the reclamation and expansion of cotton cultivation, numerous grasslands, bare lands and woodlands have been reclaimed into croplands (Liu et al., 2016). As an extremely arid zone, the study area is irrigated primarily by rivers, reservoirs and groundwater. Then the competition between irrigation and ecological water becomes a conflict point. Due to increases in irrigation levels for agricultural production, ecological water for ecosystems has been significantly decreased, leading to declines in natural vegetation mass. Meanwhile, numerous artificial dams and reservoirs constructed in the upper and middle reaches of the Tarim River have led to water deficits and vegetation declines in the lower reaches of the Tarim vegetation area known as the "Green Corridor" (Liu et al., 2014a). A reasonable and effective irrigation schedule not only ensures crop growth and yield but also minimizes irrigation requirements. Therefore, a project pertaining to the sustainable management of river oases along the Tarim River was proposed by the Bundesministerium für Bildung und Forschung in Germany in 2010 (<http://www.sumario.de/>). Its main objective is the reasonable and sustainable management of oases along the Tarim River under the regime of a changing climate and society (<http://www.sumario.de/objectives>).

The oasis area along the Tarim River is also one of the most important regions for cotton cultivation in China (Feike et al., 2015). An optimal fertilization and irrigation schedule for cotton would be beneficial for maintaining the balance between agricultural and ecological water supplies. However, the excessive irrigation and fertilization application caused a series of environmental issues, such as degenerated ecosystems, increasing water mineralization along the Tarim River, soil salinization, land degradation, desertification and dust storm formation (Zhao et al., 2012; Liu et al., 2016). Therefore, specific objectives of this research aim to improve the agricultural production process of cotton using the crop growth model, remote sensing and geoinformatic tools and to optimize agricultural managements to reduce damages to the environment along the Tarim River.

## 1.2 Introduction to crop growth models

Crop growth models are generally developed based on the transmission and conversion theory of matter and energy within Soil-Vegetation-Atmosphere transfer models (SVATs) that investigate important land surface model ([Avisar, 1998](#)). Driven by meteorological factors associated with soil water and nitrogen, other environmental conditions and agronomic practices, crop growth models simulate the photosynthesis, respiration, transpiration and nutrition during the crop growth process, crop morphological development, and yield formation, as well as their response to climate and soil ([Xing et al., 2009](#); [Thorp et al., 2014](#)). Thus, the crop model was employed in this research to simulate the mechanism of cotton growth processes: (1) the productivity of cotton in the end of growth season; (2) the response of cotton growth, development and yield formation to environmental changes and agronomic practices in cotton growth processes.

Crop growth models have gone from initially purely theoretical studies to practical application through an evolution involving three stages: model development in the early stage, initial application in the mid-stage and practical application in the current stage ([Li, 2012](#)). With the development of crop growth models, unified model parameters and input/output formats are critical for improving the universality, accuracy and operability of crop models ([Jones et al., 2003](#)). A series of crop growth models based on these objectives have been proposed based on a generic platform and set of modules. These crop growth models are developed based on the theory of canopy photosynthesis ([de Wit, 1965](#); [Monsi and Saeki, 2005](#); [Loomis and Williams, 1963](#)) and the physiological process theory ([Curry and Chen, 1971](#); [Stapleton and Meyers, 1971](#)). Meanwhile, these models consider environmental stresses and limitations influencing the crop growth process ([Childs et al., 1977](#); [Van Keulen, 1975](#); [Penning de Vries et al., 1982](#)). The more notable crop growth models are generally divided into three categories: Wageningen, USA and Australian model series.

### *Wageningen crop models*

The Wageningen crop model series in the Netherlands, also named “de Wit Scholl” ([Bouman et al., 1996](#)), emphasizes the universality of crop growth simulations. These crop models simulate the physiological mechanisms and ecological processes of crop growth and yield formation ([Bouman et al., 1996](#)). Based on the ELCROS (Elementary Crop Simulator) ([de Wit, 1970](#)) and BACROS (Basic Crop Growth Simulator) model ([de Wit et al., 1978](#)), a Simple and Universal Crop Growth Simulator (SUCROS) model was developed ([Spitters et](#)

al., 1989) to simulate the growth process of crops. In order to explore the possibility of increasing productivity in developing countries (Van Keulen and Wolf, 1986), the World Food Research Centre developed a famous World Food Studies (WOFOST) Model (Boogaard et al., 1998). The WOFOST software simulates crop growth processes at three different levels, namely potential crop growth, crop growth under water restrictions and crop growth under nutrient restrictions (Boogaard et al., 1998). The WOFOST model can also express simulated results using graphics and provide users a menu interface to select crop types, production level, climate, soil and crop genetic characteristics (Boogaard et al., 1998). Additionally, Wageningen University and International Rice Research Institute (IRRI) co-developed the ORYZA model series, such as ORYZA2000, based on the physiological and ecological processes of rice (Bouman et al., 2001).

#### *Crop growth models in the USA*

Based on the characteristics of American agriculture and climate (Wang, 2013), many crop growth models in the USA were developed, such as the CERES (Crop Estimation through Resource and Environment Synthesis) model, CROPGRO (Crop Growth) model, EPIC (Environmental Policy Integrated Climate Model) model and GOSSYM model. CERES series models fully consider the dynamics of the crop-soil-atmosphere system to simulate crop growth, development and yield (Jones and Kiniry, 1986). CERES series models are oriented towards a variety of crops, such as wheat (Ritchie and Otter, 1985), rice (Ritchie et al., 1986), maize (Jones and Kiniry, 1986) and barley (Otter-Nacke et al., 1991). The CROPGRO model, initially developed for seed legumes (Hoogenboom et al., 1992), simulates the growth, development and yield of soybeans (Wilkerson et al., 1983), dry beans (Hoogenboom et al., 1994) and non-leguminous crops (Boote et al., 2012). The EPIC model (Mitchell et al., 1996) includes physiological crop growth, soil erosion modules, soil water and transport of nutrients. Characteristics of the EPIC model are developed into a main frame based on generic physiological and ecological processes for a variety of crops combined with a variety of crop growth and agronomic parameters (Mitchell et al., 1996). The GOSSYM model, developed to simulate cotton growth and yield (Baker et al., 1983; Lemmon, 1986), also considers effects of climatic factors, agronomic practices, hydraulic properties of soil and other environmental factors on the physiological process of cotton (Reddy and Baker, 1988).

Because numerous parameters and variables restrict wide applications of models, an IBSNAT (International Benchmark Sites for Agro-technology Transfer) project (Uehara and Tsuji,

1991) was implemented by the U.S. Department of Agriculture (USDA) in 1986 to develop DSSAT (Decision Support System for Agro-technology Transfer) software (Jones et al., 2001; Jones et al., 2003). The DSSAT model aims to summarize various crop growth models and standardize input and output variables for universal applications (Jones et al., 2003). The DSSAT model, including CERES and CROPGRO modules, is a landmark for the practical application of crop models in the USA.

#### *Australian crop model schools*

The Agricultural Production Systems Simulator (APSIM) model was developed by the Agricultural Production Systems Research Unit (APSRU) and the Queensland government (Keating et al., 2003). This model includes fertilization, irrigation, soil erosion, soil nitrogen balance, soil moisture balance and the solute transport and residue decomposition modules (Holzworth et al., 2014). Similar to the DSSAT model, the APSIM model integrates a variety of crop growth models by establishing a generic platform (McCown et al., 1996). The APSIM model also uses the “plug in and plug out” approach (McCown et al., 1996) to integrate findings from a single crop model into a unified decision support system (**Figure 1.1**). It shows the model pedigree of APSIM, the models that have influenced the inception of the APSIM and the external models that have been incorporated into APSIM (Holzworth et al., 2014). The largest difference between the APSIM and other crop models is that soil rather than vegetation is considered the core of the APSIM model (Keating et al., 2003). The APSIM model is widely applied in numerous functions, including crop management, crop breeding, cultivation systems, regional water balance, climate change and land use (Keating et al., 2003).

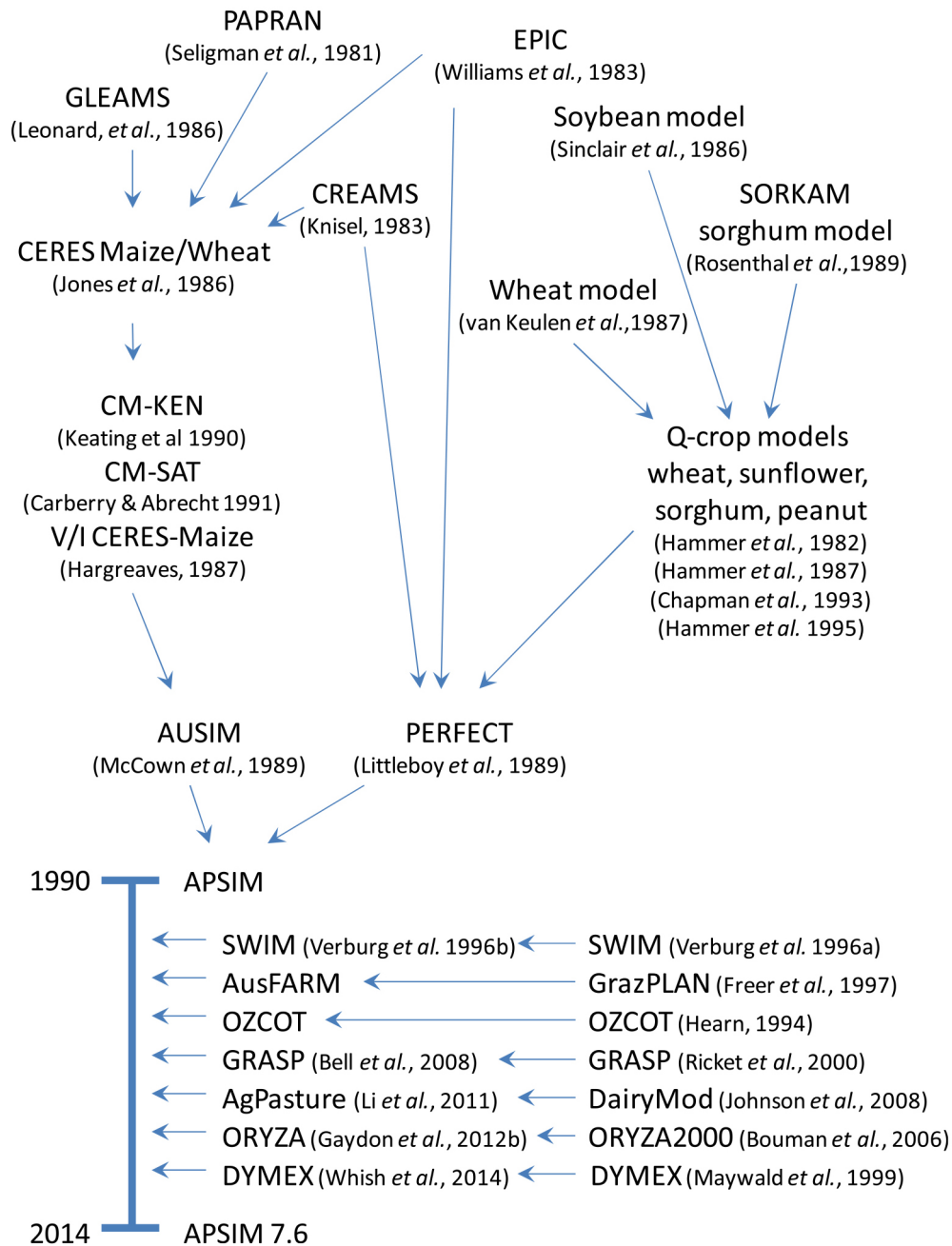


Figure 1.1 The development process of APSIM model (Holzworth et al., 2014)

### *The OZCOT sub-model*

The cotton growth model was initially used in the southeastern U.S. in the 1960s, and then was expanded to major cotton producing regions (Thorp et al., 2014). Existing cotton models are divided into models specific to cotton (e.g., GOSSYM, Cotton2K, COTCO2, OZCOT and CROPGRO-Cotton) and generic crop models (e.g., EPIC, WOFOST, SUCROS, GRAMI, CropSyst and AquaCrop) (Table 1.1) (Thorp et al., 2014).

Table 1.1 Descriptions of existing cotton simulation models (Thorp et al., 2014)

Model	Predecessor Models	Programming Language	Time Step	Major Decision Support
GOSSYM	SIMCOT I SIMCOT II	Fortran	Daily	COMAX
Cotton2K	GOSSYM CALGOS	C++, formerly Fortran	Hourly	None
COTCO2	KUTUN ALFALFA	Fortran	Hourly	None
OZCOT	SIRATAC	C#, formerly Fortran	Daily	APSIM
CSM-CROPGRO-Cotton	CROPGRO-Soybean	Fortran	Daily	DSSAT

Currently, the OZCOT model has been integrated into the APSIM platform (**Figure 1.1**). Because the APSIM/OZCOT model was employed in this paper to simulate cotton growth, we mainly focus on the introduction of the OZCOT model. As a physiology-based model, the OZCOT model is driven by air temperature and radiation interception to simulate daily cotton growth, linking a fruiting dynamic model with a water balance and simple nitrogen uptake module (**Table 1.2**) (Thorp et al., 2014).

Table 1.2 Cotton growth and development processes simulated by OZCOT (Thorp et al., 2014)

Name	Descriptions	Name	Descriptions
Phenology	Develops the number of fruiting sites based on thermal time	Partitioning	Allocates carbon to cohort pools for developing bolls
	Calculates the number of squares, bolls, open bolls, and aborted fruits based on crop carrying capacity		
Potential carbon assimilation	Canopy-level radiation interception	Yield components	Calculates fiber mass as a fraction of boll mass and boll size
Respiration	Uses empirical functions of respiration based on fruiting site count and air temperature	Stress	Calculates stress due to water, nitrogen, and air temperature

Crop growth and development processes simulated by OZCOT are phenology, potential carbon assimilation, respiration, partitioning, yield components and stress (Thorp et al., 2014). Additionally, the management practices simulated in the OZCOT model are sowing date, cultivars, planting density, irrigation, fertilization, defoliation and cropping sequence (Hearn, 1994). In the OZCOT model, phenological phases are parallel to growth process of cotton. Regarding the OZCOT model, the three categories of phenological parameters are the sowing date, base temperature of cotton growth and growing degree-day (hereafter GDD) for critical events. Phenological development stages of cotton were considered in the OZCOT model (**Table 1.3**). In the OZCOT model, the major simulated phenological phases were the emergence date, the first square event, boll formations and harvesting. The phenological

development stages of cotton span the period from sowing to physiological maturity, which are mainly controlled by thermal time and modified by stress and photoperiod (Hargreaves et al., 2013).

Table 1.3 Cotton phenological development stages (Hearn, 1994; Hargreaves et al., 2013)

Fractional Boll Development	Developmental Name	Starting Processes
	Sowing	Seed germination
	Emergence	Vegetative growth
	First Square	Reproductive development
	Small Squares (3.0-5.0mm)	
	Medium Squares (5.0-10.0mm)	
	Large Squares (>10.0mm)	
0.0	Flowering	
0.07	Small bolls (<25mm)	
0.21	Medium bolls (25.0-37.5mm)	
0.33	Large bolls (37.5-42.5mm)	
0.55	Inedible bolls	
1.0	Open bolls	

To better understand the physiological cotton model, cotton phenology in the study area is firstly analysed. Generally, the growth period of cotton is divided into five critical growth stages (**Table 1.4**): (1) sowing to emergence, (2) seedling, (3) squaring, (4) flowering and boll formation (small, medium and large bolls) and (5) boll opening and harvesting (DAXUAR, 2001; Wang et al., 2002). As a thermophilic and light-loving plant, cotton has a base temperature for growth of approximately 12 °C in the study area (<http://nzw.funonglu.com/mianhua/szhj.html>). In order to vividly understand these special events during the cotton growth period, we have also provided pictures from field campaigns in 2014 illustrating these cotton growth stages (**Figure 1.2**).

Table 1.4 Cotton growth stages in Alar (DAXUAR, 2001; Wang et al., 2002)

Major phenological events	Period
Sowing	4 April-20 April
Emergence	16 April-30 April
Seedling	30 April-20 May
Square (1 <sup>st</sup> )	20 May-27 May
Squaring (flower buds)	27 May-20 June
Flowering/Blooming	20 June-26 June
Boll formation	26 June-29 August
Opening boll	29 August-6 October
Whole stage	4 April-6 October





Figure 1.2 Photos illustrating the major growth stages of cotton (from field works in 2014 and [http://blog.sina.com.cn/s/blog\\_409096490101o5ps.html](http://blog.sina.com.cn/s/blog_409096490101o5ps.html))

Regarding the leaf development, its appearance and leaf area expansion is also a function of the growing degree-day (Hearn, 1994). LAI is also a critical indicator in this research, and therefore, it is an important factor that must be discussed. The first square event in the OZCOT model is the critical demarcation point between vegetative and reproductive growth. Ideally, simulations of LAI within the OZCOT model can be found in the **Table 1.5**. The potential growth of the leaf is subject to the solar radiation interception and transpiration and to agronomic practices. In addition, the leaf senescence is also a factor influencing LAI dynamics, and it is mainly caused by the soil water and nitrogen stress (Hearn, 1994).

Table 1.5 Simulation of LAI within OZCOT model (Hearn, 1994)

	LAI
Emergence	$LAI=f(\text{plant population, cotyledons area per plant})$
Vegetative growth	LAI expands exponentially until the 1 <sup>st</sup> square event
Reproductive growth	$LAI=f(\text{numbers of fruiting sites})$
Leaf senescence	$SENLF=f(\text{soil moisture index, fruit load})$

However, crop growth models have also some flaws on optimizing the agricultural production and growth process. Crop growth models cannot obtain effects of disasters and pest on canopy growth status of crop. Additionally, crop growth models can not accurately simulate the agricultural production on a regional scale. However, remote sensing can capture the timely canopy information of crop to provide true observations of cotton growth status on a regional scale. Meanwhile, remote sensing also overcomes the time-consuming and labour-intensive

task obtaining in-situ measured input parameters and initial conditions within crop growth models. Then remote sensing images can provide accurate parameters to calibrate crop growth models. Therefore, the simulated accuracy on agricultural production of crop growth models are improved by the inclusion of remote sensing data in many regions for various crops (**Table 1.6**) while rarely previous researches were reported in this study area.

### **1.3 Strategies for optimizing crop growth models**

The rapid development of remote sensing and geographic information systems (GIS) provides a scientific approach to apply crop growth models on a regional scale. Based on the classification of parameters within crop growth models (Claverie et al., 2012), parameters are generally divided into crop-specific and field-specific parameters. Field-specific parameters can be acquired from multi-temporal remote sensing images and GIS interpolation, such as the emergence date and the effective accumulated temperature for the various growth stages. Generated regional data are used as input parameters to drive crop growth models. This simulation method is called “simulation after interpolation” (McVicar and Jupp, 2002). Conversely, the approach simulating spatial crop growth by interpolating many field specific simulations is called “interpolation after simulation” (Wu et al., 2006). Many scholars have used these methods to upscale the application of crop models to the regional scale by GIS interpolation (Tan and Shibasaki, 2003; Bastiaanssen and Ali, 2003; Liu et al., 2007; Hebbar et al., 2008; Muslim et al., 2015). However, the largest shortcoming of these two approaches is the spatial heterogeneity involved in upscaling. Therefore, the use of remote sensing data in a wide range of applications is needed to gradually resolve this issue.

After Wiegand et al. (1979) introduced remote sensing data into the crop model to improve model simulation accuracy, remote sensing derived parameters coupled with various crop models have been widely used to estimate yield and simulate crop growth. Remote sensing observations are generally acquired from in-situ spectral observations, spaceborne and airborne data. Many studies have described various criteria for integrating remote sensing observations into crop growth models (Bach and Mauser, 2003; Dorigo et al., 2007; Zhao et al., 2013). Based on previous studies, the combination of remote sensing observations and crop models can be divided into three major strategies: the forcing strategy, continuous assimilation strategy and sequence assimilation strategy (Delécolle et al., 1992).

### Forcing strategy

The forcing strategy is implemented by directly driving crop model variables retrieved from remote sensing images or updating corresponding state variables (such as LAI) in crop models using remote sensing observations ([Delécolle et al., 1992](#)) (**Figure 1.3**). The input data retrieved from remote sensing images are equivalent to the state variables within the crop models ([Delécolle et al., 1992](#)). The hypothesis of the forcing strategy is that state variables derived from remote sensing observations are more accurate than crop model simulations ([Dorigo et al., 2007](#)). This strategy overcomes the deficit of the inversion of biophysical parameters directly derived from remote sensing images to accurately obtain these parameters ([Delécolle et al., 1992](#)). Crop models generally simulate the daily growth of crops while available remote sensing images have no such high temporal resolution. In order to keep consistent time-stepping with crop models, remote sensing observations are usually integrated into the simulated curve, and then they are interpolated in accordance with the crop model time step and remote sensing observations ([Delécolle et al., 1992](#)). Therefore, numerous interpolation approaches, such as the wavelet method ([Dorigo et al., 2007](#)), linear interpolation and fast Fourier transformations ([Roerink et al., 2000](#)), have been proposed to fill gaps among the observations. The forcing strategy is generally applied in the early stage of combining remote sensing observations with crop growth models on a regional scale ([Maas, 1988](#); [Liu et al., 1997](#); [Matsushita and Tamura, 2002](#); [Chiesi et al., 2002](#); [Yun, 2003](#); [Morari et al., 2004](#); [Xiong et al., 2008](#); [Mo et al., 2009](#)).

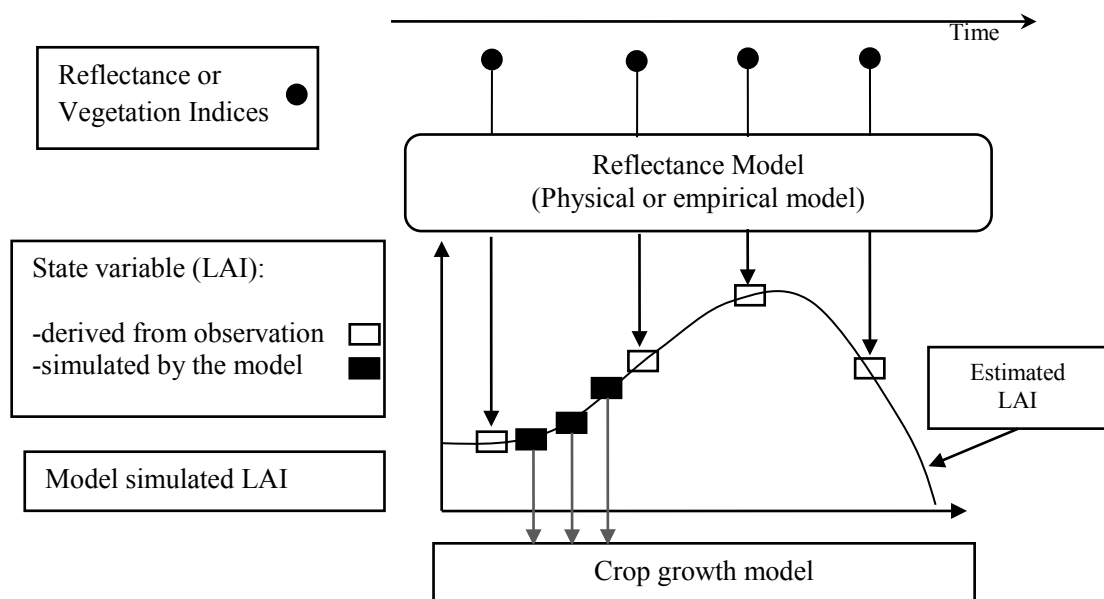


Figure 1.3 Schematic diagram for the forcing strategy ([Delécolle et al., 1992](#))

### *Continuous assimilation strategy*

The continuous assimilation strategy mainly determines the initial states and input parameters of the crop model by minimizing the difference between crop model simulation results and remote sensing observations (Delécolle et al., 1992). Then the optimized initial states and parameters within the crop model are determined for simulations of growth process and yield formation (Delécolle et al., 1992). This strategy is also called crop model re-initialization/re-parameterization and it can be divided into two specific approaches.

The model initialization/parameterization strategy employs retrieved biophysical parameters such as the LAI to adjust the relevant parameters and initial states of the crop model to reduce the differences between model simulations and synchronous remote sensing observations (Delécolle et al., 1992) (**Figure 1.4**). Adjusted initial values and parameters are regarded as initial conditions and parameters of crop growth model. The assimilation of remote sensing observed state variables for the model initialization/parameterization has also been applied for winter wheat (Maas, 1991), maize (Maas, 1993), sugar beet (Clevers and van Leeuwen, 1996; Clevers et al., 1997) and grassland ecosystems (Nouvellon et al., 2001) based on the observed ground radiation, airborne remote sensing images and satellite remote sensing images.

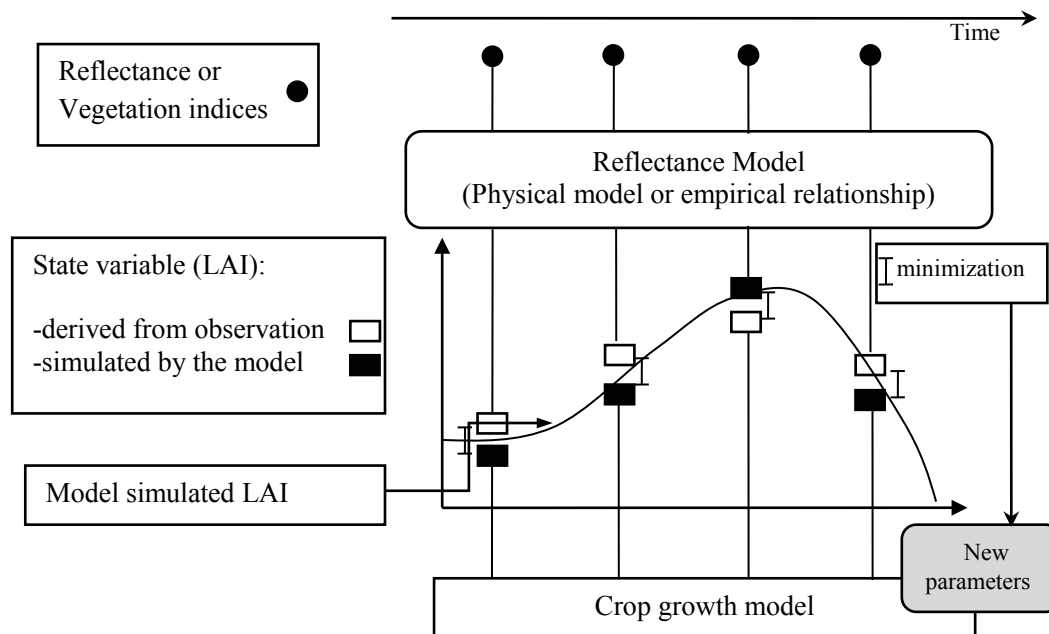


Figure 1.4 Schematic diagram for the recalibration strategy (Delécolle et al., 1992)

The other strategy (initialization and parameterization of crop model using spectroscopic data) couples crop growth models with remote sensing reflectance (or vegetation index), based on a radiative transfer model, to initialize and parameterize crop growth models (Bouman, 1992;

Moulin et al., 1995). Key parameters and initial states of crop growth are determined by directly comparing the observed reflectance from remote sensing images to the simulated reflectance from the coupled crop model (**Figure 1.5**). This strategy has also been further implemented by coupling remote sensing data, crop models and radiative transfer models together (Supit, 1997; Guérif and Duke, 1998; Weiss et al., 2001; Fang et al., 2011; Launay and Guérif, 2005).

#### *Sequence assimilation strategy*

The sequence assimilation strategy, also called the updating strategy, continuously updates the state variables of crop models using externally observed data (Dorigo et al., 2007) (**Figure 1.6**). When new observed data appear, the status of crop model prediction becomes the background and is updated by observed data (Curnel et al., 2011). The updated status restarts the crop model integration until all observations are used (Curnel et al., 2011). The assumption of this strategy is that if there is a model state variable with a higher accuracy at time T, this state variable will improve the accuracy of the future simulated state variables (Delécolle et al., 1992). The advantage of the sequence assimilation strategy is that new observed data are used to update the predicted state of the model in a stable fashion (Delécolle et al., 1992). Based on this strategy, a series of assimilation algorithms (Dorigo et al., 2007), such as the EnKF (Ensemble Kalman Filter) algorithm, have been employed to improve the accuracy of crop yield estimation by linking crop models and remote sensing images (de Wit et al., 2007; Curnel et al., 2011).

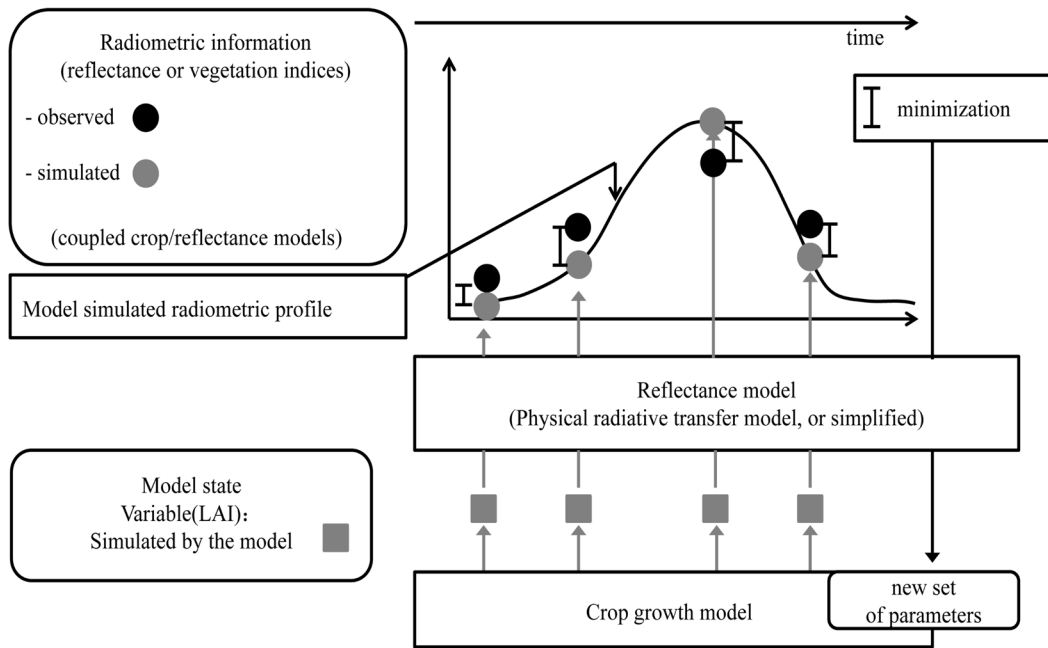


Figure 1.5 Assimilation strategy by comparing simulated reflectance and satellite reflectance (Delécolle et al., 1992)

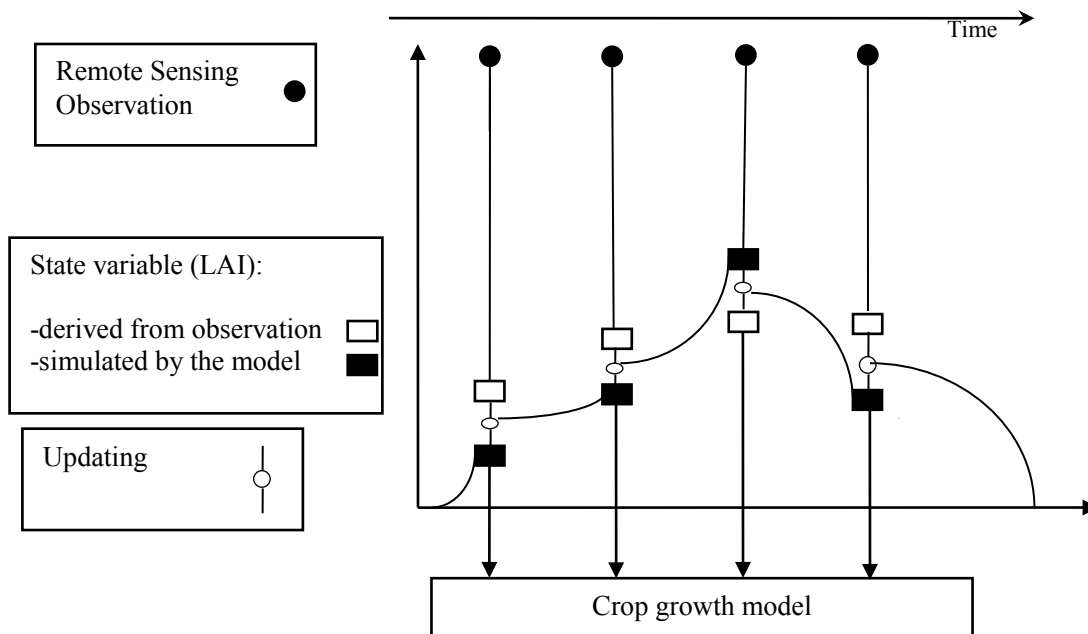


Figure 1.6 Schematic diagram for the sequence assimilation strategy (Delécolle et al., 1992)

*Summary of assimilations between remote sensing and crop models*

We have used remote sensing data, assimilation algorithms, crop types, crop models and variables as indicators to summarize assimilation studies about coupling remote sensing and

crop models together (**Table 1.6**). This table shows some of the studies that have been conducted. Few studies have included remote sensing images with high spatial resolution. Medium and low resolution images were used in these studies, such as Landsat TM and MODIS images. The LAI is one of the most important coupling variables between remote sensing data and crop models. Regarding assimilation algorithms, previous studies have given a variety of algorithms.

These investigations used various strategies and state variables in the assimilation between the remote sensing inversion and the crop model simulation. The first strategy reinitializes and recalibrates parameters using the biophysical and chemical parameters from the crop model simulation and remote sensing inversion. These state variables include the LAI, soil water content, fraction of absorbed photosynthetic active radiation (FPAR), leaf nitrogen, phenological information and chlorophyll. The second strategy acquires a better yield by comparing the reflectance from remote sensing images and the crop model nested with a radiation transfer model. In addition, vegetation indices have been also used instead of reflectance to optimize the simulation by minimizing differences between simulated and retrieved vegetation indices.

Compared to the first strategy, the second one is more scientific from a physical perspective by directly comparing the physical reflectance. However, this strategy has also led to numerous problems. After introducing radiation transfer models into the assimilation scheme, additional uncertainties have been introduced, such as uncertainties in the input parameters and initial conditions within the radiation transfer model. Simultaneously, computing resources have also increased, decreasing the computing efficiency.

According to the EU (European Union) program on “climate change, agriculture and food security”, three major crop types, namely Maize, Wheat and Rice, were mainly mentioned (Hoefsloot et al., 2012). Similarly, numerous scholars have focused on wheat, maize and rice (**Table 1.6**). Few studies on cotton have been reported. Correspondingly, numerous common crop models have been employed such as the SWAP, DSSAT and WOFOST models while the APSIM model has been rarely used. Regarding the assimilation between remote sensing and crop models, the state variable is most important for linking variables from model simulations and remote sensing inversion. During this EU-Project, scientists have also frequently used the LAI, GAI (Green Area Index) and NDVI (or reflectance). The most frequently used parameter is the LAI (Watson, 1947), a parameter was developed for revealing vegetation canopy status in field experiments (Hoefsloot et al., 2012). This result is

also consistent with other similar investigations (Fang et al., 2008; Mo et al., 2005; Ma et al., 2008).

The remote sensing images used were mainly MODIS, SPOT, AVHRR and Landsat TM/ETM+ images. Both the summary of related studies and the EU project give useful examples for the assimilation between the LAI derived from remote sensing data and the LAI simulated from the APSIM/OZCOT model. Therefore, coupled crop growth models with remote sensing and GIS has become a popular and state of the art area of research from the field to the regional scale.



Table 1.6 Previous researches on assimilation between remote sensing and crop models

RS data	Assimilation algorithms	Crop model	Crop types	Variables	Authors
ASD	PSO	RiceGrow	Rice	LAI, LNA	<a href="#">Zhu et al., 2010</a>
ASD	PSO and EnSRF	RiceGrow	Rice	LAI, LNA	<a href="#">Wang et al., 2012</a>
MODIS HJ CCD	PSO	WOFOST	Rice	SAVI	<a href="#">Wu et al., 2012</a>
MODIS	SCE-UA and SA	COSIM	Cotton	LAI	<a href="#">Zhao et al., 2005</a>
ASD	VFSA	CERES-Wheat	Winter wheat	LAI	<a href="#">Liu et al., 2011a</a>
MODIS	Cost function	CERES-Wheat	Winter wheat	LAI	<a href="#">Wang et al., 2011</a>
MODIS TM	SCE-UA	CERES-Maize	Maize	LAI	<a href="#">Jin et al., 2012</a>
SAR	Cost function	WOFOST	Rice	Biomass	<a href="#">Tan et al., 2011</a>
ENVISAT ASAR	SCE-UA	ORYZA2000	Rice	LAI	<a href="#">Shen et al., 2009</a>
MODIS LAI	EnKF	WOFOST	Winter wheat	LAI	<a href="#">Wu, 2012</a>
MODIS	Forward deducing + pixel model	WOFOST	Winter wheat	LAI	<a href="#">Guo et al., 2014</a>
MODIS LAI GPP	SA, SCE-UA	WOFOST	Wheat	LAI GPP	<a href="#">Wang, 2013</a>
MODIS LAI GPP	EnKF	WOFOST-HYDRUS	Maize	LAI	<a href="#">Li, 2012</a>
MODIS LAI	EnKF	WOFOST	Winter wheat	LAI	<a href="#">Huang et al., 2012</a>
MODIS	FSEOPT software	WOFOST	Winter wheat	LAI, ET	<a href="#">Zhang et al., 2007</a>
HJ-1A/B	SCE-UA	WOFOST	Rice	LAI	<a href="#">Chen et al., 2010</a>
MODIS LAI	SCE-UA	CERES-wheat	Wheat	LAI	<a href="#">Yan et al., 2006</a>
MODIS	FSEOPT software	WOFOST	Winter wheat	LAI	<a href="#">Ma et al., 2005</a>
MODIS NDVI	SCE-UA	EPIC	Maize	LAI	<a href="#">Ren et al., 2011</a>
ASD HJ TM	SCE-UA	WheatGrow	Wheat	LAI LNA	<a href="#">Huang et al., 2011</a>
Observed LAI	Constrained analysis	WOFOST	Maize	LAI, TAGP	<a href="#">Sun et al., 2013</a>
SPOT, Airborne images	Optimization algorithm	SUCROS	Sugar beet	TSAVI	<a href="#">Launay and Guérif, 2005</a>
HJ-1A/B CCD	POD4DVar	CERES-wheat	Wheat	LAI	<a href="#">Jiang et al., 2014</a>
SPOT, Airborne images	Optimization algorithm	SUCROS	Sugar beet	TSAVI	<a href="#">Guérif and Duke, 2000</a>
Ground radiometry	Updating and forcing	CERES-Wheat	Wheat	LAI	<a href="#">Thorp et al., 2010</a>
MODIS	FSEOPT	WOFOST	Winter wheat	SAVI	<a href="#">Ma et al., 2008</a>
ASD	EnKF	CERES-Wheat	Wheat	NDVI	<a href="#">Li et al., 2011</a>
MODIS LAI	EnKF	WOFOST	Wheat	LAI	<a href="#">Zhu et al., 2013</a>
ENVISAT/ASAR, MERIS	variational assimilation	CERES-wheat	Wheat	LAI	<a href="#">Dente et al., 2008</a>
MODIS-LAI	EnKF	DSSAT	Maize	LAI	<a href="#">Ines et al., 2013</a>
IRS LISS-III	Modified corrective approach	WTGROWS	Wheat	LAI	<a href="#">Sehgal et al., 2005</a>
MODIS LAI	POWELL optimization	CERERS-Maize	maize	LAI	<a href="#">Fang et al., 2011</a>
MODIS MOD15A2	EnKF	DSSAT	Wheat	LAI	<a href="#">Nearing et al., 2012</a>
Landsat 8 OLI	PSO	WOFOST	Rice	LAI	<a href="#">Jin et al., 2015</a>
ASD spectral data	PSO	WOFOST	Rice	Vegetation index	<a href="#">Wu et al., 2013</a>
MODIS L1B	GA	SWAP	Wheat	ET	<a href="#">Irmak and Kamble, 2009</a>
MODIS L1B	GA	SWAP	NA	ET, LAI	<a href="#">Charoehirunyingvos et al., 2011</a>
MODIS	constant gain Kalman filter	SWAP	Wheat	LAI, ET	<a href="#">Vazifedoust et al., 2009</a>

*Continued*

Table 1.6 Continued

RS data	Assimilation algorithms	Crop model	Crop types	Variables	Authors
Landsat 5 TM	PEST	SWAP	NA	ET	<a href="#">Droogers et al., 2010</a>
MODIS LAI	EnKF	PyWOFOST	Maize	LAI	<a href="#">Zhao et al., 2013</a>
hand-held radiometer	FSEOPT	SUCROS	Sugar beet	reflectance	<a href="#">Guérif and Duke, 1998</a>
MODIS LAI	EnKF	WOFOST	Winter wheat	LAI	<a href="#">Liu et al., 2014b</a>
ASD spectral data	PSO	DSSAT-CERES	Wheat	Canopy Nitrogen accumulation	<a href="#">Li et al., 2015</a>
MODIS LAI	SCE-UA	SWAP	Winter wheat	Phenological information	<a href="#">Xu et al., 2011</a>
IRTS-P3 infrared radiative thermometer	SCE-UA	SVAT	NA	Surface radiometric temperature	<a href="#">Crow et al., 2008</a>

## 2 Objectives

Based on the background and problems mentioned above, five main objectives for this study are proposed as follows:

### **Objective 1: Implementing APSIM/OZCOT model in a spatial mode (GIS-based crop growth model)**

In order to solve the flaws within crop growth models, a GIS-based crop growth model coupled with remote sensing images is proposed (**Figure 2.1**). This flowchart illustrates the procedure for comparing the LAI derived from remote sensing images and the APSIM/OZCOT model by tuning sensitive parameters within the crop growth model, based on an assimilation method. This GIS-based crop growth model includes two important parts: the earth observation and APSIM/OZCOT model. First, the PVI is retrieved from time series Landsat-8 OLI remote sensing images after the radiometric correction. Then, a statistical model is used to analyse the relationship between the PVI and the observed in-situ LAI by correlation analysis. In addition, the APSIM/OZCOT model is employed after the parameterization to simulate the LAI of cotton. Afterwards, the comparison between the simulated and the retrieved LAI is analysed to parameterize the relevant parameters in the APSIM/OZCOT model. Finally, the regional yield of cotton can be obtained based on these optimized parameters in the APSIM/OZCOT model.

### **Objective 2: Land use mapping of cotton cultivation**

Prior to the assimilation, the explicit distribution of cotton cultivation is the first step. Then a series of remote sensing images within a whole growth period are used to extract cotton pattern combined with phenological events of different vegetation types.

### **Objective 3: LAI retrieval from Landsat 8 OLI remote sensing data**

LAI is an important state variable in this coupling model between remote sensing and crop growth models. Timely LAI observations of cotton canopy derived from multi-temporal remote sensing images can provide the true LAI status to the APSIM/OZCOT model. Then seasonal LAI maps within the cotton cultivation region are retrieved from remote sensing data in this research.

**Objective 4: APSIM/OZCOT model for yield prediction at the field level**

After the calibration of cultivar parameters within the APSIM/OZCOT model, the APSIM/OZCOT model can accurately simulate the growth process and yield formation of cotton. Then this coupling model is implemented to simulate the LAI dynamics and yield formation at the field scale.

**Objective 5: APSIM/OZCOT model for regional yield prediction**

After the implementation of this coupling model, this strategy is then applied to the regional scale. In order to increase the computational efficiency, we also implement the assimilation during two growth periods of cotton: the early stage and mid-late growth stage.

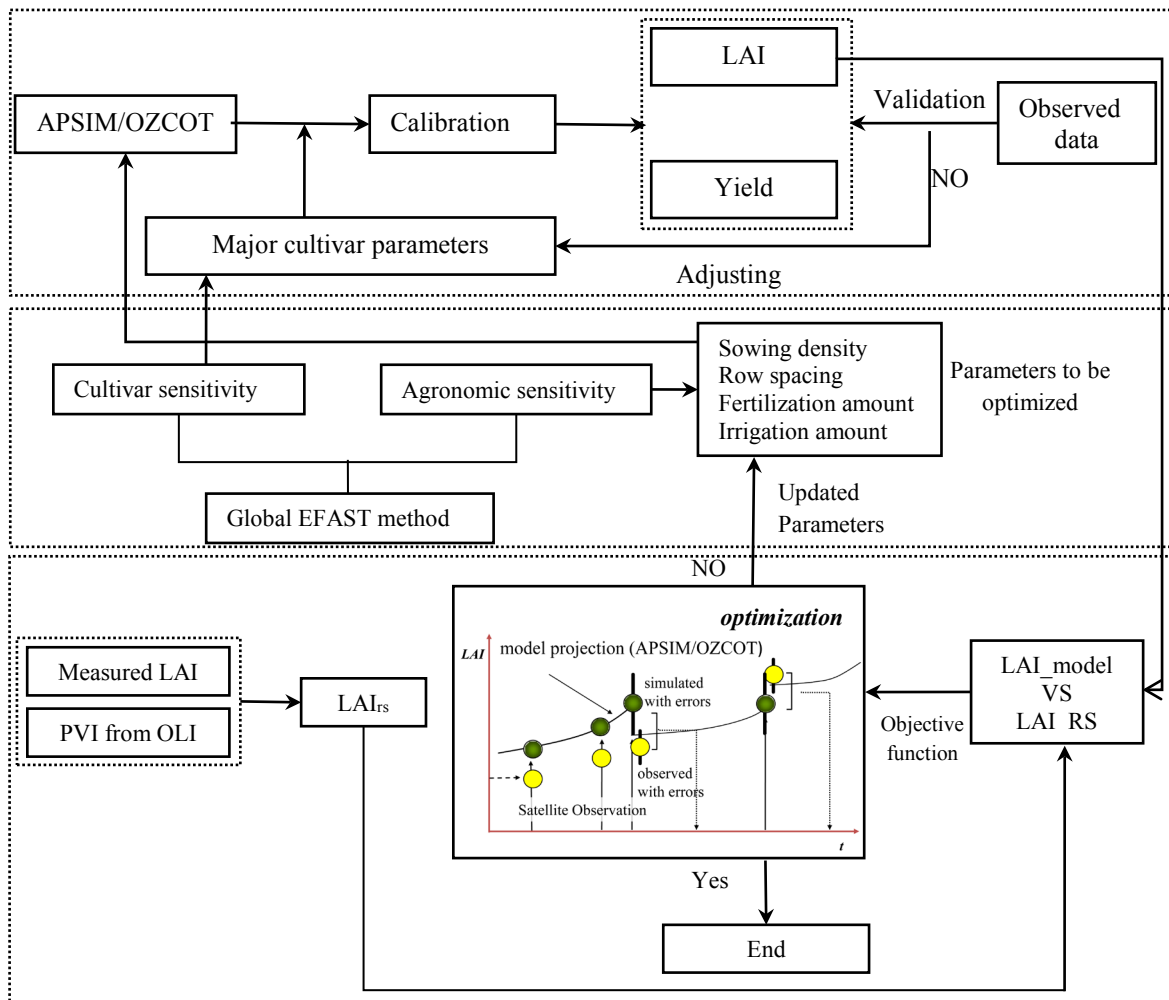


Figure 2.1 Flowchart of the assimilation between remote sensing and APSIM/OZCOT model

## 3 Study Site

### 3.1 Characterisation of study site

The study area, administered by Alar City, is located in the Xinjiang Uygur Autonomous Region, NW China, residing at the northern edge of the Taklamakan Desert. It is also located at the intersection of three rivers namely the Aksu, Yarkand and Hotan Rivers (**Figure 3.1**). Alar is administrated by both the Xinjiang Uygur Autonomous Region and the Xinjiang Production and Construction Corps (XPCC), in which a hybrid management system is implemented. Since 1998, private farms, local government and XPCC have expanded their farmland and reclaimed arable land driven by increases in the price of cotton. Most recent reclamations were devoted to cultivated cotton.

According to data from the Alar Statistical Year Book (<http://www.ale.gov.cn/structure/zjale/ssrk.htm>), the population of Alar is about 310 100 in 2014 and the number of employees is about 152 500 while the agricultural employees are only 41 300. In the year of 2014, the agricultural GDP is about 20.85 billion Chinese Yuan (CNY) based on data from the Alar Statistical Year Book. Among them, the output value of cultivation was 18.67 billion CNY while the output value of forestry, animal husbandry and fishery was 0.2 billion, 1.15 billion and 0.08 billion CNY, respectively. In 2014, based on data from the Alar Statistical Year Book, the cultivation area of cotton, grain and vegetable was 150.67, 21.41 and 4.81 thousand ha, respectively, while their production was  $35.46 \times 10^7$ ,  $20.97 \times 10^7$  and  $14.11 \times 10^7$  kg respectively (**Figure 3.2**). The percentage of cotton cultivation was approximately 85.2% of crop cultivation in 2014. Based on questionnaires during field works, we know that Alar is the main upland cotton cultivation region and a cultivation region for island cotton in China.

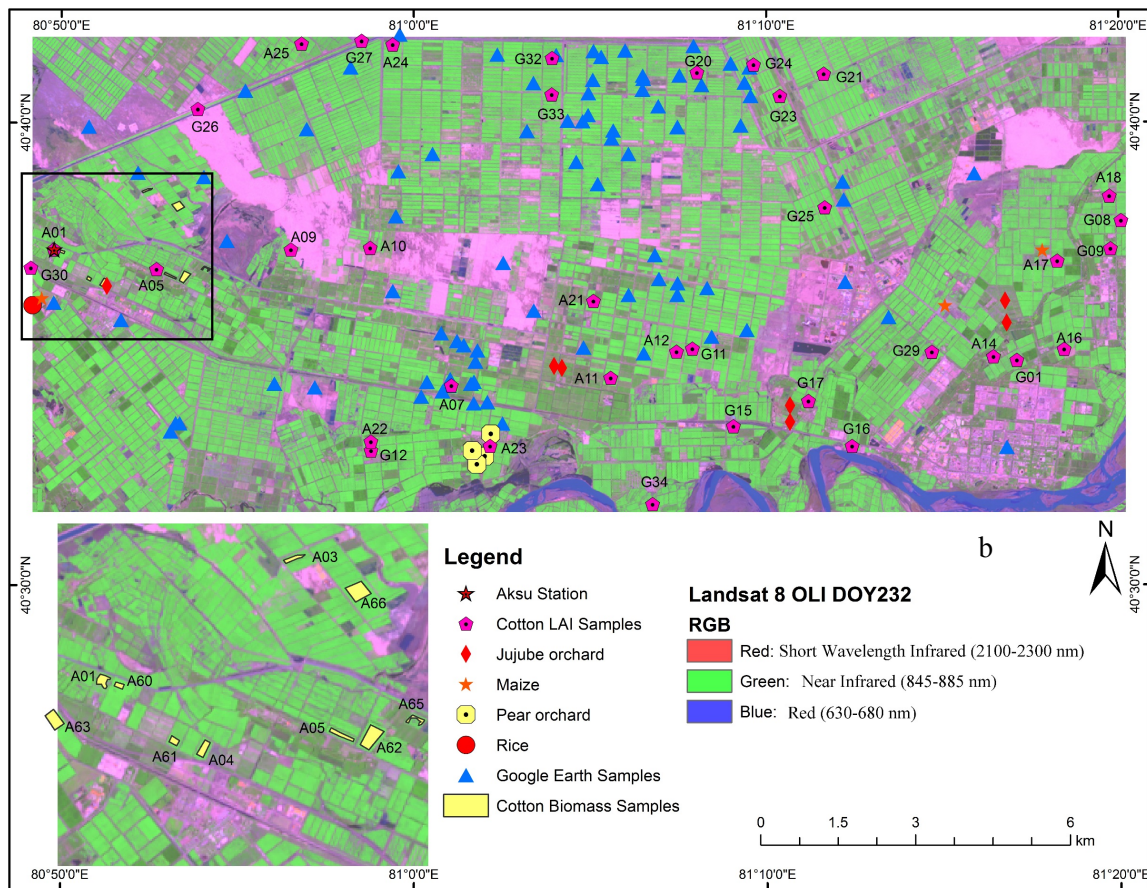
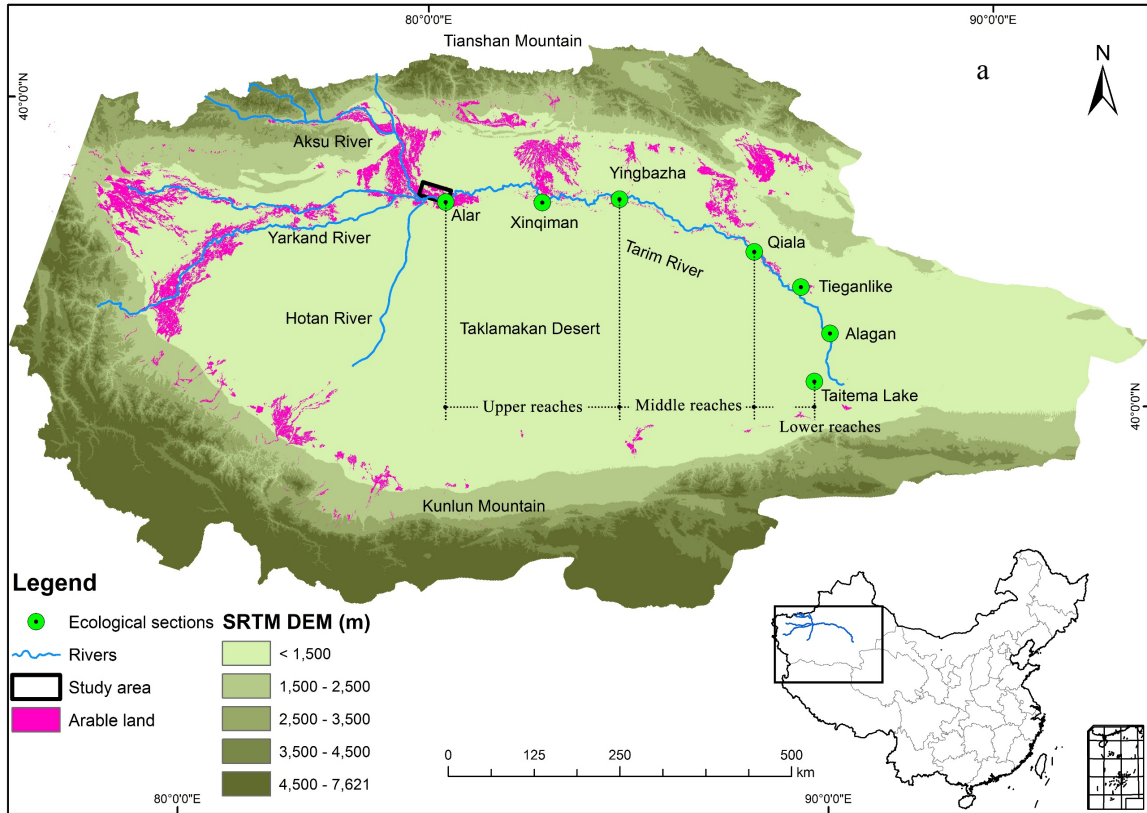


Figure 3.1 (a) Study area location in China; (b) LAI, yield and land cover samples in the study area

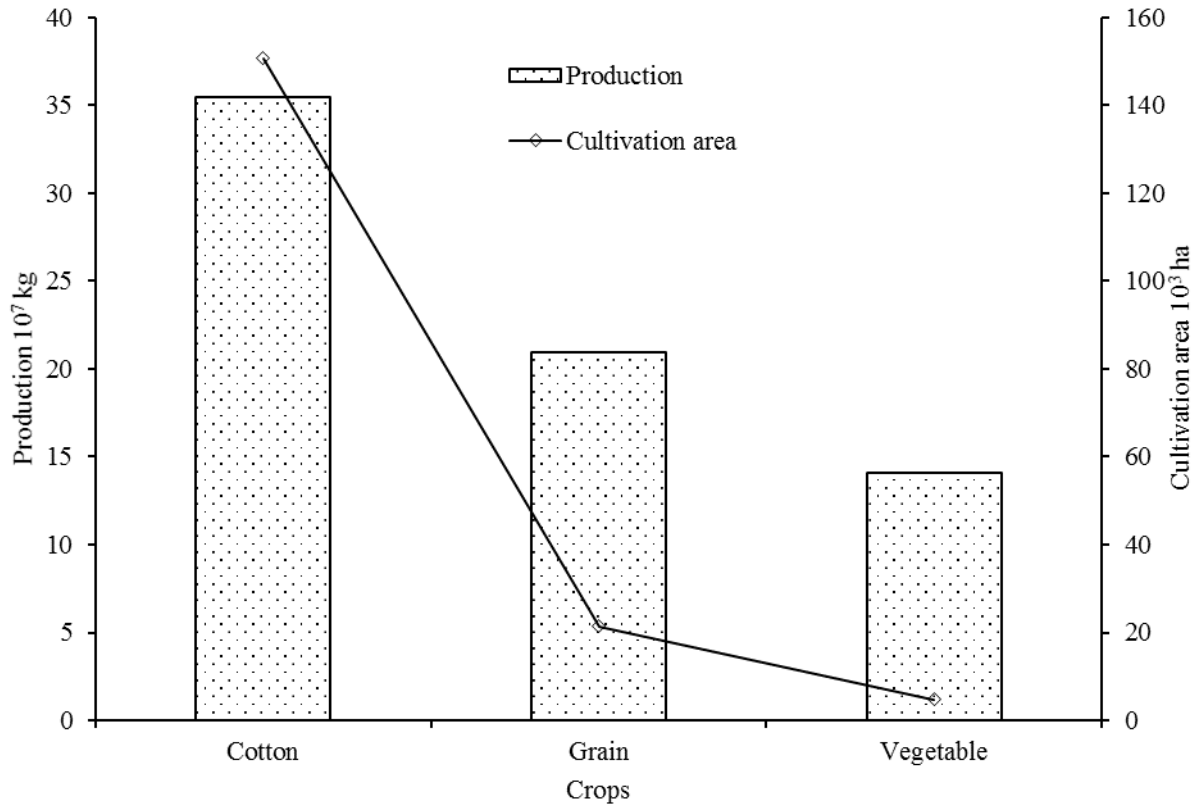


Figure 3.2 Cultivation and production of three major crops in 2014

Based on the SRTM (Shuttle Radar Topographic Mission) DEM (Digital Elevation Model) data (Jarvis et al., 2008), the terrain of the study area is relatively flat with an altitude ranging from 994 to 1045 m (Figure 3.3a). Generally, the terrain trends higher in the northwest and lower in the southeast of study area. There is a total of 17 types of soil in the study area based on a soil map from the University of Hohenheim using the Harmonized World Soil Database (HSWD) (FAO et al., 2012) (Figure 3.3b). Alar is the interchange of the Aksu, Hotan and Yarkand Rivers and also the source of the Tarim River. The study area is a cotton region irrigated by groundwater and runoff pumping.

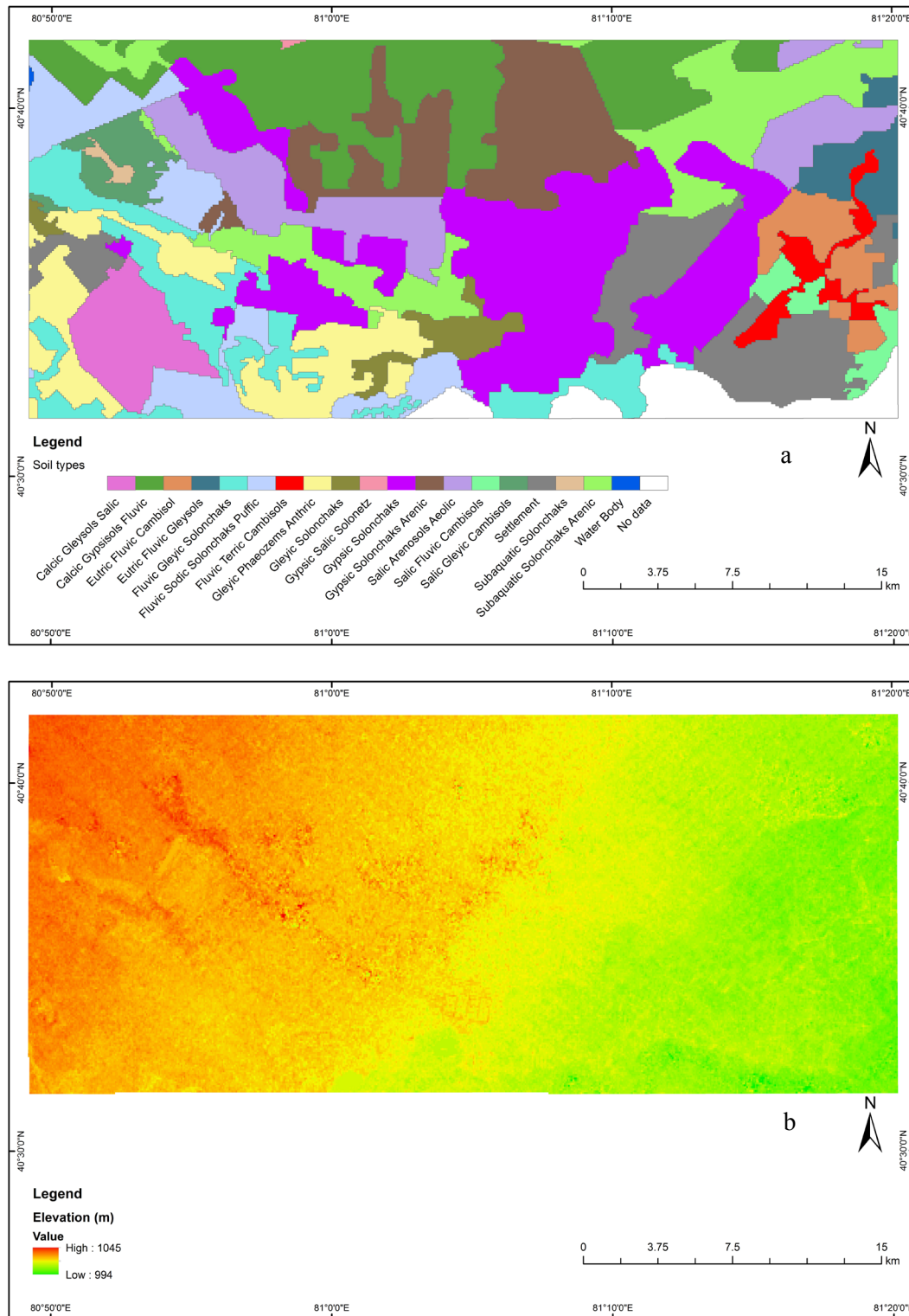


Figure 3.3 (a) Soil types map (FAO et al., 2012); (b) the digital elevation model (Jarvis et al., 2008)

Alar belongs to the extremely arid continental desert climate in the warm temperate zone. According to meteorological data during 1959–2014 at the Alar National Weather Station, the annual average temperature, rainfall and solar radiation in this region was approximately 10.7 °C, 48.5 mm and 16.8 MJ/m<sup>2</sup> (Figure 3.4), respectively. Based on seasonal dynamics of the annual average temperature, rainfall and solar radiation reached maximum in summer and



minimum in winter. The total rainfall in July from 1959 to 2014 was about 626.28 mm while the lowest was 34.5 mm in January. The highest average radiation in June was about 24.78 MJ/m<sup>2</sup> while the lowest average radiation in December was 8.25 MJ/m<sup>2</sup>. The highest average temperature in July was 24.73 °C while the lowest average temperature was -8.37 °C in January.

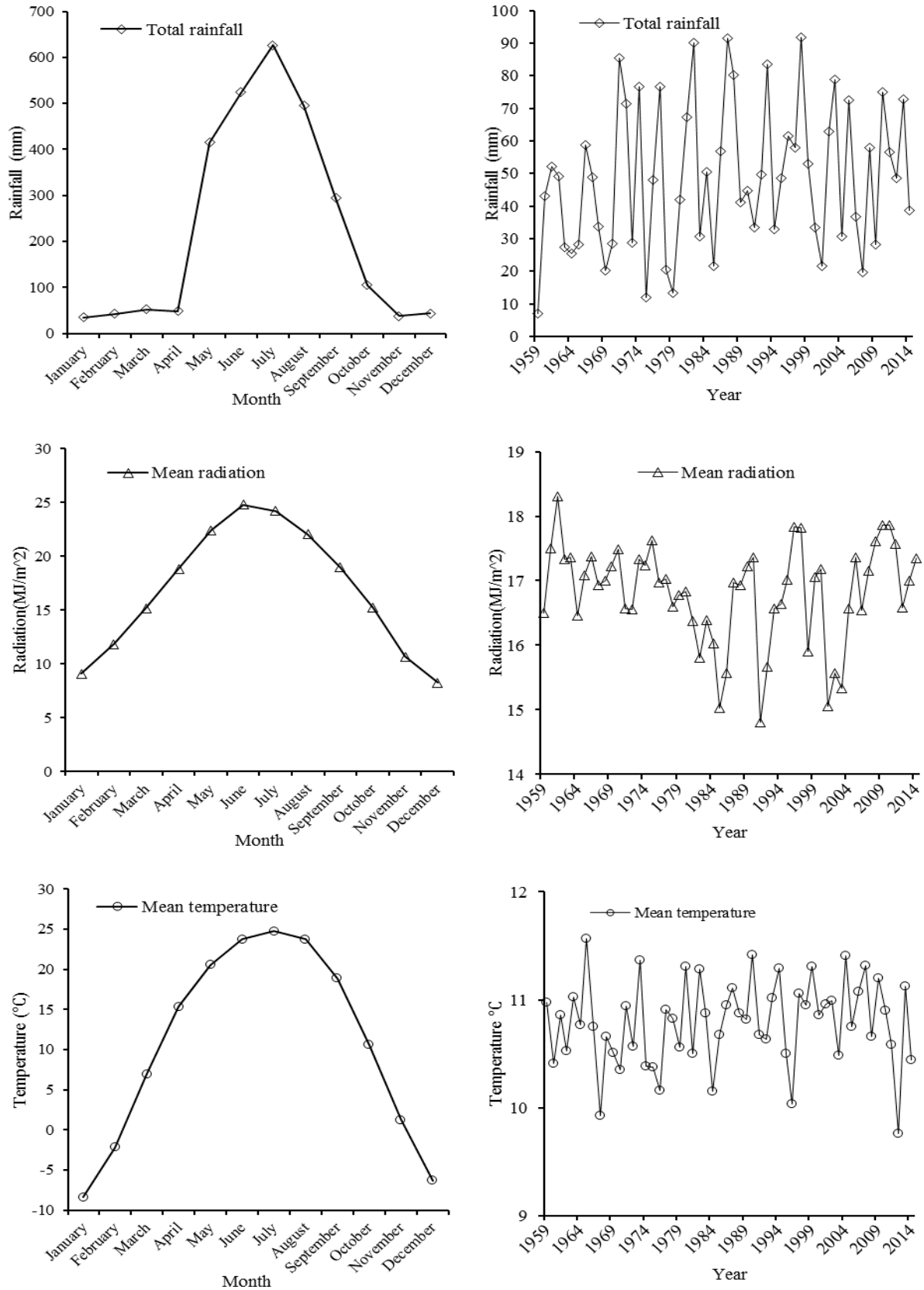


Figure 3.4 Inter and intra-annual changes of rainfall, radiation and temperature in Alar, 1959-2014

### 3.2 Selection of test area

Agronomic practices such as specific cotton variety, fertilization, irrigation and cultivation modes are all allocated and managed by the various corps of XPCC. Homogeneous and large cotton fields, approximately  $700 \times 120$  m in size, are useful for the large-scale cultivation and management of cotton. Additionally, a station ( $80^{\circ} 45' E$ ,  $40^{\circ} 37' N$  and altitude 1028 m) belonging to the Chinese Ecosystem Research Network, namely the Aksu National Field Scientific Observation and Research Station for Farmland Ecosystem (hereafter Aksu station), is located in the study area (**Figure 3.1e**). Because the Aksu station is designed to represent a typical oasis agricultural ecosystem, numerous long term monitoring data regarding soil water, salt, nutrients and agronomic practices for cotton were obtained.

Variations in the organization of agricultural production patterns and the type of arable land use resulted from the two different modes of agronomic management from the XPCC and private farms. Therefore, Alar is a typical study area for analysing cotton growth modelling coupled with remote sensing images. In order to acquire an optimal boundary for the study area that includes all cotton fields within field campaigns, we further selected four border points as follows (**Table 3.1**). Then, we used the rectangle with the four border points to define the study area (**Figure 3.1e**).

Table 3.1 Description of study area used for the assimilation

	UTM 44 N Easting (meter)	Longitude (degree)	UTM 44 N Northing (meter)	Latitude (degree)	Field
West	484761.283	80.81985	4496028.297	40.614936	G30
North	497916.852	80.975343	4505204.538	40.69774	G27
South	509519.015	81.112385	4486232.118	40.526769	G34
East	528420.000	81.336066	4498048.597	40.632788	G08

## **4 Data and Methods**

### **4.1 Remote sensing images and pre-processing**

Because the revisit time of Landsat-8 is 16 days, Landsat-8 Operational Land Imager (OLI) remote sensing images are not continuous daily observations. Furthermore, cloudiness caused missing visible and near-infrared (VIS-NIR) remote sensing images. Meanwhile, the APSIM/OZCOT model has a daily simulation step. Thus, selecting optimal state variables derived from remote sensing images is critical for describing the physiological process of the APSIM/OZCOT model. In this paper, we selected seven cloud-free Landsat-8 OLI remote sensing images at DOY 72 (13 March), DOY 136 (16 May), DOY 168 (17 June), DOY 200 (19 July), DOY232 (20 August), DOY 248 (5 September) and DOY 280 (7 October). These Landsat-8 OLI remote sensing images covered the phenological stages from seedling to boll opening and maturation. Thus, LAI values retrieved from Landsat-8 OLI time series images are considered trusted state variables for the assimilation strategy between the APSIM/OZCOT model and remote sensing images.

In addition, MODIS MCD43A3 Albedo and MOD/MYD 09A1 reflectance images were also obtained during the same period as OLI images to assist the atmospheric correction of the Landsat-8 OLI images. The spatial resolution of the MCD43A3 product (nadir BRDF-adjusted reflectance) is 500 meters while its temporal resolution is 16 days. The spatial resolution of MOD/MYD 09A1 is 500 m and the temporal resolution is 8 days. The MODIS EVI (enhanced vegetation index) products in 2001, 2008 and 2013 were also obtained to generate EVI magnitude maps for modelling the spatiotemporal dynamics of reclamation. All remote sensing images were acquired from the NASA's Earth Observing System Data and Information System.

An MRT (MODIS Re-projection Tool) was used to transform an ISIN (Integerized Sinusoidal) projection of MODIS images into a Universal Transverse Mercator (UTM) 44 and a World Geodetic System 1984 (WGS84) datum ellipsoid. Meanwhile, the data format of MODIS was also converted into the ENVI standard from HDF-EOS (Hierarchical Data Format-Earth Observing System) and the spectral band order was adjusted to be the same as Landsat-8 OLI images. Then a Gaussian Low Pass method was employed to generate a template with the kernel size of  $17 \times 17$  (the size is greater than  $500/30$ ). Afterwards, Landsat-8 OLI images were aggregated into 500 m level by the Gaussian Low Pass downscaling approach. Downscaling OLI images with 500 m were resampled into 500 m by a pixel aggregate

method, which using the mean value of all pixels contributing to the output pixel as the value of output pixels.

Then land cover sampling was implemented based on MODIS MCD43A3 and Landsat-8 OLI images. Thus, some dark targets such as the water body, shade, dense cotton coverage and low reflectance soil, as well as the high reflectance soil and sand, were selected. After selecting the Region of Interest (ROI), spectral curves of various ROIs were checked to avoid errors caused by failures related to the MODIS algorithm. Afterwards, the estimated atmospheric parameters were obtained by estimating the relationship between the MODIS MCD43A4 and Landsat-8 OLI images using AtCPro software, developed by the environmental remote sensing department, University of Trier (Hill, 2013) (Figure 4.1). The RMSE between the MODIS MCD 43A4 and Landsat OLI image at DOY 200 was only 0.03844, and the angstrom beta, angstrom nu and water vapour were all obtained. Based on estimated atmospheric parameters, we implemented the atmospheric correction of Landsat-8 OLI image combined with the SRTM DEM data for the topographic correction. Then, we compared vegetation reflectance between the MODIS MCD43A4 products and Landsat-8 OLI remote sensing images at DOY 200 (Figure 4.2). The atmospherically-corrected Landsat OLI image showed better performance against the MODIS spectral curve of vegetation.

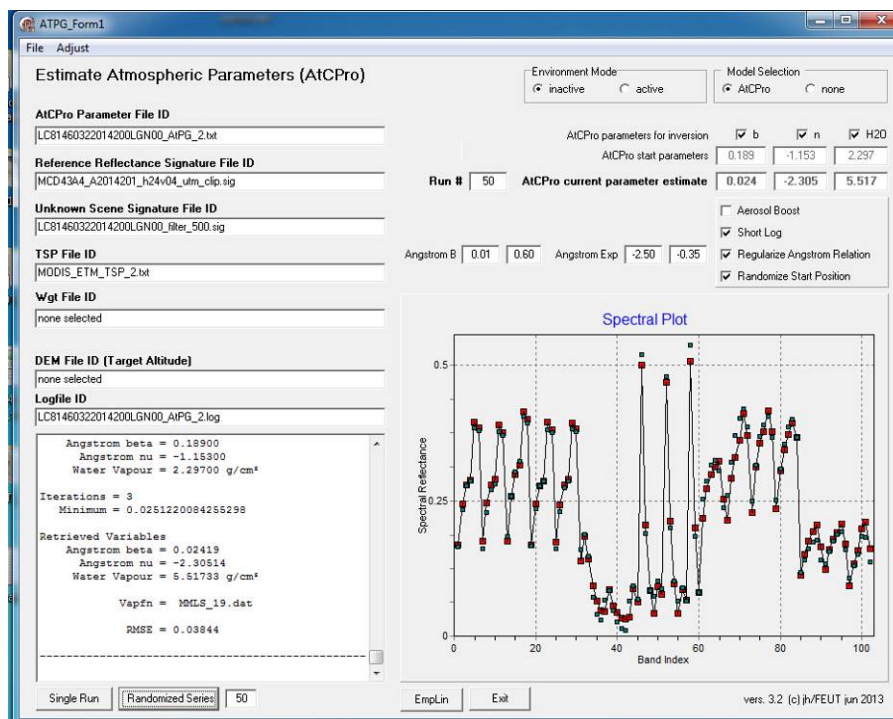


Figure 4.1 The estimated atmospheric parameters based on an AtCPro software (Hill, 2013)

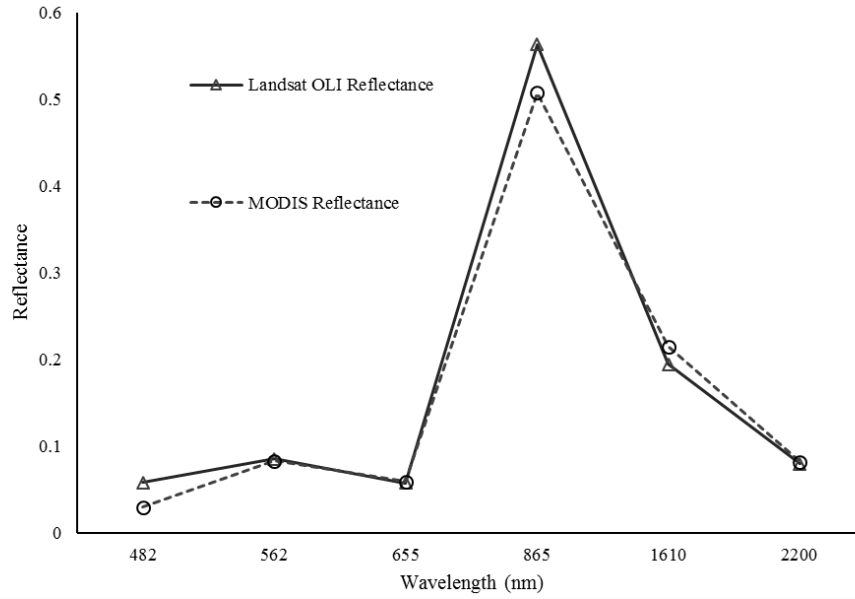


Figure 4.2 Comparison of MODIS and corrected Landsat 8 OLI vegetation reflectance responses

## 4.2 Ground data collection

The daily climate data during 1958–2014 were recorded by the Alar National Principal Station of China Meteorological Administration (code 51730) affiliated to World Meteorological Organization (WMO), located in the study area. As a driver for the APSIM/OZCOT model, daily climate data include maximum and minimum temperature, rainfall and sunshine hours. All these daily climate data were obtained from China Meteorological Data Sharing Service System. According to the metadata, maximum and minimum temperature, rainfall and sunshine hours were all first multiplied by 0.1. Then sunshine hours were converted into solar radiation since the solar radiation is a climatic factor driving the APSIM/OZCOT model. The daily solar radiation was calculated using the following formula proposed by Doorenbos and Pruitt (1977). These formulas are as follows:

$$H = H_L \times \left(a + b \times \frac{S}{S_L}\right) = 0.8 \times H_0 \times \left(a + b \times \frac{S}{S_L}\right) \quad (4.1)$$

$$S_L = (2/15) \cdot W_s; W_s = \cos^{-1}(-\tan \Phi \cdot \tan \delta) \quad (4.2)$$

where  $H$  is the daily solar radiation;  $H_L$  is the daily solar radiation under the sunny state;  $S$  and  $S_L$  represent the actual sunshine hour and the day length;  $\Phi$  is the latitude;  $\delta$  is the solar declination;  $W_s$  is the hour angle;  $a$  and  $b$  are empirical constants of 0.248 and 0.752, respectively, according to Chinese conditions (Zuo et al., 1963);  $H_0$  is the extraterrestrial

irradiation and the atmospheric transparency coefficient is 0.8 in Western China (Tong et al., 2005).

Additionally, the formula of the extraterrestrial irradiation (Zuo et al., 1963) is as follows:

$$H_0 = (1/\pi) \cdot G_{sc} \times E_0 \cdot (\cos \Phi \cdot \cos \delta \cdot \sin W_s + (\pi/180) \cdot \sin \Phi \cdot \sin \delta \cdot W_s) \quad (4.3)$$

$$E_0 = 1.00011 + 0.034221 \cos \Gamma + 0.00128 \sin \Gamma + 0.000719 \cos 2\Gamma + 0.000077 \sin 2\Gamma \quad (4.4)$$

$$\delta = (180/\pi) \cdot (0.006918 - 0.399912 \cdot \cos \Gamma + 0.070257 \cdot \sin \Gamma - 0.006758 \cdot \cos 2\Gamma + 0.000907 \cdot \sin 2\Gamma - 0.002697 \cdot \cos 3\Gamma + 0.00148 \cdot \sin 3\Gamma)$$

$$\Gamma = 2\pi \cdot (n-1)/365 \quad (4.5)$$

where  $G_{sc}$  is the solar constant;  $E_0$  is the correction factor of Earth's orbital eccentricity;  $\Gamma$  is year angle and  $n$  is the DOY (day of year).

The climatic data including the maximum temperature, minimal temperature, precipitation and solar radiation in 2014 at the Alar State Station of Meteorology was listed (Figure 4.3).

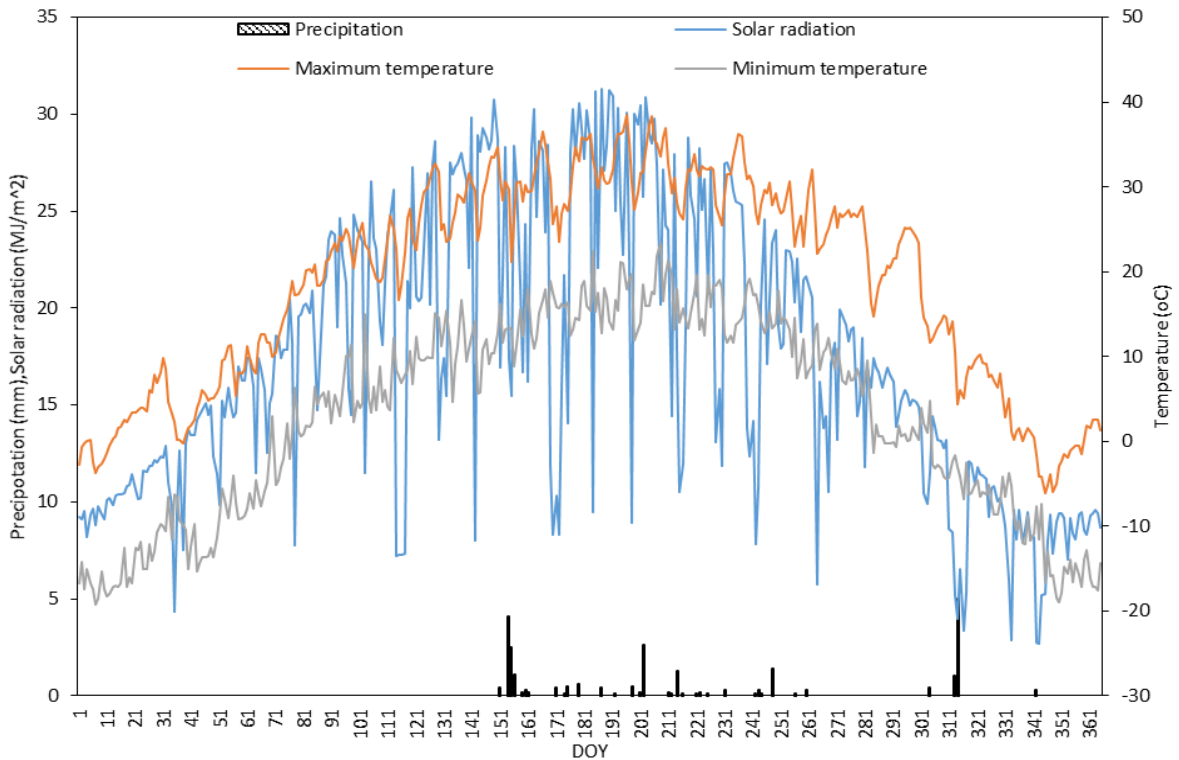


Figure 4.3 Daily climate data within 2014 at the Alar State Station of Meteorology

A total of 26 observed in-situ soil profiles were acquired from the University of Hohenheim in Germany, a member of the SuMaRiO project (Figure 3.1e). Meanwhile, cotton yield and

biomass data before harvesting from a total of ten fields (**Figure 3.1e**) in 2014 was collected by staff at the University of Hohenheim and provided for this research (**Table 4.1**).

Table 4.1 In situ observed cotton yield in 2014 (provided by University of Hohenheim)

	A01	A03	A04	A05	A60	A61	A62	A63	A65	A66
Cotton Yield ( $\times 10^3$ kg/ha)	4.57	5.76	6.12	7.36	5.46	7.97	6.64	7.75	7.87	7.67
Biomass ( $\times 10^3$ kg/ha)	11.67	14.81	9.38	16.41	8.90	14.21	12.88	14.26	16.18	13.89

In addition to 16 cotton fields with soil profiles, a total of 20 uniformly distributed cotton fields without soil profiles covering the entire study area were selected as LAI sampling plots according to the corresponding administration that they were affiliated with. The distribution of sampling plots not only reflects variations in agronomic practices, but also reveals spatial variations of cotton growth. In each sampling plot, about 9–12 points over an interval of greater than 30 meters (the pixel size of Landsat OLI image) were selected to reflect the heterogeneity of cotton growth. Field campaigns were implemented during three major cotton growth stages, namely the seedling, flower-boll and boll opening-mature stage. Finally, the LAI measurement, plant height measurement was both performed by employing a LAI-2000 Plant Canopy Analyser (LI-COR Inc., Lincoln, Nebraska) and a rule with millimetre-level accuracy (**Figure 4.4**; **Figure 4.5**). The LAI within cotton fields was estimated using this non-destructive method. Simultaneously, about five measurements of the plant canopy height nearby each sampling point were taken and averaged to a mean height per sampling point. About 9–12 plant canopy height values per cotton field were acquired.



Figure 4.4 LAI and height measurement during three major cotton growth stages



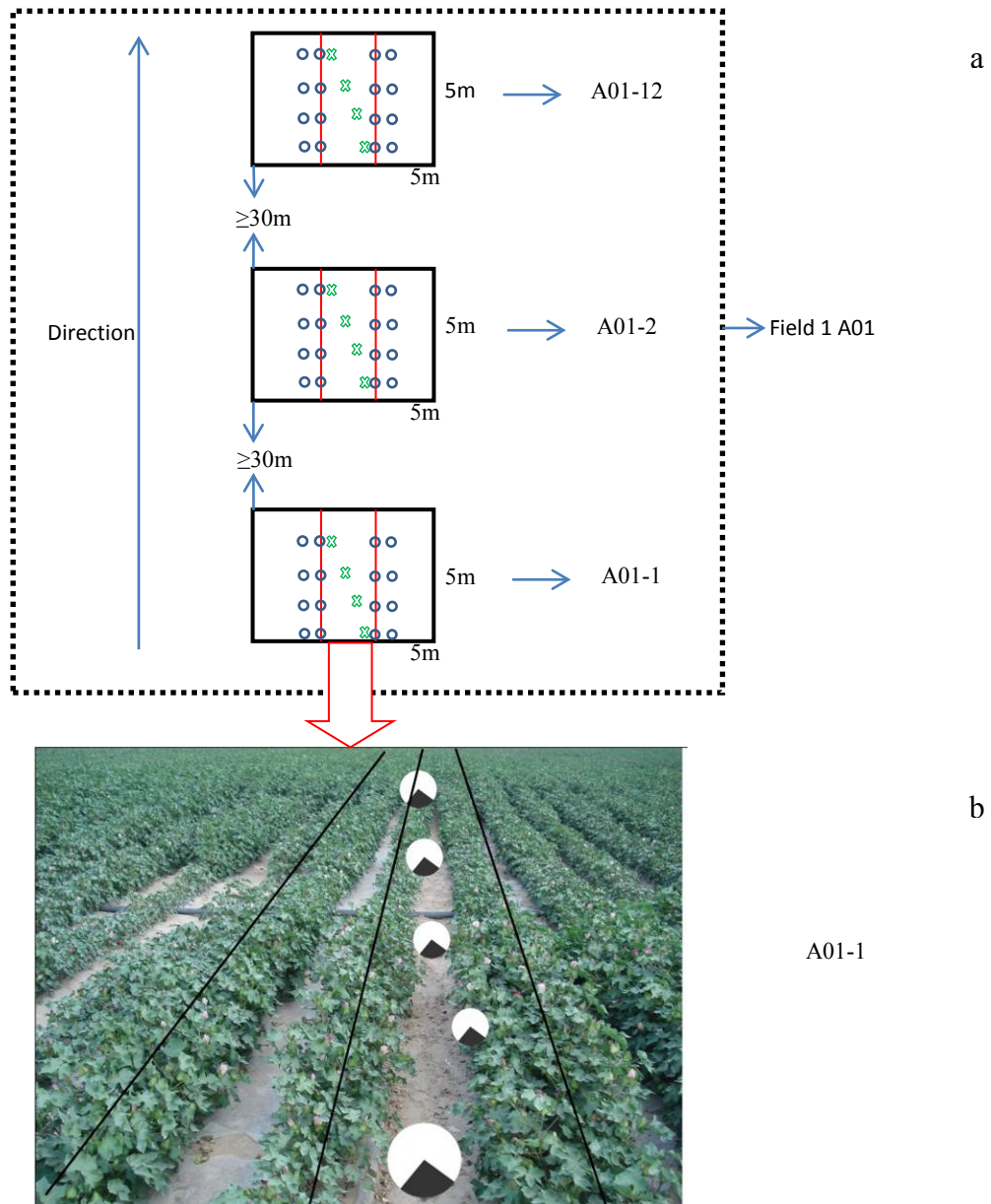


Figure 4.5 Sampling strategy for LAI-2000 over cotton field A01: (a) LAI was measured in a total of 12 plots, the size of each plot was about 5×5 meters and distance between them was  $> 30$  meters (the pixel size of Landsat OLI image); (b) illustrate a detailed measurement about the first plot (A01-1) within field A01

Meanwhile, data pertaining to agronomic practices, cotton price and disasters of each plot were acquired using numerous questionnaires and interviews with local residents (**Figure 4.6**). Agronomic practices mainly include the cotton variety, cultivation mode, sowing date, irrigation and fertilization (amount and date). Among these cotton varieties, a cultivar titled XLZ37 created by the local company, has been cultivated since 2010, exceeding 60% of the total cotton cultivation area in Southern Xinjiang (Wang, 2010). A test in 2009 of the XLZ37 cotton variety showed that the boll weight and lint percentage were 6.1 g and 45.7%,

respectively (<http://baike.baidu.com/view/8227023.htm>). Generally, cotton was cultivated using the tractor sowing machine (**Figure 4.7**). During the field campaign, the wide space is about 65 cm and the narrow space is 12 cm, while the plant space is 10 cm. This row configuration can be used as a reference for determining the range of the row spacing parameter in the assimilation strategy.



Questionnaire



Interview



Pesticide spraying



Irrigation and fertilization

Figure 4.6 Field campaigns during three major cotton growth stages

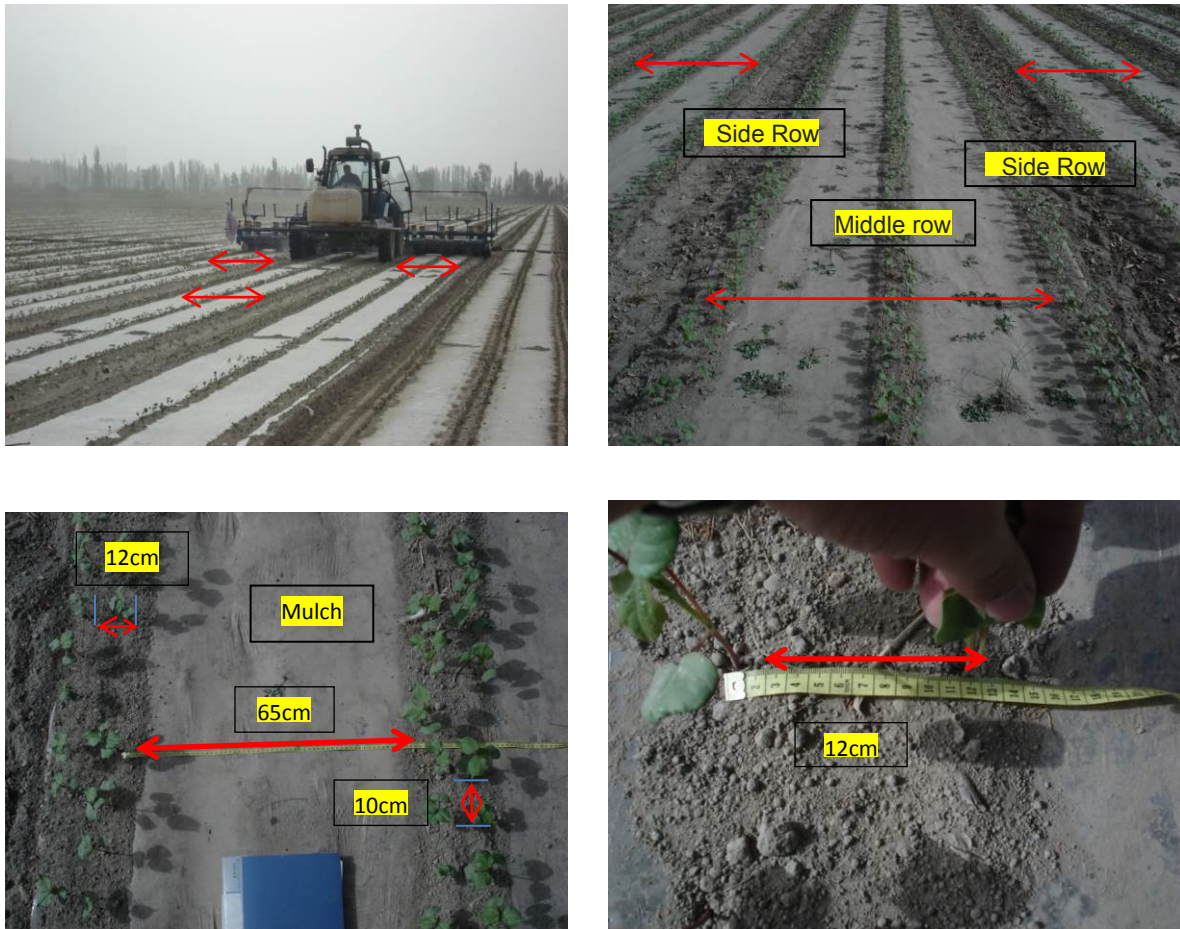


Figure 4.7 Cultivation configuration of cotton using tracker sowing in study area

Additionally, about 15 land cover types including cotton, maize, rice, jujube and pear orchard were obtained using the handheld GPS (Global Positioning System) (**Figure 3.1b**). These data were used for assessing the accuracy of cotton cultivation extraction based on Landsat-8 OLI remote sensing images.

### 4.3 LAI retrieval from Landsat 8 OLI images

To obtain the regional LAI maps within a growth period of crop, the relationship between the observed LAI and corresponding vegetation index derived from remote sensing images was modelled. In these relationships, many kinds of vegetation indices are from the composition of visible, near infrared red and shortwave infrared bands (Kaufman and Remer, 1994; Hansen and Schjoerring, 2003; Stenberg et al., 2004; Yang et al., 2012) were used, such as NDVI and EVI. The relationship between the observed LAI and vegetation indices derived from remote sensing images was limited to the canopy closure and soil reflectance (Peddle et al., 1999). In the study area, the soil background noise in cotton fields with low vegetation closure at the early growth stage affects the accurate extraction of vegetation index. Thus, a



soil line concept was proposed and extracted from remote sensing images ([Baret et al., 1993a](#)). Then, based on this soil line concept, a perpendicular vegetation index (PVI) was proposed to eliminate soil effects ([Richardson and Wiegand, 1977](#)). The formula of the PVI is as follows,

$$PVI = \frac{1}{\sqrt{a^2 + 1}} (\rho_{NIR} - a \times \rho_{RED} - b) \quad (4.6)$$

where  $a$  and  $b$  are slope and intercept of the soil line, respectively and  $\rho_{NIR}$  and  $\rho_{RED}$  are the near infrared and red band, respectively.

Then we selected DOY 136 (May), DOY 200 (July) and DOY 248 (September) in 2014 as three critical dates to obtain the PVI synchronized to LAI measurements. In addition, we also selected DOY 72 (March) before the cotton cultivation event to construct a whole and continuous PVI growth curve of cotton during 2014. Correspondingly, the actual LAI of cotton field is nil for DOY 72. Then a mathematical statistical method was employed to model the relationship between the average observed LAI and PVI values within all observed cotton fields during the entire growth period of cotton.

#### 4.4 Mapping cotton cultivation pattern

Because the phenological events of vegetation are different, available remote sensing images in the leaf-on (full foliation) and leaf-off (defoliation) period ([Loveland et al., 1995](#)) provide near real time observations to track phenological events and indicators of the vegetation canopy on the rational spatial and temporal scale ([Fan et al., 2015](#)). Thus, this information can be used as temporal indicators of remote sensing images to extract vegetation and crop types in many researches ([Rembold and Maselli, 2006](#); [Wardlow et al., 2007](#)) with a higher accuracy than using a single remote sensing image classification ([Peng et al., 2009](#)). This phenology-based remote sensing classification method generally establishes the crop growth curve using vegetation indices derived from time series remote sensing images, and then extracts crop types based on the rulesets from the temporal variations in vegetation indices caused by various phenological events of vegetation types ([Wardlow and Egbert, 2008](#)).

Compared to distinguishing vegetated pixels from non-vegetated pixels, the cotton cultivation extraction from the vegetated area is more worth analysing. Thus, feature bands and combinations associated with their thresholds were proposed to extract the cotton cultivation pattern based on phenological differences between cotton and woodland, orchard and the

other crops. The phenological variations between cotton and woodland shelterbelt, orchard (including apple, pear and jujube) in the study area were used to assist remote sensing images for obtaining the cotton cultivation pattern. At the seedling stage, the individual cotton plant is small, and the cotton population is relatively sparse while the woodland shelterbelt and orchard type have already turned green with significant signals on the remote sensing images. The cotton population shows the opposite characteristics at the blooming stage compared to the seedling stage of cotton (**Figure 4.8**).



Figure 4.8 Temporal variations of vegetated signals between cotton and woodland, orchard

In addition to the massive cotton cultivation, the study area is also sporadically mixed with the rice and the spring-summer maize silage. The spring maize was usually sown in early April and harvested in early July. After the harvest, maize fields were then ploughed by farmers to re-cultivate the summer maize. The duration of summer maize ranges from mid-July to early October. The spring and summer maize both belong to maize silage. As a major crop, cotton was sown in early-mid April and harvested in early-mid October, 2014. Rice was sown during late April-early May and harvested in mid-late October. The sowing, growth and harvest calendars of various crops are listed in this paper (**Figure 4.9**) and the changing trend

of NDVI is mapped (**Figure 4.10a**). Because the NDVI of maize is higher than rice and cotton at DOY 136, the maize pattern can be easily excluded. Since the rice field is generally irrigated during mid-June (DOY 168), the NDVI of rice closely equals nil.

Specifically, land cover types in regions affected by human activities seriously fluctuate due to environmental disasters and anthropogenic activities (Gómez et al., 2016). Therefore, we considered the disruptive effects of hail and sandstorm disasters on cotton growth at the emergence and seedling stage of cotton. After these disasters, farmers usually re-cultivate cotton or cultivate rice instead of cotton to guarantee the minimum harvest loss and reduce soil salinization, pests and diseases within cotton fields. During field campaigns, we obtained several cotton fields attacked by hail disaster in the late May, 2013. Therefore, we selected three Landsat 8 OLI images after May in 2013: DOY 165 (14-June), DOY 181 (30-June) and DOY197 (16-July). Then a NDVI curve was constructed based on these three images and the other images in 2014 (**Figure 4.10b**). Similar to rice type, the NDVI curve of rice cultivation after disasters is also different from the normal growth and re-cultivation of cotton after disasters (**Figure 4.10b**). Although farmers' behaviours caused the delay of cotton growth, the seasonal NDVI dynamics appear the similar trend, which is different from other vegetation types. Although there are some errors caused by the annual variations of cotton growth, the NDVI dynamic trend for re-cultivation of cotton after disasters can still reveal its phenology development. Moreover, the percentage of re-cultivation of cotton after disasters usually occupies less than healthy (or stable) cotton. However, based on these rulesets, the method about extracting cotton cultivation map is more robust and accurate. In conclusion, based on temporal NDVI variations of cotton, the other vegetation types and non-vegetation types, a cotton extraction model with related rulesets and their thresholds was established to extract cotton cultivation patterns.

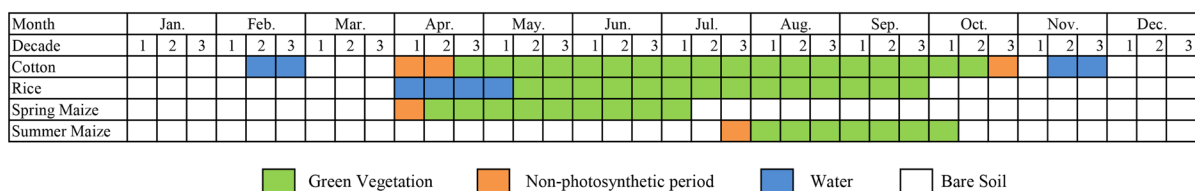


Figure 4.9 Crop cultivation and harvesting calendar in the study area

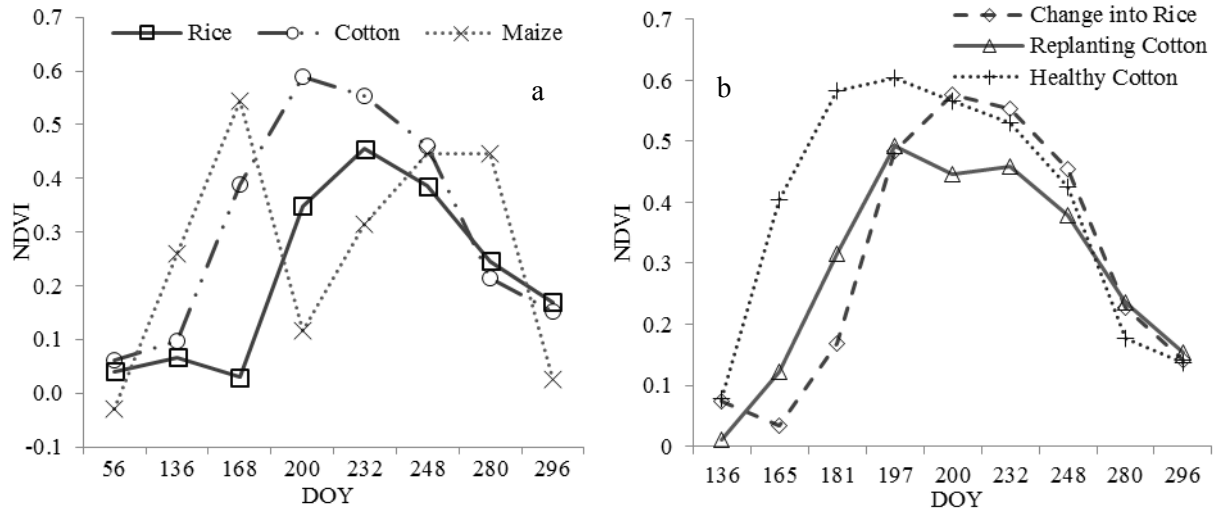


Figure 4.10 (a) Changes in NDVI of three crops, (b) NDVI changes of crops caused by hail disaster

## 4.5 APSIM/OZCOT model

### 4.5.1 Sensitivity analysis

Prior to the application of the APSIM/OZCOT model, the sensitivity analysis of input parameters and initial conditions is a convenient pathway to understand the mechanism and adjust parameters within the model (Zhao et al., 2014). All parameters in the APSIM/OZCOT model are divided into three categories: cultivar, soil and agronomic parameters. Then a total of 36 cultivar parameters, 20 soil parameters and 4 agronomic parameters were selected to test their sensitivities to LAI dynamics (Table 4.2; Table 4.3; Table 4.4). These selected cultivar parameters control the phenological development simulation, leaf development simulation and biomass formation (Hearn and da Roza, 1985; Hearn, 1994). Additionally, selected soil and agronomic parameters can affect dynamics of soil moisture and nitrogen content, thereby affecting the phenological development, leaf development and biomass formation of cotton (Hearn, 1994).

Sensitivity analysis approaches include local and global sensitivity analysis (Saltelli et al., 1999). As a local sensitivity analysis, the “one-at-a-time” (OAT) approach tests the impact of an individual parameter on model results by adjusting an individual parameter and fixing the other parameters (Hamby, 1994; McCarthy, 2010). Although this method is easy to implement, it only reveals the direct influence of parameters on results but ignores the indirect effects of mutual coupling among parameters (He, 2015). Additionally, a global sensitivity analysis can test the effects of changes in multiple parameters on the simulated results and analyse the direct and indirect effects of each parameter on model results (Crosetto et al., 2000). Global sensitivity analysis approaches based on the variance, such as the Extended

Fourier Amplitude Sensitivity Test (EFAST) method, have been widely applied in crop growth models ([Jiang et al., 2011](#); [Zhao et al., 2014](#); [He, 2015](#)). The EFAST method was proposed based on the advantage of the Sobol' approach ([Saltelli and Sobol', 1995](#)) and the Fourier Amplitude Sensitivity Test (FAST) method ([Saltelli et al., 1999](#)). The EFAST method is based on variance analysis, and variances of simulated results can reflect the sensitivity of input parameters ([Saltelli et al., 1999](#)). The variance of model results is decided by individual input parameters and their interactions ([Saltelli et al., 1999](#)). The independent sensitivity of a single input parameter is measured by a first-order sensitivity while the overall sensitivity of parameters (independence and interaction) is measured by a global sensitivity ([Crosetto and Tarantola, 2001](#)). Therefore, the decomposition of the variance can obtain contribution to the variance of various parameters and coupling between the parameters, that is, the sensitivity index of various parameters ([Crosetto and Tarantola, 2001](#); [Zhao et al., 2014](#)).

Based on ranges of these cultivar and agronomic parameters, we selected several values between maximal and minimal values to test the sensitivity of each parameter to LAI dynamics. We considered the observed in-situ values of the soil parameters as a baseline, including a plus and minus 5%, to generate the range of observed values. Meanwhile, the OAT approach and EFAST approach were both employed to analyse the sensitivity of these parameters to the LAI.



Table 4.2 Description of parameters in OZCOT model (Hearn, 1994; McCarthy, 2010)

Code	Parameter	Unit	Range	Description	
1	RATE_EMERGENCE	mm/DD	0.0-1.0	Growth rate (mm per day) from sowing to emergence	
2	ACOTYL	mm <sup>2</sup>	0.0-1000.0	Leaf area of cotyledons	
3	RLAI	mm <sup>2</sup> /mm <sup>2</sup>	0.0-1.0	Base rate of leaf growth pre first square	
4	DLDS_MAX	mm <sup>2</sup> /site	0.0-5.0	Maximum leaf area increase per site	
5	FLAI	mm <sup>2</sup> /site	0.0-1.0	Varietal adjustment for rate of LAI gain per fruiting site	
6	DDISQ	DD	>400	Thermal time between emergence and the appearance of the first square	
7	SQCON	squares/plant/DD	0.001-0.030	Squaring constant for generating sites per DD	
8	TIPOUT	days	>52	Day degrees delay caused by tipping out damage	
9	FCUTOUT	nil	0.0-1.0	Constant used to determine when site production stops due to boll load	
10	FBURR	nil	0.0-5.0	Proportional boll weight with Burr Fraction included	
11	POPCON	nil	0.0-1.0	Plant population constant for adjustment of daily site production	
12	RESPCON	nil	0.001-0.030	Respiration constant	
13	FRUDD1		40-60		
14	FRUDD2		124-216		
15	FRUDD3		230-420		
16	FRUDD4	DD	252-456	Array of values of cumulative Day Degrees for each growth phase of fruit development (8 categories)	
17	FRUDD5		365-624		
18	FRUDD6		479-792		
19	FRUDD7		649-1051		
20	FRUDD8		824-1338		
21	BLTME1				0.000-0.000
22	BLTME2				0.000-0.000
23	BLTME3				0.000-0.000
24	BLTME4	nil	0.056-0.084	Thermal time for fruit categories as a proportion of the total required to develop a complete boll (categories 4-8)	
25	BLTME5		0.168-0.252		
26	BLTME6		0.264-0.396		
27	BLTME7		0.440-0.660		
28	BLTME8		0.800-1.000		
29	WT1				0.00832-0.01248
30	WT2				0.02176-0.03264
31	WT3				0.11528-0.17292
32	WT4	nil	0.07904-0.11856	Relative weight of each category relative to a mature (inedible) green boll (cat 7)	
33	WT5		0.40336-0.60504		
34	WT6		0.76936-1.15404		
35	WT7		0.80000-1.00000		
36	WT8		0.46280-0.69420		

Table 4.3 Soil properties used in the APSIM/OZCOT model (provided by University of Hohenheim)

Code	Parameter	Description	Observation	Min (-5%)	Max (5%)
37	SAT1	Saturated water content at soil layer 1	0.426	0.4047	0.4473
38	SAT2	Saturated water content at soil layer 2	0.463	0.43985	0.48615
39	SAT3	Saturated water content at soil layer 3	0.471	0.44745	0.49455
40	SAT4	Saturated water content at soil layer 4	0.441	0.41895	0.46305
41	DUL1	Drained upper limit of soil water content at soil layer 1	0.246	0.2337	0.2583
42	DUL2	Drained upper limit of soil water content at soil layer 2	0.159	0.15105	0.16695
43	DUL3	Drained upper limit of soil water content at soil layer 3	0.22	0.209	0.231
44	DUL4	Drained upper limit of soil water content at soil layer 4	0.241	0.22895	0.25305
45	LL151	15Bar lower limit of soil water content at soil layer 1	0.062	0.0589	0.0651
46	LL152	15Bar lower limit of soil water content at soil layer 2	0.048	0.0456	0.0504
47	LL153	15Bar lower limit of soil water content at soil layer 3	0.055	0.05225	0.05775
48	LL154	15Bar lower limit of soil water content at soil layer 4	0.061	0.05795	0.06405
49	airdry1	Volumetric water content for air dry soil at soil layer 1	0.062	0.0589	0.0651
50	airdry2	Volumetric water content for air dry soil at soil layer 2	0.016	0.0152	0.0168
51	airdry3	Volumetric water content for air dry soil at soil layer 3	0.018	0.0171	0.0189
52	airdry4	Volumetric water content for air dry soil at soil layer 4	0.02	0.019	0.021
53	bd1	Bulk density at soil layer 1	1.52	1.444	1.596
54	bd2	Bulk density at soil layer 2	1.42	1.349	1.491
55	bd3	Bulk density at soil layer 3	1.4	1.33	1.47
56	bd4	Bulk density at soil layer 4	1.48	1.406	1.554

Table 4.4 Agronomic parameters used in the APSIM/OZCOT model

Code	Parameter	Description	Min	Max
57	Irrigate_amount	The amount of irrigation application (unit: mm)	50	300
58	Fert_amount	The amount of fertilization application (unit: kg/ha)	50	300
59	Row_spacing	The spacing between cotton rows (unit: mm)	300	600
60	Sowing density	Sowing density per row (unit: plant/m <sup>2</sup> in row)	20	50

### 4.5.2 Local calibration

Variations of cotton varieties in different regions are mainly subject to the local climate, soil, water and other environmental factors. Although physiology-based cotton growth models can simulate the growth and development processes of cotton, detailed parameters between various cotton cultivars are also specific. Especially, the temperature and accumulated temperature controlling a rational phenology of cotton vary among different cultivars. Because the APSIM/OZCOT model was developed based on cotton varieties and growth environment in Australia, cultivar parameters are first calibrated based on local crop varieties and climate prior to the application in different regions to minimize cultivar-related uncertainties (Zhao et al., 2014). These cultivar parameters used to calibrate are generally sensitive to the LAI and yield while non-sensitive parameters can be briefly treated (Cavero et

al., 1998). The calibration procedure for cotton mainly includes the calibration of cotton phenology and the growth process (such as yield and LAI). During the cotton growth period, the most influentially phenological parameters were calibrated first and then the yield and LAI parameters were calibrated for the APSIM model (Zhao et al., 2014). A logical phenology of cotton simulation is therefore a pre-step for LAI simulation.

We proposed that cultivar parameters about phenological development within all cotton varieties in the study area are similar while the differences between them are only parameters controlling the yield formation, insect and disease resistance. Because these cotton varieties are all affected by the similar climatic condition, all cotton varieties belong to mid-late maturing varieties. In addition, most crop cultivar parameters are genetic and decided by crop varieties (Ma et al., 2013). Thus, parameters controlling the phenological development of cotton are basically consistent in the study area during 2006–2014.

In order to obtain local cultivar parameters, we designed a test at the Aksu Station based on the observed soil, climate and agronomic data (such as the application date and amount of irrigation/fertilization, plant density, sowing date and row spacing) during two successive cotton seasons (2006–2007) at the Aksu station (Zhao and Hu, 2010). These data provide the detailed input data and initial conditions of the APSIM/OZCOT model, greatly reducing uncertainties in these data within the model. Meanwhile, we selected three sensitive parameters (FLAI, FRUDD8 and DDISQ) to calibrate local cultivars based on the sensitivity analysis of cultivar parameters. These parameters mainly focused on the LAI growth and phenological development of cotton. Since the phenology is controlled by GDD, a series of temperature parameters such as DDISQ and FRUDD were selected to adjust the phenology and yield formation of cotton. Additionally, the leaf area growth during the reproductive growth is controlled by the FLAI parameter. Similar to numerous researches (Ma et al., 2008; Guérif and Duke, 2000), a trial and error method and an optimization method were both employed to determine the selected parameters within crop models by minimizing the differences between the simulated values and the in-situ measurements. Additionally, the relevant article regarding the calibration of parameters at the Aksu Station (Yang et al., 2014) was used as a reference to obtain parameters for local cultivars. Meanwhile, the lint percentage and seed cotton weight per boll of a cotton variety were both obtained.

The flowchart illustrates the procedure for executing and calibrating the APSIM/OZCOT model using meteorological, soil and agronomic data (Figure 4.11). First, the APSIM/OZCOT model was primarily modelled, driven by the meteorological data by

plugging in OZCOT, soil nitrogen and water, and other sub-modules as well as a series of agronomic practices. Then the simulated LAI and yield was validated against in-situ observed data by adjusting three selected parameters. After that, the best values for three selected parameters between 2006 and 2007 were obtained by minimizing the gap between the simulated and observed LAI and yield after a loop process. Finally, a trial and error method was employed to determine a hybrid cotton variety based on three optimized parameters between 2006 and 2007. Meanwhile, the validation to simulated LAI and yield based on the hybrid cotton variety was also assessed using three indicators. The relevant formulas (Jachner et al., 2007) are as follows:

$$RMSE = \sqrt{\frac{\sum_{i=1}^n (LAI_{obs} - LAI_{sim})^2}{n}} \quad MAE = \frac{\sum_{i=1}^n |LAI_{obs} - LAI_{sim}|}{n}$$

$$R = \frac{\sum_{i=1}^n (LAI_{sim} - \bar{LAI}_{sim})(LAI_{obs} - \bar{LAI}_{obs})}{\sqrt{\sum_{i=1}^n (LAI_{sim} - \bar{LAI}_{sim})^2} \sqrt{\sum_{i=1}^n (LAI_{obs} - \bar{LAI}_{obs})^2}} \quad (4.7)$$

where  $RMSE$  is root-mean-square error;  $MAE$  is mean absolute error;  $R$  is the Pearson's correlation;  $LAI_{obs}$  and  $LAI_{sim}$  are the observed and simulated LAI, respectively;  $\bar{LAI}_{obs}$  and  $\bar{LAI}_{sim}$  are average observed and simulated LAI;  $n$  is number of external samples (remote sensing or field observations); and  $i$  is the number index.

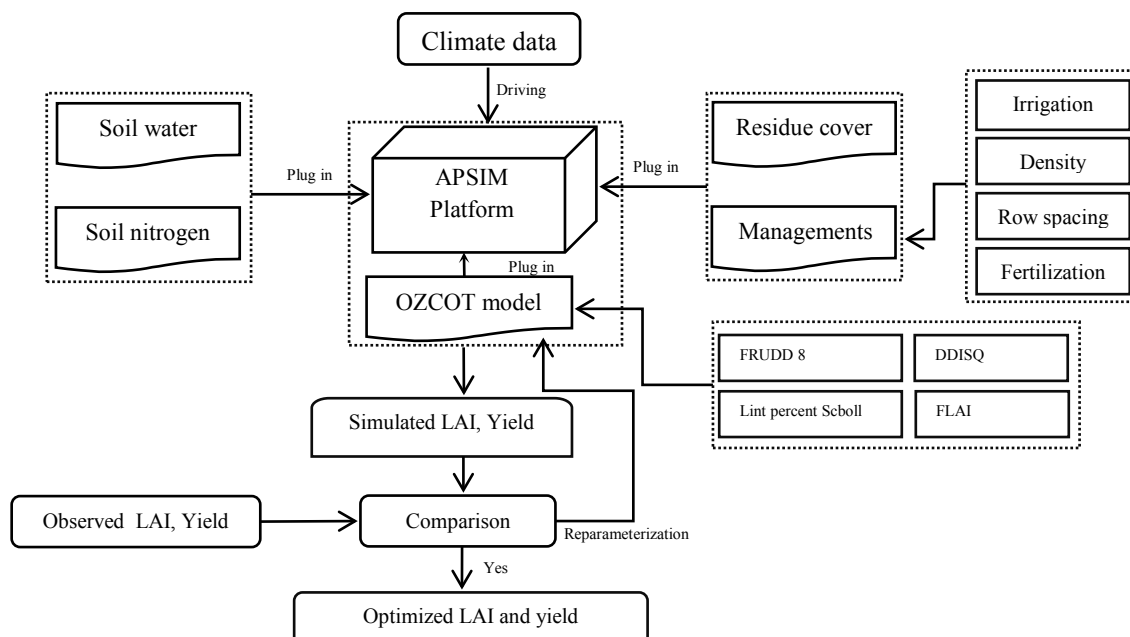


Figure 4.11 Schematic diagram of the calibration process of the APSIM/OZCOT cotton model

### 4.5.3 Assimilation strategies

Based on the proposed framework in the second chapter, we emphasize on the detailed assimilation strategies (**Figure 2.1**). In addition to the APSIM/OZCOT model and remote sensing, an optimization platform with appropriate algorithms is critical to link these two parts. Meanwhile, an objective function is used to reflect the difference between the LAI derived from remote sensing, and crop model simulation. In this paper, the objective function of coupling remote sensing with the crop model is the root mean squared error (RMSE) between the simulated and observed LAI.

#### *Optimization algorithms*

Based on a summary of the literature regarding assimilation strategies between crop models and remote sensing, we also analysed and reclassified a series of assimilation algorithms, evaluating the computational speed, efficiency, accuracy and stability (Ines et al., 2013). This paper selected a Particle Swarm Optimization (PSO) approach and a general-purpose optimization based on the Nelder-Mead algorithm (Nelder and Mead, 1965) as assimilation algorithms because they are easy to implement with high computational efficiency and optimal performance. The general-purpose optimization based on the Nelder-Mead algorithm is included as an option for box-constrained optimization and simulated annealing (Nash, 1990).

The PSO algorithm was proposed in 1995 (Eberhart and Kennedy, 1995), which was derived from the predatory behaviour of birds. The most easy and effective predatory approach for birds is searching in regions where the nearest bird is near the food source (Kennedy et al., 2001). A bird flock is considered a swarm and each individual in the swarm is considered a particle without quality and volume. If we assume that the swarm consisting of  $m$  particles flies in a  $D$ -dimensional space with a certain velocity, each particle searches the historically best position and the best position of other particles in the swarm by updating the direction of movement and magnitude of velocity for each particle after iterations (Kennedy, 1997). Then their expressions are as follows (Eberhart and Shi, 2001; Wang et al., 2014),

- ① the position of particle  $i$  is expressed as follows:  $x_i = (x_{i1}, x_{i2}, \dots, x_{id})$ ,  $1 \leq i \leq m$ ,  $1 \leq d \leq D$
- ② the velocity of particle  $i$  is expressed as  $v_i = (v_{i1}, v_{i2}, \dots, v_{id})$
- ③ the historically best position of particle  $i$  is expressed as  $p_i = (p_{i1}, p_{i2}, \dots, p_{id})$
- ④ the historically best position of all particles within a swarm is expressed

as  $p_g = (p_{g1}, p_{g2}, \dots, p_{gd})$ .

During each iteration, the position and velocity of a particle is generally updated based on individually and globally best positions. Their formulas ([Eberhart and Shi, 2001](#)) are as follows,

$$v_{id}^{k+1} = w \times v_{id}^k + c_1 \varepsilon (p_{id}^k - x_{id}^k) + c_2 \eta (p_{gd}^k - x_{id}^k) \quad (4.8)$$

$$x_{id}^{k+1} = x_{id}^k + v_{id}^{k+1} \quad (4.9)$$

where  $k$  is the iteration;  $w$  is the inertia weight;  $c_1$  and  $c_2$  are acceleration constants;  $\varepsilon$  and  $\eta$  are uniformly distributed random numbers in the range  $[0, 1]$ . In order to prevent the particles from drifting away from the searching space, the velocity of particle is limited to a maximum velocity range  $[-Vmax, Vmax]$ . In this research, both  $c_1$  and  $c_2$  generally take on a value of 2 ([Eberhart and Shi, 2001](#)) and the iteration ( $w$ ) is 0.4 ([Eberhart and Shi, 2001](#)). The number of dimensions in the study is the number of agronomic parameters in the APSIM/OZCOT model.

Specific processes of the PSO algorithm are as follows ([Kennedy, 1997](#); [Eberhart and Shi, 2001](#)) (**Figure 4.12**):

Step 1: Setting up the threshold range for each parameter and randomly initializing the position and velocity of each particle within a swarm.

Step 2: Evaluating the optimization fitness function (i.e., the cost function) of each particle in the APSIM/OZCOT model

Step 3: For each particle, the cost function value (or position) of this iteration was used to compare with its best position (***pbest***) for all iterations. If the current value is better than ***pbest***, its position is considered to be the current optimal position. Otherwise, its optimal position is not changed.

Step 4: The optimal position of each particle in this iteration (***pbest***) is used to compare with the best position of the whole swarm (***gbest***) in previous iterations. If the value of a certain particle is better, its value is then considered to be the current global best position (***gbest***). Otherwise, the optimal position of the swarm is not changed.

Step 5: Setting parameters of the velocity and position formula ([Eberhart and Shi, 2001](#)), and changing the velocity and position of each particle, respectively.

Step 6: If there is no cost function value or iteration that reaches a preset maximum number, the program returns to Step 2 and continues the iterative optimization until the termination condition is satisfied.

#### *Computational efficiency of PSO*

Prior to application of the PSO assimilation method, we tested the computational efficiency of the PSO assimilation method. There are two factors influencing the PSO efficiency, namely particles and iterations. In order to acquire the best results with a fast computational speed, a series of particles and iterations were selected to test their responses to PSO capacity based on the RMSE between the simulated and retrieved LAI from Landsat-8 OLI images (**Figure 4.13**). According to the performance of particles, the RMSE decreased dramatically from 10 to 15 particles while the change of RMSE was not significant. Therefore, the optimal number of particles was 15. Similarly, the performance of iterations showed that the optimal number of iterations was 60. Thus, the particles and iterations used in the assimilation at the field level were set as 15 and 60, respectively.

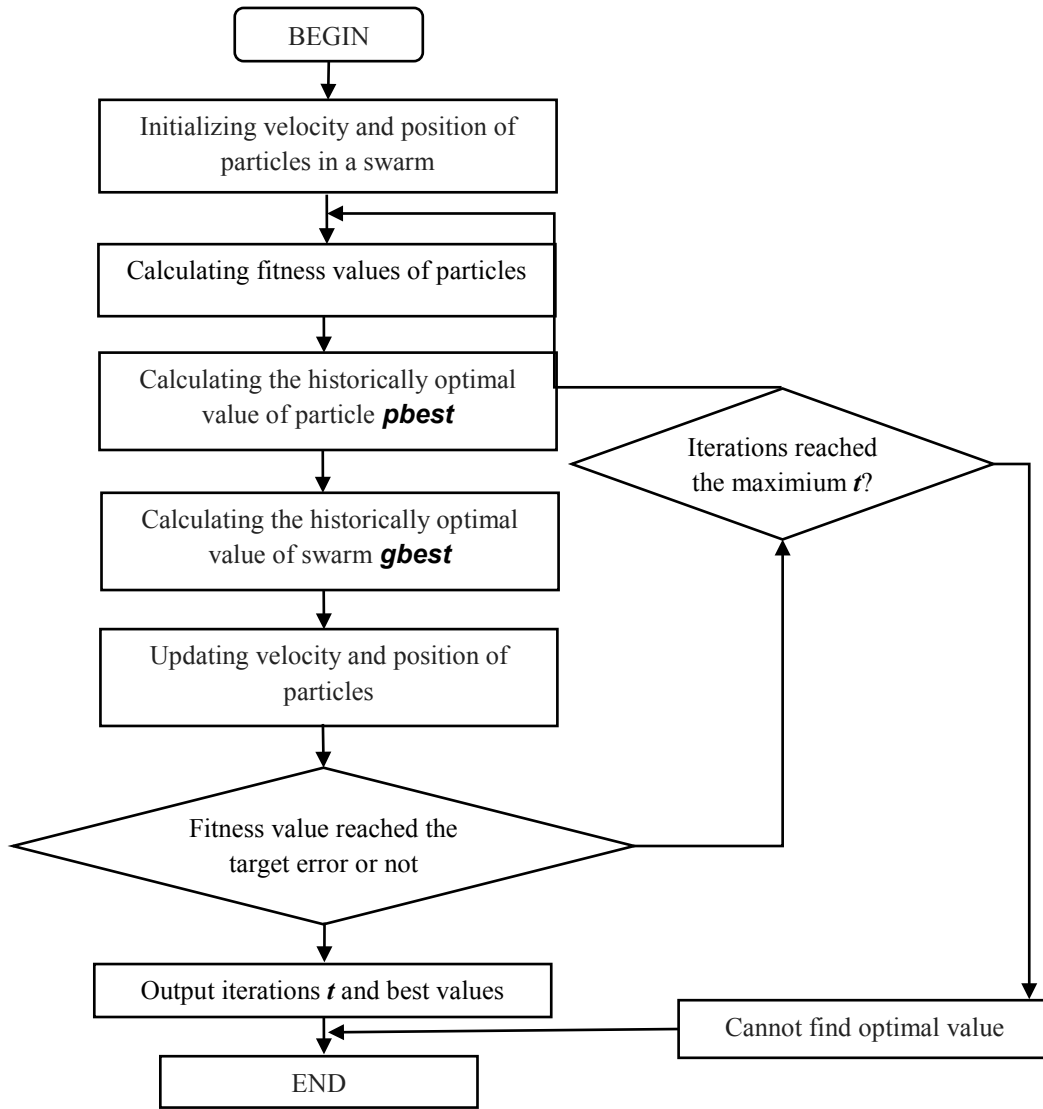


Figure 4.12 The flowchart of PSO algorithm (Kennedy, 1997)

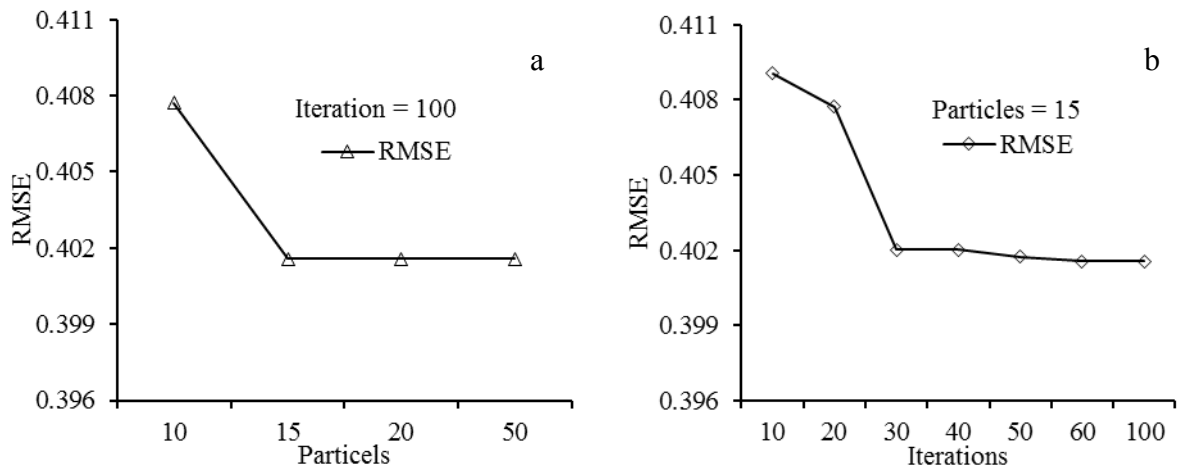


Figure 4.13 (a) The response of particles; (b) iterations to PSO capacity



# 5 Results and Discussion

## 5.1 Cotton cultivation pattern

According to the proposed cotton extraction model, the cotton cultivation pattern in 2014 was obtained based on Landsat-8 remote sensing images coupled with thresholds (Figure 5.1). The cotton extraction model includes three steps. First, the NDVI derived from DOY 168 was used to exclude non-vegetated areas (water, rice field with water, artificial land and bare land). The NDVI map at DOY 200 was used to extract arable land and woodland with high vegetation coverage. Then, the NDVI map at DOY 136 was used to extract lower coverage of vegetation and exclude the woodland. Finally, the cotton cultivation pattern was extracted (Figure 5.2) based on the rule that “If  $(NDVI_{168} > 0.09)$  and  $(NDVI_{136} < 0.1)$  and  $(NDVI_{200} > 0.3)$  then we have a cotton cultivation area”.

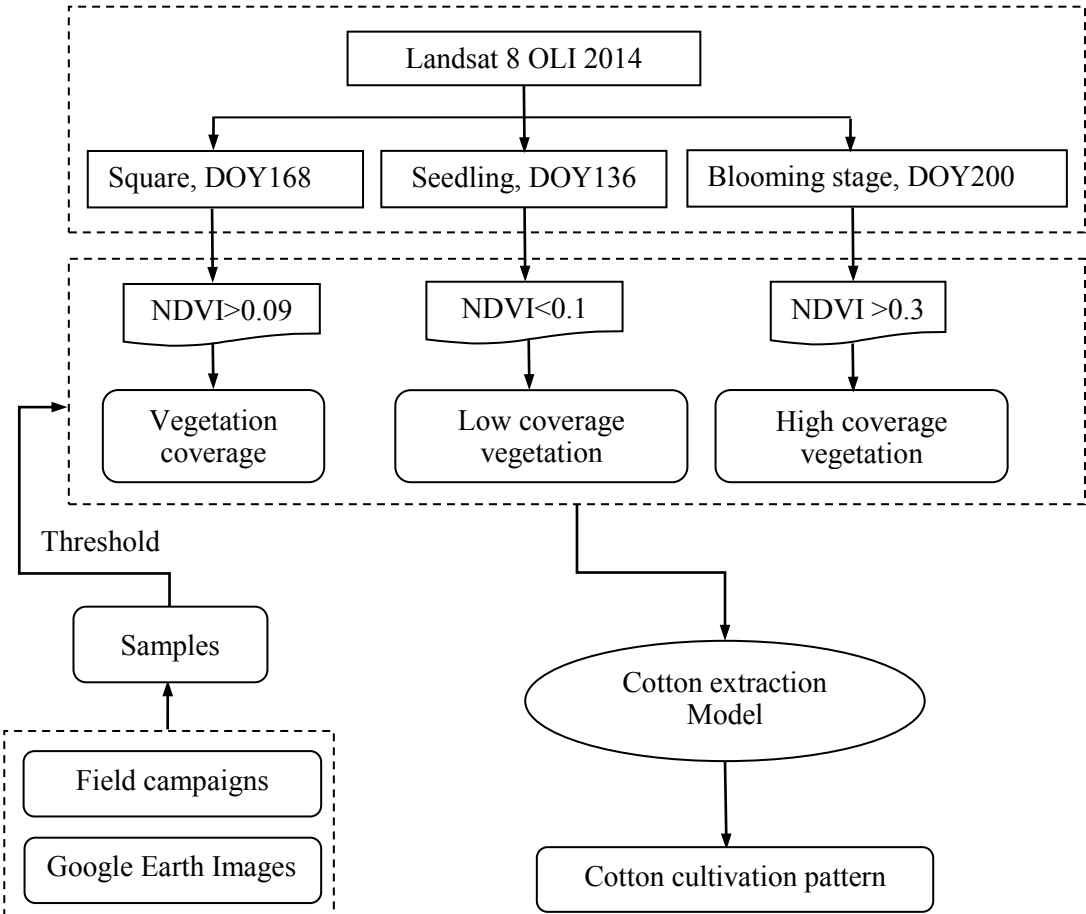


Figure 5.1 Flowchart of cotton cultivation extraction process

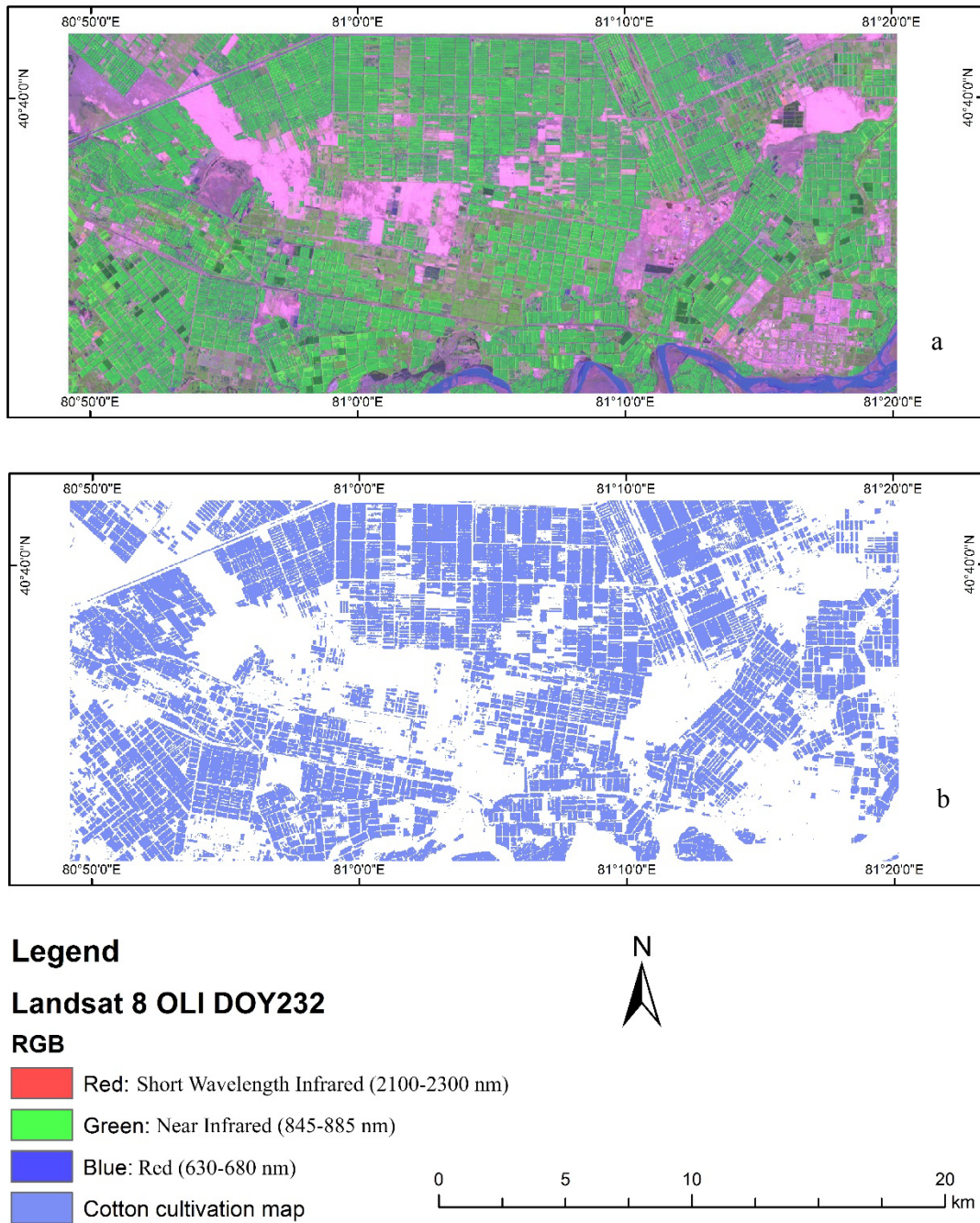


Figure 5.2 (a) Landsat 8 OLI images at DOY 232; (b) cotton cultivation pattern in 2014

Regarding the accuracy of cotton cultivation classification, we mainly focused on the accuracy of small-size cotton fields. A long and narrow cotton field along a road in the northwestern study area was specifically used to test the accuracy of this classification algorithm. We used high spatial resolution images from Google Earth to ensure whether the region was a road or cotton field (**Figure 5.3**). The result showed that the long and narrow cotton field was accurately extracted and the classification algorithm based on phenology was creditable. Simultaneously, a total of 47 cotton fields for in situ LAI and yield observations and 15 other land cover samples (non-cotton farmlands) during field campaigns were also

introduced to test the accuracy of the classification. Additionally, 40 cotton field samples and 43 non-cotton field samples were also collected from the Google Earth, which are evenly distributed in the study area. The ratio of the correct sample to the total sample is considered an indicator for evaluating the accuracy of cotton cultivation extraction. The results show that the classification accuracy of the cotton cultivation pattern is 89.7% (Table 5.1). Therefore, this classification algorithm was determined as a highly accurate method through the acquisition of the cotton distribution.

Table 5.1 Accuracy assessment of cotton cultivation mapping

Sample numbers	Incorrect samples	Correct samples	Accuracy (%)
145	15	130	89.7

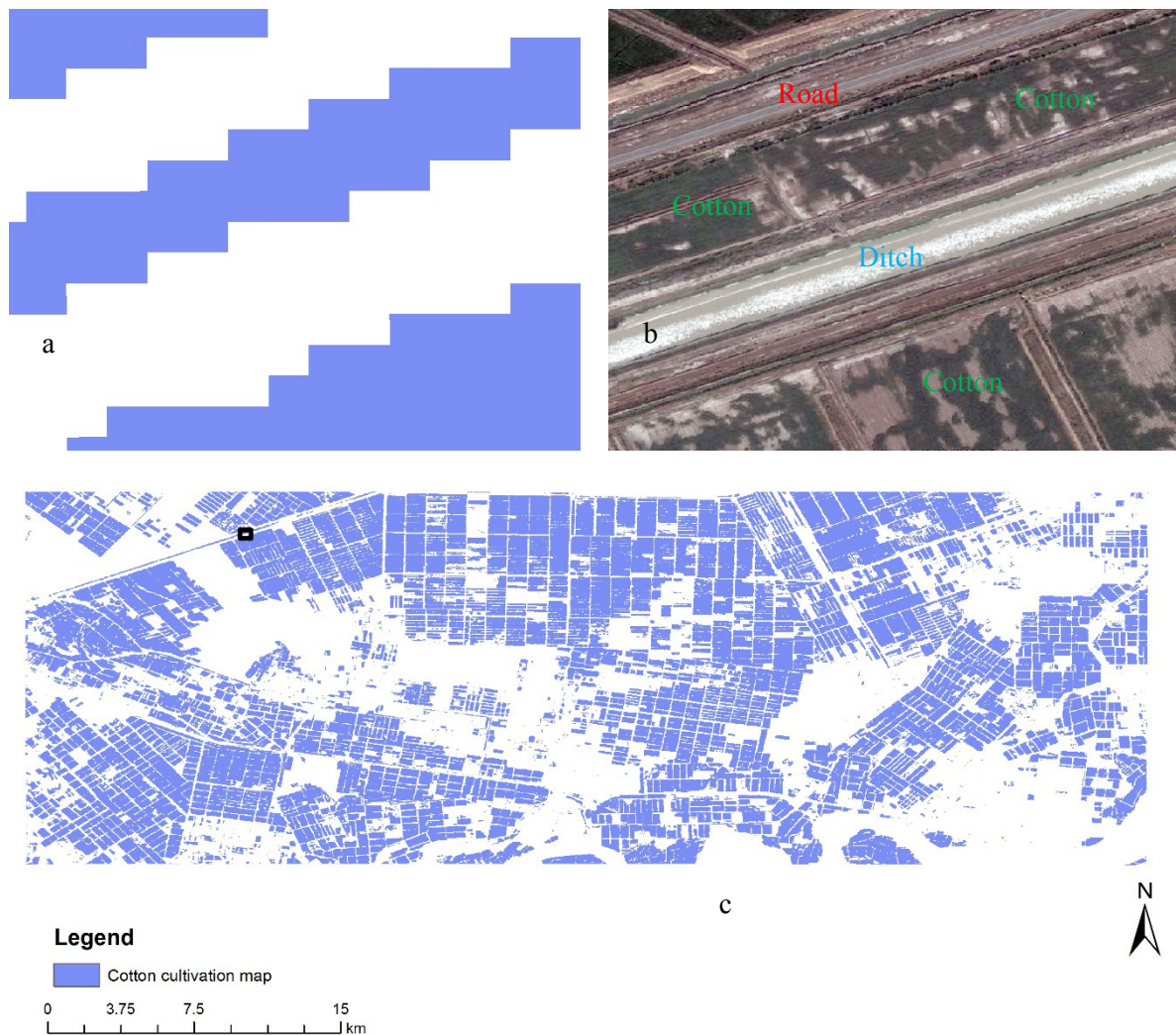
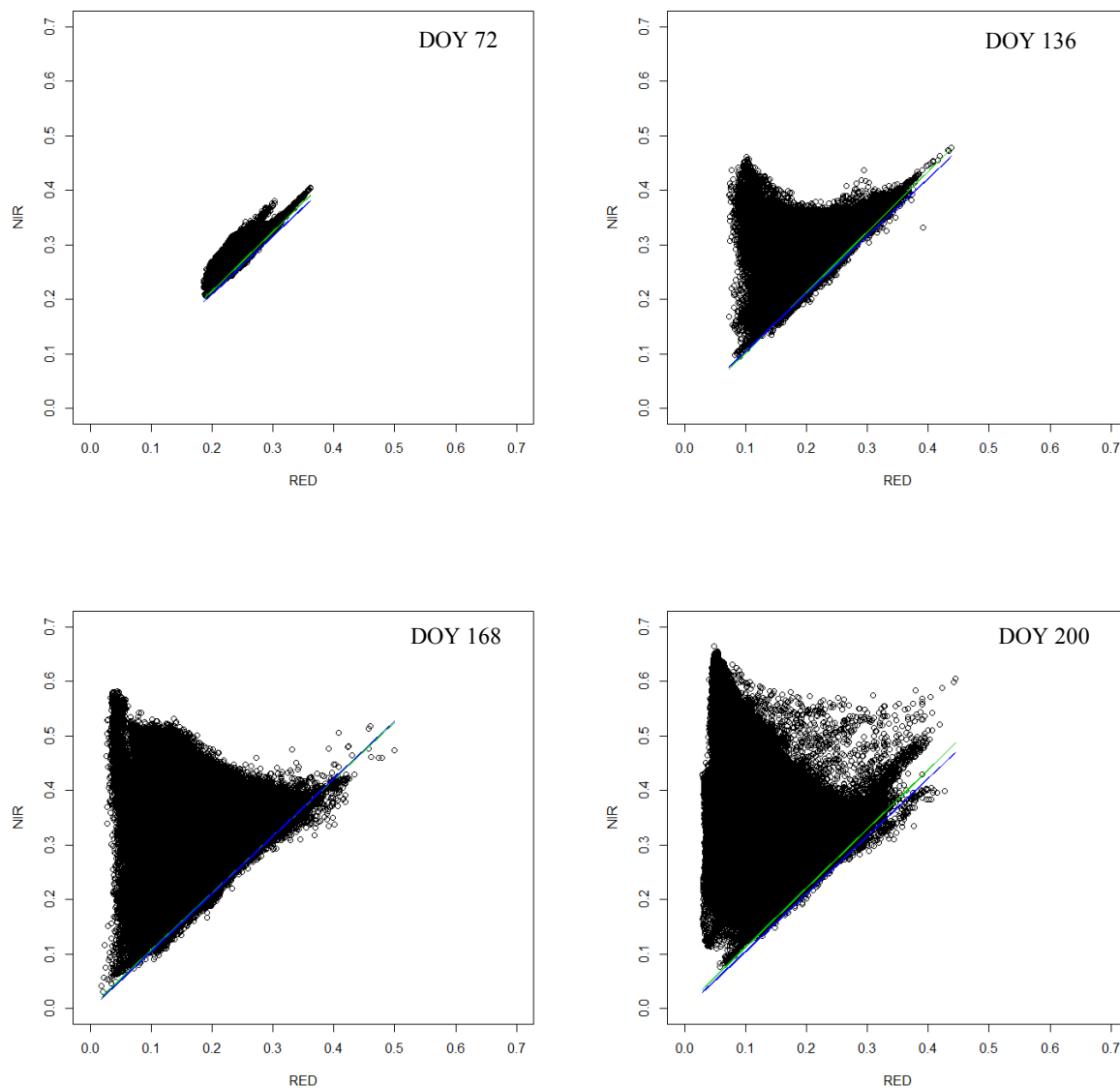


Figure 5.3 (a) Cotton extraction of linear fields; (b) Google Earth image; (c) the location of linear field

## 5.2 LAI maps derived from Landsat-8 OLI images

The soil line determination from Landsat-8 OLI remote sensing images is the first step to extract PVI images. A two-dimensional space is then constituted by the red and near-infrared channels to acquire a soil line (**Figure 5.4**). In order to minimize the effects of water on the soil line, an NDWI (Normalized Difference Water Index) index was used to mask the water body information. Then, an algorithm proposed by Baret ([Maas and Rajan, 2010](#)) was performed to extract the soil line from Landsat-8 OLI remote sensing images. Thereby, the slope and intercept of the soil line were both obtained.



*Continued*

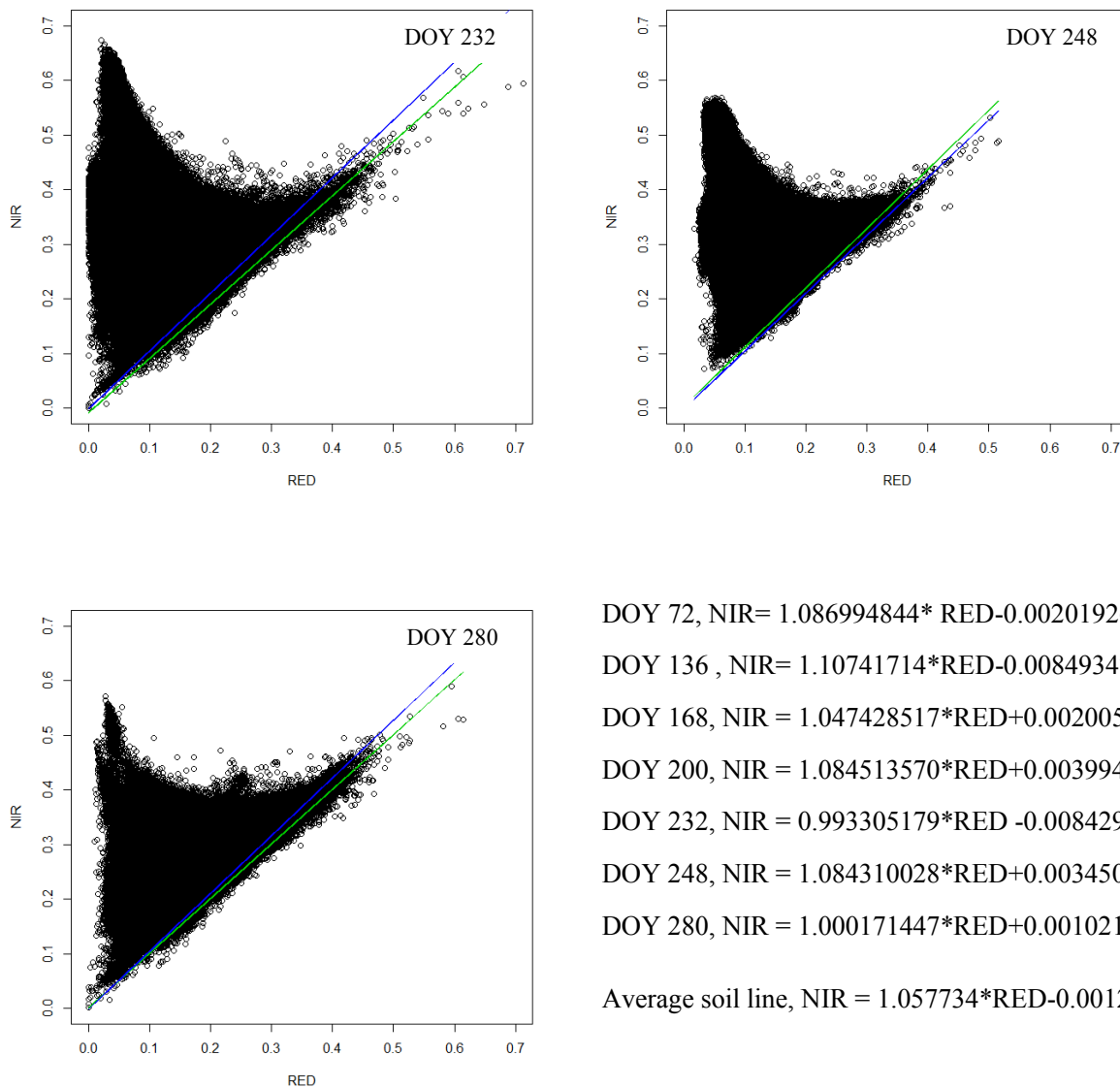


Figure 5.4 Soil lines from Landsat 8 OLI images of 2014 (the green line is the individual soil line corresponding to each image, and the blue line is the average soil line)

The soil line is not a strictly straight line but a stripe with a suitable width. Therefore, the slopes of soil lines are different. In addition, the main factors ([Baret et al., 1993b](#)) affecting the bare soil line are: (1) external factors unrelated to the observed surface (sensor parameters, observation and illumination direction and atmospheric conditions); (2) soil surface conditions (e.g., orientation, roughness, shadow, crust and straw residues); (3) the inherent physical and chemical form impacting the spectral characteristics of soil (e.g., mineral composition, organic matter, moisture, particle size, soil structure). The soil water and the roughness on soil line have weaker impact ([Baret et al., 1993b](#)). Additionally, errors from the atmospheric correction can also lead to differences in slopes of soil lines.



For the same region, although parameters of the soil line fluctuate over time and are influenced by many factors, these changes are totally stable. Thus, we selected seven epoch Landsat-8 OLI images for soil line extraction based on the method mentioned above. The slope and intercept of the soil line were both analysed. Slopes of the seven soil lines ranged from 0.993305 to 1.107417 while the intercepts of the seven soil lines ranged from  $-0.00849$  to 0.003994 (**Table 5.1**). Stoner and Baumgardner (1981) published the results of soil lines with slopes ranging from 1.06 to 1.60 and intercepts ranging from  $-0.01$  to 0.07. Thus, the slope and intercept parameters of these seven soil lines coincide with the results from Stoner and Baumgardner (1981), as the maximal slope of the seven soil lines is 1.107 and the minimal slope is 0.993305, with a mean and average deviation of slope of 1.06 and 0.038, respectively. The average deviation of slope is less than 0.1 indicating that the soil line changes over time but is relatively stable in the study area (Qin et al., 2012). This stability also explains the validity and reliability of this method in extracting the soil line. Additionally, the best soil line corresponding to remote sensing images was determined by comparing the position of the individual and average soil line in the NIR-RED plotting space (**Figure 5.4**). In addition to DOY 232 and 280, the other images used average soil line (**Table 5.2**). Finally, a series of Landsat-8 OLI remote sensing images from 2014 were all used to obtain PVI maps based on corresponding soil lines.

Table 5.2 Comparison of individual soil line and average soil line

DOY	Slope	Intercept	The best soil line
72	1.086995	-0.00202	Average soil line
136	1.107417	-0.00849	Average soil line
168	1.047429	0.002006	Average soil line
200	1.084514	0.003994	Average soil line
232	0.993305	-0.00843	
248	1.08431	0.00345	Average soil line
280	1.000171	0.001022	
Average	1.057734	-0.00121	

A linear relationship between the observed LAI and PVI was obtained with a  $R^2$  of 0.8777 (**Figure 5.5**). The relationship shows that there is data gap within the PVI range between 0.1 and 0.2 due to lack of observed LAI in June. The designed field campaign planning aims to collect the LAI at early (May), middle (July) and late growth stage (September) of cotton. However, cotton grows rapidly and LAI expands exponentially in June. Additionally, the soil disturbance within cotton fields at the early growth stage, personal errors and systematic errors from the LAI-2000 equipment also affect the accurate LAI measurement. After

supplementing these observed LAI data, the relationship between observed LAI and PVI probably appears nonlinear since the relationship between biophysical, chemical parameters of vegetation and the spectral reflectance has been proven nonlinear (Kokaly and Clark, 1999). LAI maps within 2014 were then mapped according to this regression model between the observed LAI and PVI derived from Landsat-8 OLI remote sensing images (**Figure 5.6**).

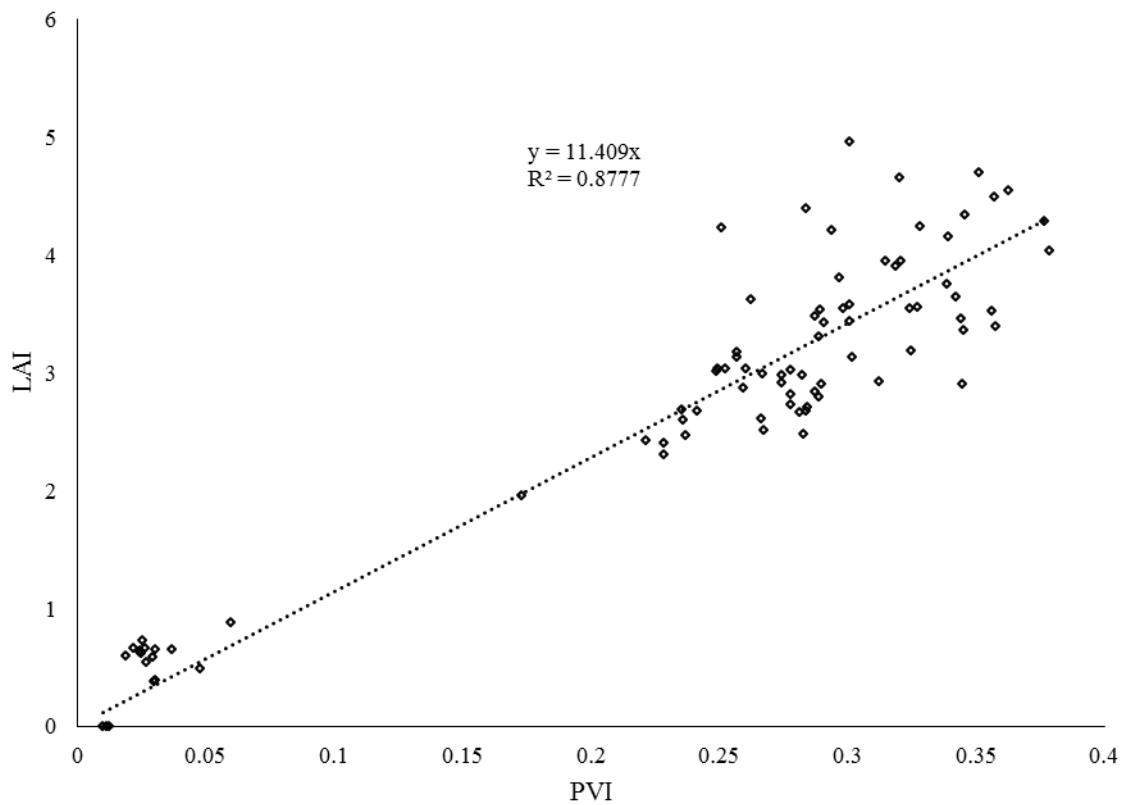


Figure 5.5 The relationship between observed LAI and PVI derived from Landsat 8 OLI images

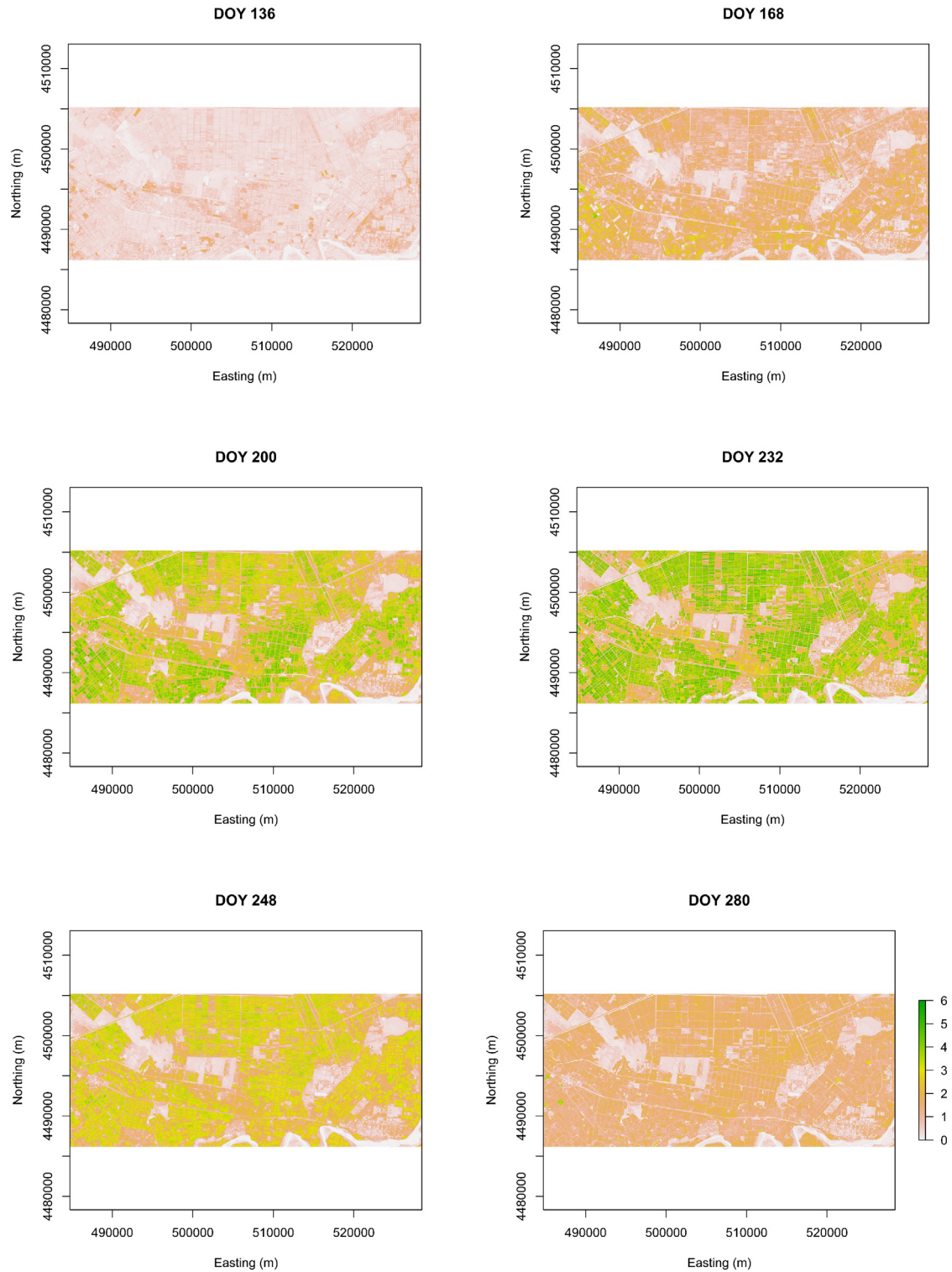


Figure 5.6 LAI maps derived from Landsat 8 OLI remotely sensed images within 2014

Due to personal and systematic errors, lack of LAI observations in June as well as non-fully synchronized time (day-to-day) between remote sensing observations and field observations,



the observed LAI resulted in a bias of the remote sensing derived LAI. Then we analysed the bias between remote sensing derived and observed LAI. The observed LAI from these six cotton fields (namely A09, A10, A21, A23, A24 and G20) was weakly affected by soil disturbances and personal errors during the field campaign in May. Therefore, these six cotton fields were selected to reveal the bias of remote sensing derived LAI. The in situ observed LAI in these six cotton fields may be higher or lower than LAI derived from remote sensing images. Then the RMSE between remote sensing derived LAI and observed LAI for these six cotton fields during three field campaigns was obtained. Afterwards, the error bars (remote sensing derived LAI  $\pm \frac{1}{2}$  RMSE) at DOY 136, 200 and 248 (three field campaigns) were obtained to reveal the accuracy of remote sensing derived LAI. Additionally, we also used the optimized LAI curves from the APSIM/OZCOT model to check the reliability of the LAI from the equation between the remote sensing derived PVI and observed LAI (**Figure 5.7**). The result showed that the LAI curves after the optimization for the six fields were close to the error range at DOY 136, 200 and 248 though these curves did not fully pass through these error ranges. Thus, the remote sensing derived LAI can be considered an accurately external observation for the APSIM/OZCOT model simulation though they have some biases.

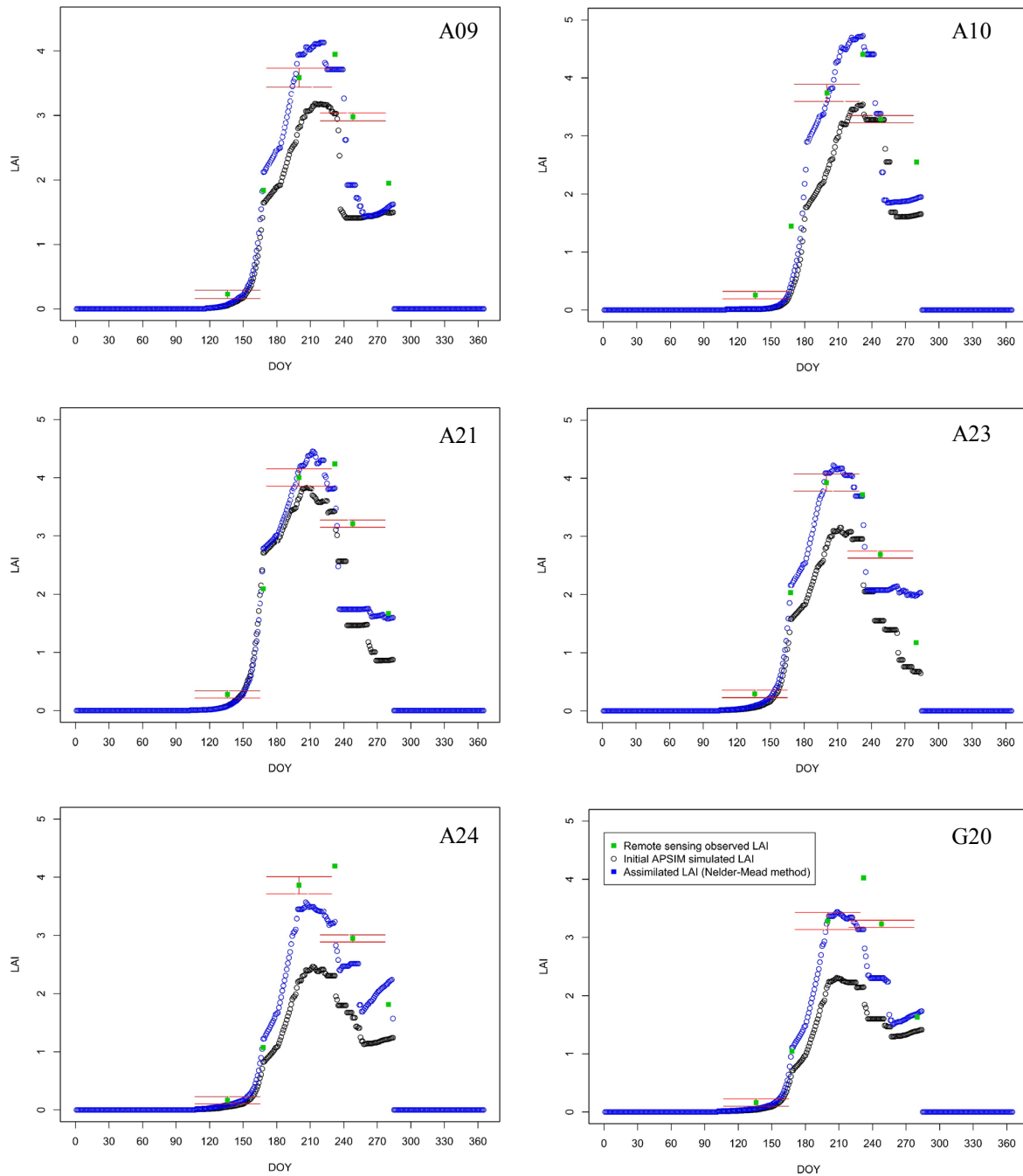


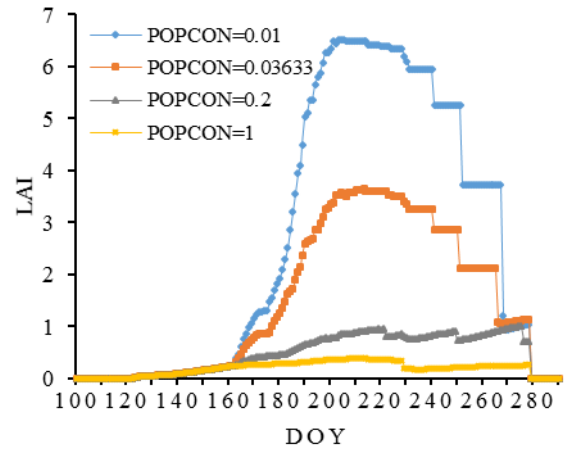
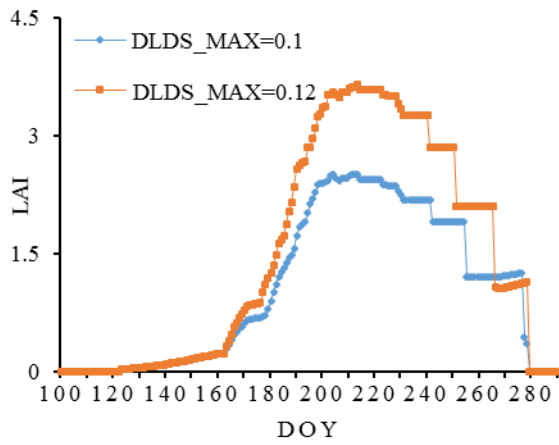
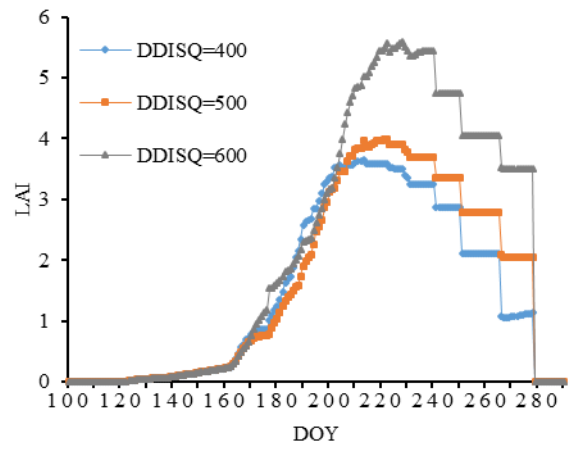
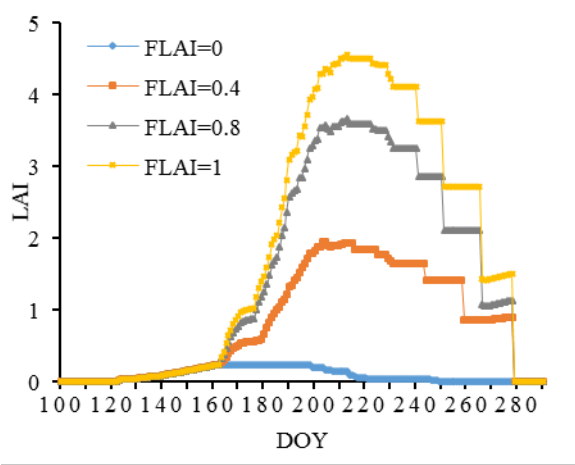
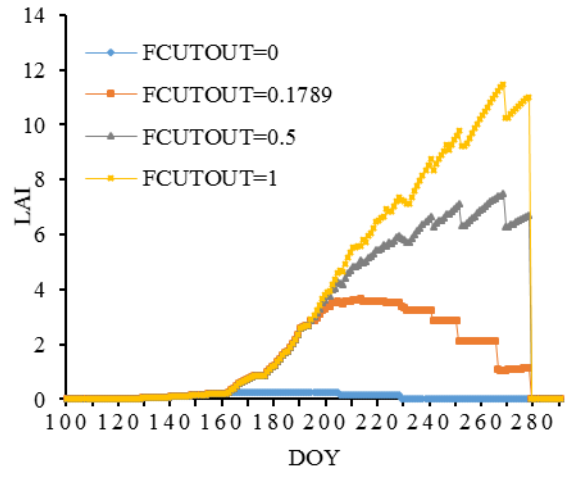
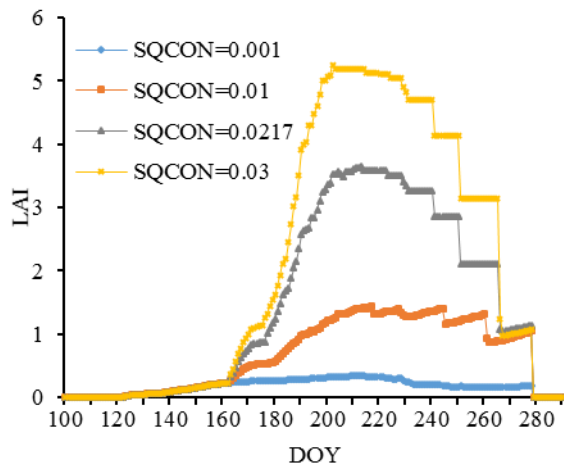
Figure 5.7 The error bar of 6 fields between remote sensing derived and in situ observed LAI (the red error bar is the RMSE between remote sensing derived LAI and in situ observed LAI)

### 5.3 APSIM-based yield prediction

#### *Sensitive parameters*

The OAT method was initially used to test the sensitivity of parameters to LAI dynamics. The result showed that there were ten cultivar parameters (**Table 4.2**) sensitive to LAI dynamics, namely SQCON, FCUTOUT, FLAI, DDISQ, DLDS\_MAX, POPCON, FBURR, ACOTYL, RLAI and FRUDD3 (**Figure 5.8**). The sensitivity of soil parameters (**Table 4.3**) is less than

the cultivar parameters (**Figure 5.9**), while the four agronomic parameters (**Table 4.4**) were all sensitive to LAI dynamics (**Figure 5.10**). Then we tested the sensitivity of these cultivar parameters and four agronomic parameters to the LAI using an EFAST global sensitivity analysis method. Because five major cotton varieties were cultivated in 2014, we selected five corresponding cotton fields to test the sensitivity of parameters to LAI dynamics. **Figure 5.11** shows the distribution of the global sensitivity of parameters to the LAI of five cultivars from five cotton fields (A01, A05, A09, A22 and A10). We also obtained the average global and local sensitivity index of parameters to the LAI at these five cotton plots (**Figure 5.12**). According to sensitivity of these parameters to the LAI, the results showed that one cultivar parameter (RLAI) and four agronomic parameters (row spacing, sowing density per row, irrigation and fertilization amount) were the most sensitive to the LAI dynamics of cotton. The RLAI parameter is the base rate of leaf growth before the first square event, which makes LAI expands exponentially until the first square event. Therefore, RLAI is most sensitive to LAI dynamics. Numerous investigations have confirmed similar agronomic parameters using global and local sensitivity analysis methods based on various crop growth models ([Jiang et al., 2011](#); [Wu et al., 2009](#); [Zhang and Su, 2012](#)). Similar to these studies, these agronomic parameters of cotton in this research are difficult to obtain on a regional scale. Thus, wide application of the crop model is limited on a regional scale.



*Continued*

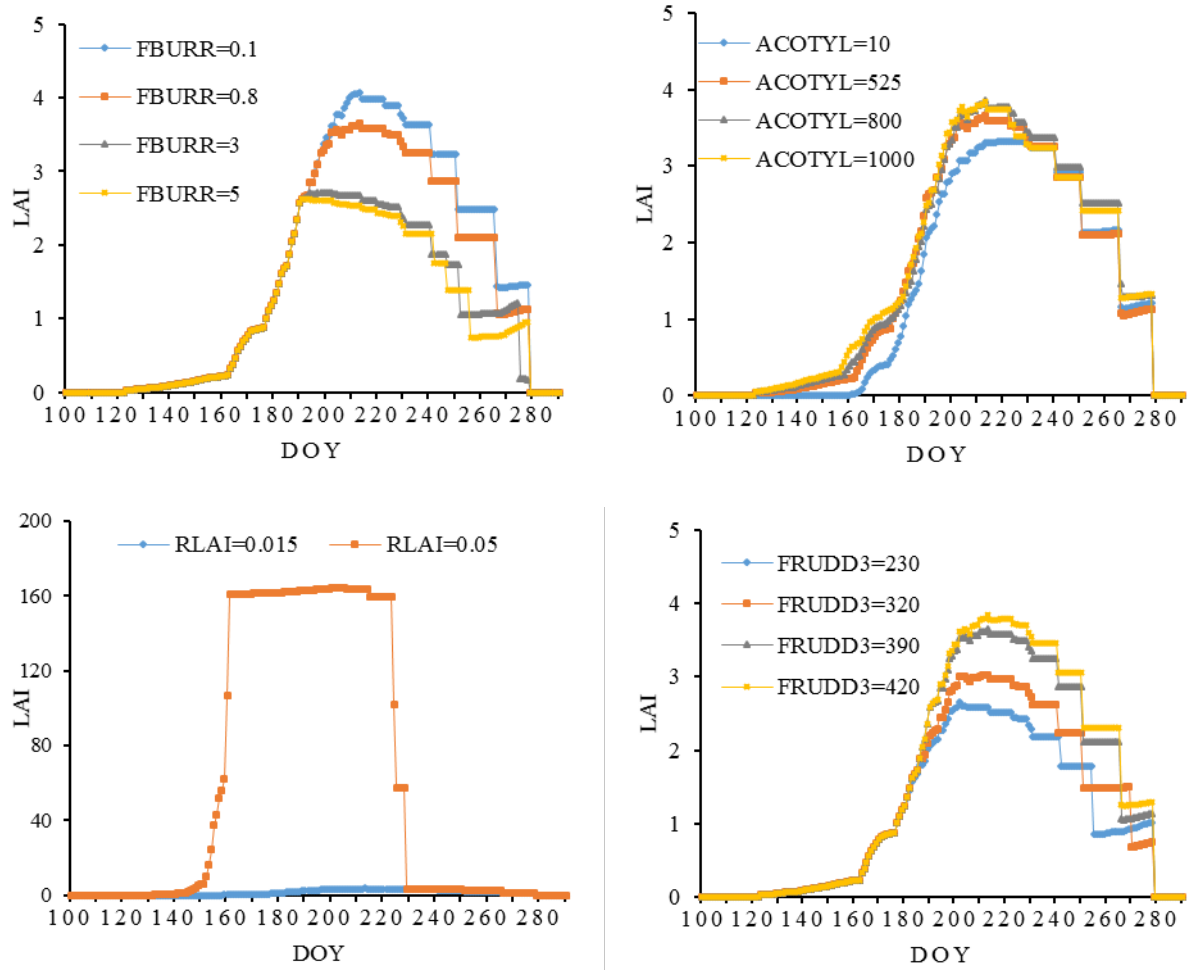


Figure 5.8 Sensitivity of 10 major cultivar parameters to LAI dynamics

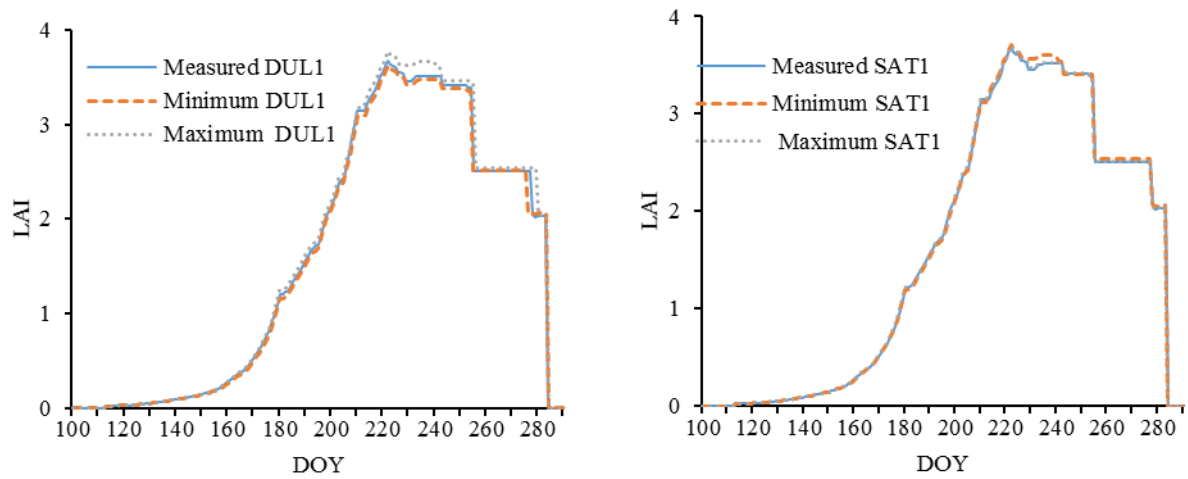


Figure 5.9 Sensitivity of two soil parameters to LAI dynamics

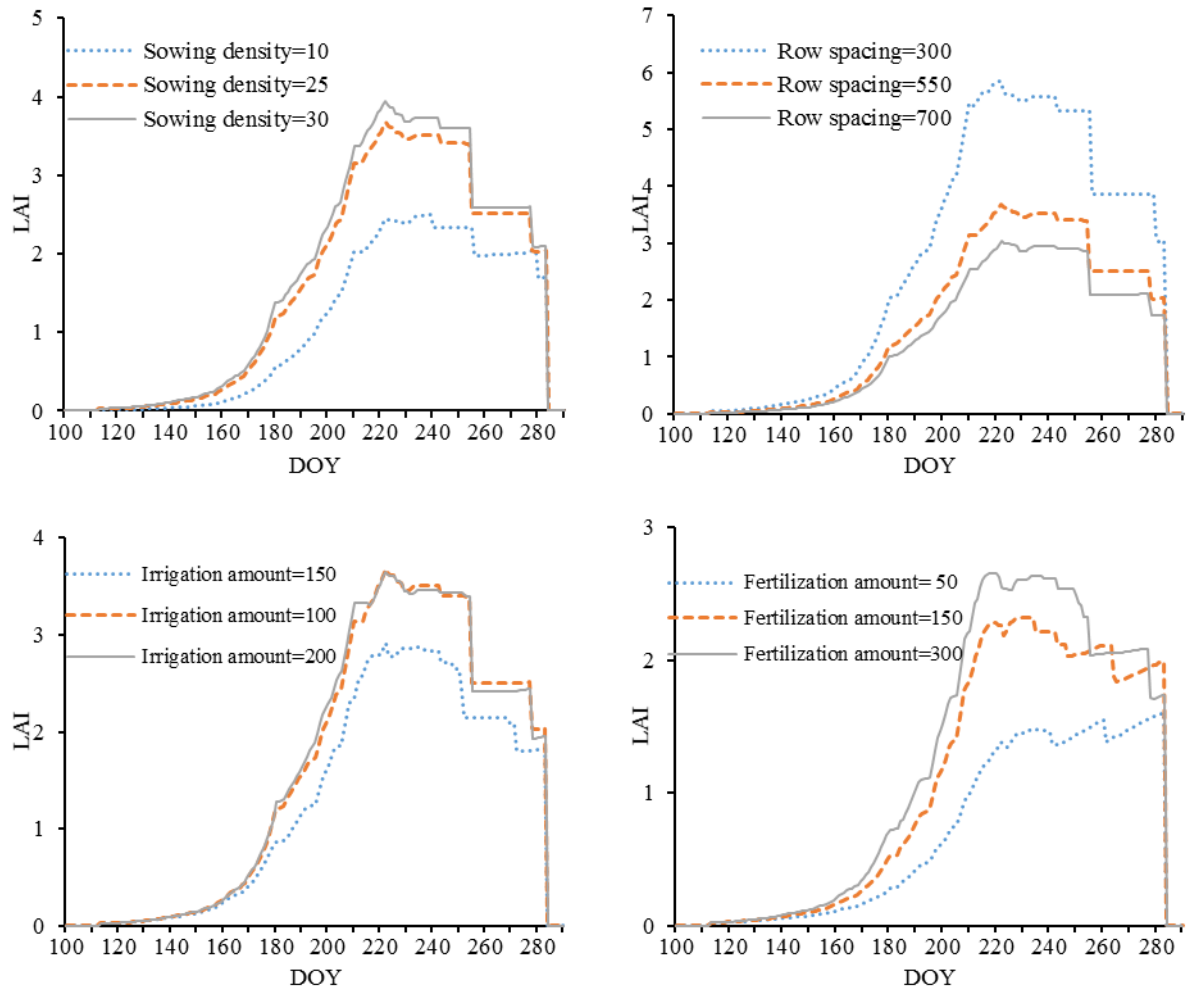


Figure 5.10 The sensitivity analysis of agronomic parameters to LAI dynamics

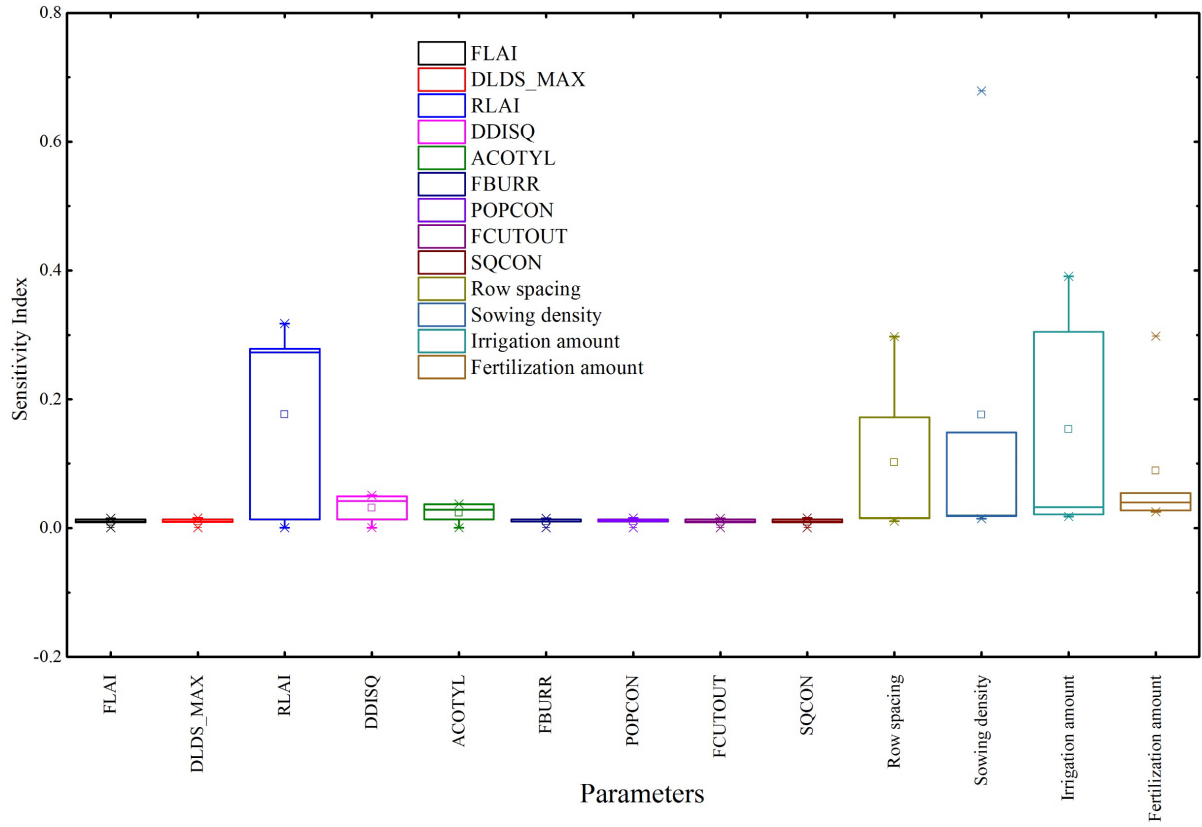


Figure 5.11 Error bar of global sensitivity of parameters at five plots to LAI dynamics

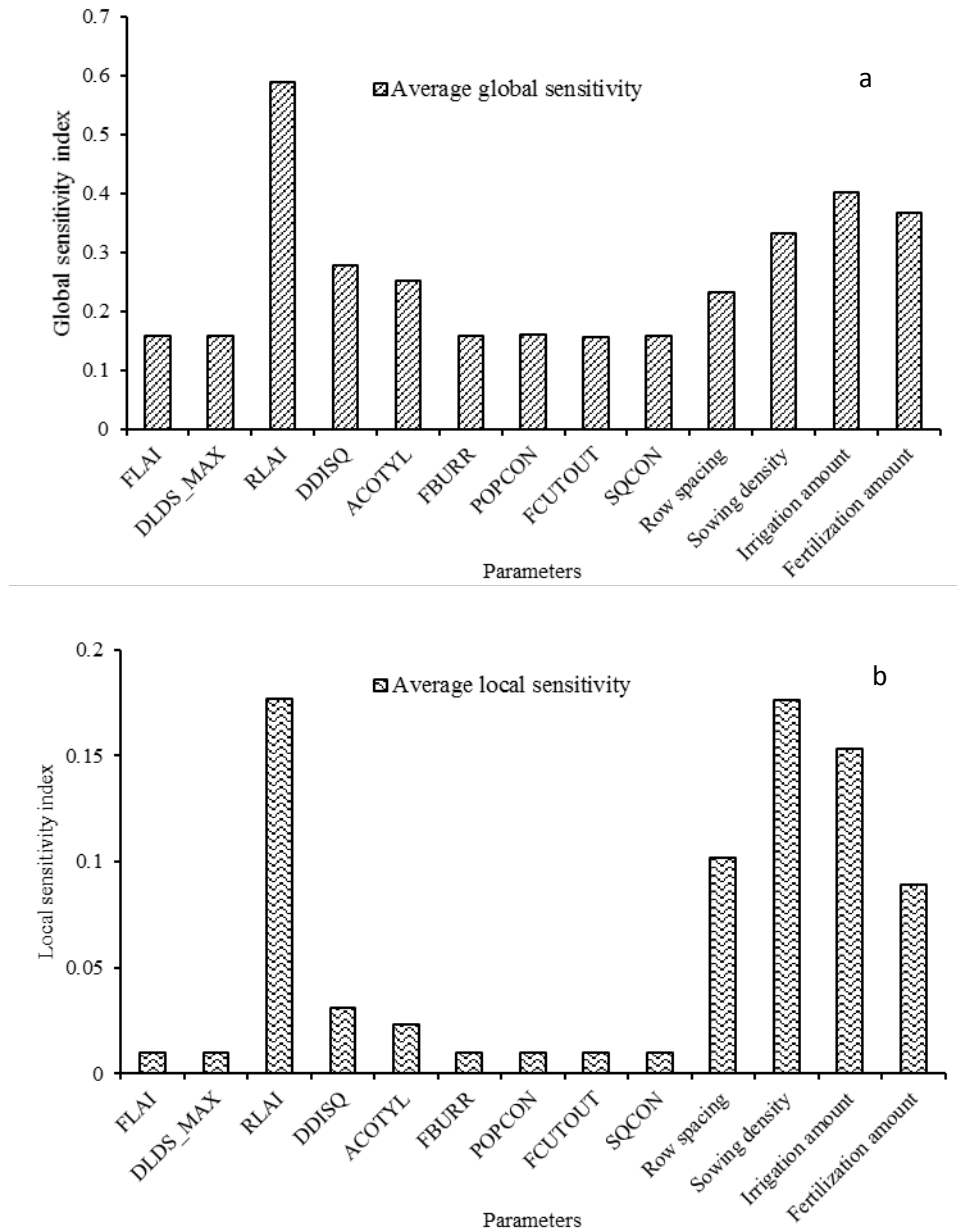


Figure 5.12 (a) Average global sensitivity; (b) and local sensitivity of parameters to LAI dynamics

#### *APSIM/OZCOT model calibration*

First, the PSO optimization method was used to optimize cultivar parameters by minimizing the difference between the simulated and observed LAI during 2006–2007 (**Figure 5.13**). The best parameters were obtained for 2006 and 2007, as follows (**Table 5.3**).

Table 5.3 Optimized cultivar parameters in the APSIM/OZCOT model

	DDISQ	FLAI	FRUDD8	RMSE
2006	300	0.50	998.49	0.388
2007	357.90	0.55	1029.03	0.367
Hybrid	330	0.52	1015	



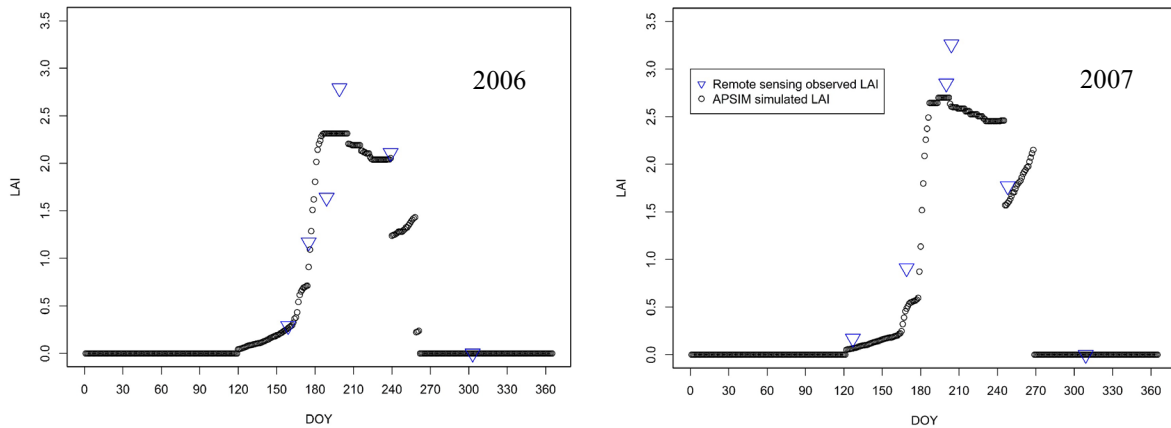


Figure 5.13 The difference between simulated and observed LAI between 2006 and 2007

According to these results and the relevant article (Yang et al., 2014), we initially determined a hybrid variety of cotton using the trial and error method (Table 5.3). The simulated lint yield of cotton using this hybrid cultivar was 2755 and 2525.1 kg/ha in 2006 and 2007, respectively, and the yield was 6028.45 and 5525.38 kg/ha. Additionally, the observed cotton yield was 5251.7 and 5265.4 kg/ha in 2006 and 2007, respectively (Table 5.4). The difference between the observed and simulated yield was 776.72 kg/ha and 259.98 kg/ha in 2006 and 2007. In total, the yield simulation of the APSIM/OZCOT model after calibration at the Aksu Station was accurate and can be widely applied.

Table 5.4 Accuracy of the simulated and observed yield during 2006-2007

	Lint yield (kg/ha)	Lint percent (%)	Yield Simulation	Yield Observation	Gap
2006	2755	45.7	6028.45	5251.73	776.72
2007	2525.1	45.7	5525.38	5265.4	259.98

Then, the comparison between the simulated and observed LAI was used to verify the accuracy of this hybrid cultivar in the APSIM/OZCOT model (Figure 5.14). The coefficient of determination was 0.83 and 0.97 in 2006 and 2007, respectively, with a significant positive correlation. The RMSE and MAE between observed and simulated LAI was 0.45 and 0.33, respectively, in 2006. Additionally, the RMSE and MAE between observed and simulated LAI was 0.46 and 0.41, respectively, in 2007. The Pearson's correlation coefficient was 0.913 at the 0.05 level (significant correlation at .05 level, bilaterally) in 2006. In addition, the Pearson's correlation coefficient was 0.988 at the 0.01 level (significant correlation at .01 level, bilaterally) in 2007.

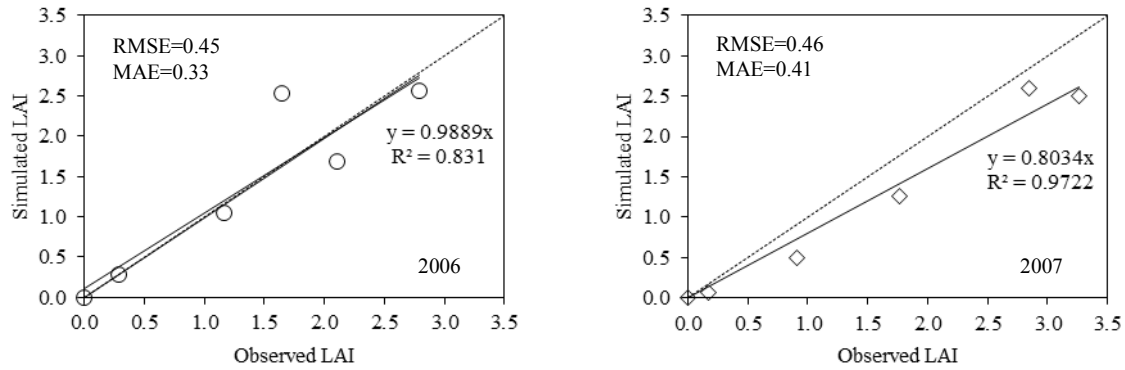


Figure 5.14 Correlation analysis of simulated and observed cotton LAI during 2006-2007

Therefore, the main cultivar parameters (**Table 5.5**) of the cotton cultivar variety (hybrid XLZ37) in the study area were finally obtained. Then the XLZ37 cotton variety within the OZCOT model can be used for the assimilation between remote sensing and crop growth model in the next step.

Table 5.5 Initial parameters of OZCOT model calibration

Parameters	Value	Definition
DDISQ	330	Growing degree-day accumulation to the first square
Percent_I	45.7	Percentage lint in boll yield by weight
SCBOLL	6.1	Weight seed cotton per boll
Baset	12	Minimum temperature as a base for temperature calculations
FLAI	0.52	Varietal adjustment for rate of LAI gain per fruiting site
FRUDD1-8	55-1015	55, 190, 390, 410, 590, 650, 900, 1015

#### *Assimilation at the field scale*

Parameters that require optimization are sensitive to the LAI; however, they are difficult to be determined and obtained on a large scale. According to the sensitivity analysis of parameters from the APSIM/OZCOT model, four agronomic parameters namely row spacing, sowing density per row, fertilization and irrigation amount were the most sensitive to LAI dynamics. Meanwhile, obtaining these four parameters on a regional scale was difficult, and the accuracy of these parameters from questionnaires is also limited. Therefore, this paper selected row spacing, sowing density per row, fertilization and irrigation amount as parameters to be optimized (**Table 5.6**). The initial values and ranges of these parameters were also defined prior to the optimization between the observed and simulated LAI. The initial values for four parameters were determined according to [Gao \(2014\)](#).

Table 5.6 Initial value and ranges of parameters within APSIM model

Parameters	Initial value	Value range
Row spacing	460 mm	350-550 mm
Sowing density per row (plants/m <sup>2</sup> in row)	9.2	1-12
Irrigation per time	60 mm	50-90 mm
Total fertilization (urea)	900 kg/ha	500-1600 kg/ha

The row spacing changes with cotton cultivar ([Wang et al., 2002](#)), machine size (the track wheel) and sowing modes ([DAXUAR, 2001](#)). **Figure 5. 15** shows a common mode of cotton cultivation in the study area. The narrow spacing ranges from 200 to 300 mm while the wide spacing ranges from 500 to 600 mm ([Liu et al., 2011b](#); [Yang et al., 2014](#); [Wang et al., 2002](#)). Additionally, the wide and narrow rows are 650 and 120 mm, respectively, during the field campaign. Additionally, salt, drought and sandstorms can minimize the number of plants. Although these two sowing modes vary, the difference in the row spacing should be narrow. Thus, the range of row spacing was assigned from 350 to 550 mm.

According to the relevant articles ([Liu et al., 2011b](#); [Yang et al., 2014](#); [Gao, 2014](#)), the sowing density ranges from 15 to 28.6 plants/m<sup>2</sup>. Therefore, we defined the sowing density as 15 to 35 plants/m<sup>2</sup>. In the APSIM model, the sowing density is controlled by two parameters: row spacing and sowing density per row (plants/m<sup>2</sup> in row). Based on ranges of row spacing and sowing density, the sowing density per row (plants/m<sup>2</sup> in row) within the APSIM model was finally determined (**Table 5.6**).

Regarding the agronomic practices in the APSIM/OZCOT model, the winter and spring irrigation were both determined by questionnaires and interviews. Generally, the winter irrigation occurs in November after harvesting while the spring irrigation occurs in February before the sowing event. Both the spring irrigation and winter irrigation are generally applied to press the salt and maintain the soil moisture within the cotton fields. The winter and spring irrigation amounts are about 225 and 285 mm, respectively, between mid-November and February. Thus, these two specific irrigation events in the study area are critical for cotton cultivation and soil moisture. During Early-Mid June, the first irrigation during the growth period is normally implemented. Prior to this event, no irrigation event occurs during the growth period. Regarding the application amount of irrigation, it is mainly decided by the soil moisture within cotton fields, generally ranging from 50 to 90 mm ([Gao, 2014](#)). According to the technical specification of cotton in the Alar ([Gao, 2014](#)), the irrigation during the growth period is approximately 60 mm per time and there is a total of 9–10 times irrigation. Irrigation

events in the growth period are terminated in late August with an interval of 7–10 days. Meanwhile, fertilization and irrigation time was averaged from 34 surveying cotton plots during 2010–2014. It is also basically consistent with relevant articles and reports from military cotton planting in Alar. The dates are as follows: 10-June, 20-June, 01-July, 10-July, 17-July, 25-July, 01-August, 10-August and 20-August.

In addition to irrigation, fertilization is also important for cotton growth and yield formation. Fertilization is generally divided into the basal manure and top dressing. The basal manure is implemented before or at the sowing event and the nitrogen amount is about 150 kg/ha. Regarding top dressing events, the date and frequencies are both consistent with irrigation events during the growth period. Meanwhile, fertilization dissolved in water is transported to the cotton fields with a total amount during growth period of approximately 500–1600 kg/ha.

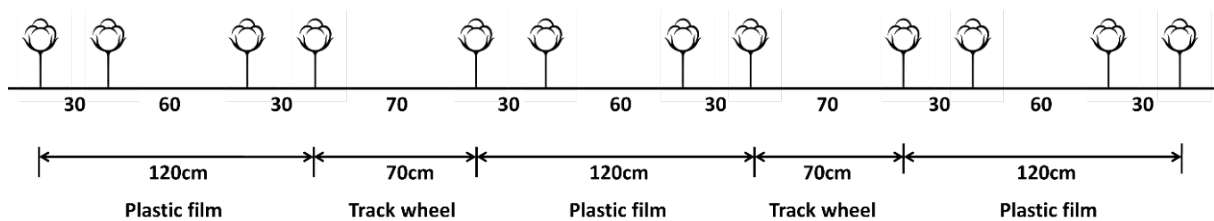


Figure 5.15 An illustration of the commonly used sowing mode in study area

We used the PSO method to minimize the variation between the LAI retrieved from Landsat-8 OLI images and the simulated LAI from the crop model. Then, we compared the simulated LAI using the mono APSIM/OZCOT model and assimilated LAI using the coupled remote sensing and APSIM/OZCOT model with the LAI retrieved from remote sensing images at the Aksu Station (**Figure 5.16**). The results showed that the difference between the remote sensing derived LAI and the assimilated LAI based on the PSO method was smaller, and the RMSE between them was only  $0.75 \text{ m}^2/\text{m}^2$ . Compared to the mono APSIM/OZCOT model simulation, the hybrid method between remote sensing and the crop model have a better fitting degree between retrieved and simulated LAI. Therefore, it perfectly met the requirement of assimilation between remote sensing and the crop model.

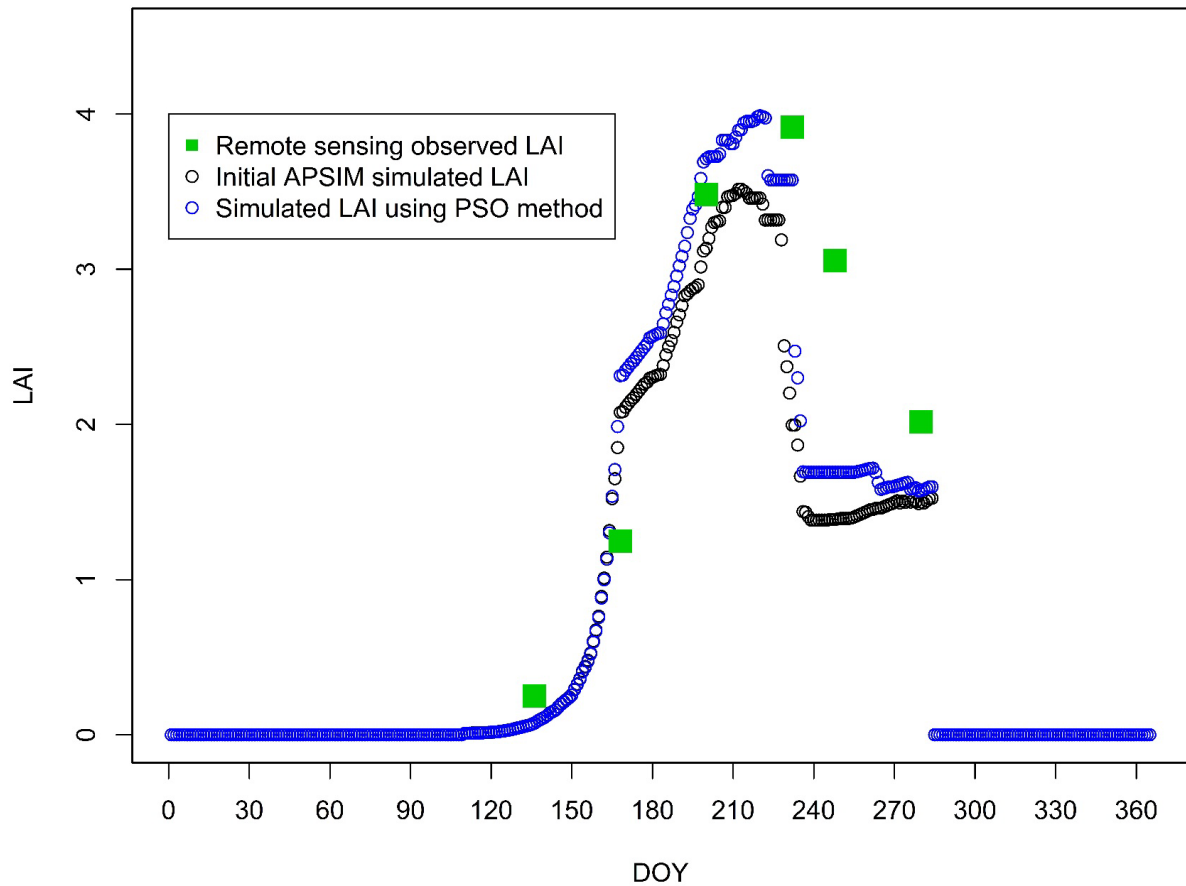


Figure 5.16 The match between remote sensing derived LAI and initial LAI using APSIM/OZCOT model, simulated LAI after the PSO assimilation at the Aksu Station

In order to validate the accuracy of assimilations from the coupled remote sensing and APSIM/OZCOT model, a total of ten cotton fields (**Figure 3.1b**) with the in-situ yield observation were selected to construct coupling models between remote sensing and the crop model based on the PSO method. A quantitative assessment of the coupled model was performed by comparing the simulated cotton yield after assimilation with the corresponding observed yield. Assimilation results showed that the yield estimation after the assimilation was very close to the field-observed values and the coefficient of determination was as high as 0.82 (**Figure 5.17b**). The difference between the observed and assimilated yields for the ten fields ranged from 18.2 to 939.7 kg/ha. Meanwhile, two indicators, RMSE and MAE, were also used to assess the error between the observed and assimilated yield. The RMSE and MAE was 417.5 and 303.1 kg/ha, respectively. The Pearson's correlation coefficient was 0.932\*\* at 0.01 level (significant correlation at .01 level, bilaterally).

Compared to the yield estimation using the mono APSIM/OZCOT model simulation based on the recommended values of parameters (**Figure 5.17a**), the assimilation strategy between remote sensing and APSIM/OZCOT model performed better on the yield simulation. In

addition to Aksu station, the simulated LAI using the APSIM/OZCOT model and remote sensing observations at the other cotton fields more closely approximated the remote sensing observation compared to the mono APSIM/OZCOT model (Figure 5.18). Thus, the strategy of coupling the APSIM/OZCOT model with the remote sensing observations is a more accurate method to obtain the LAI growth process and yield estimation of cotton.

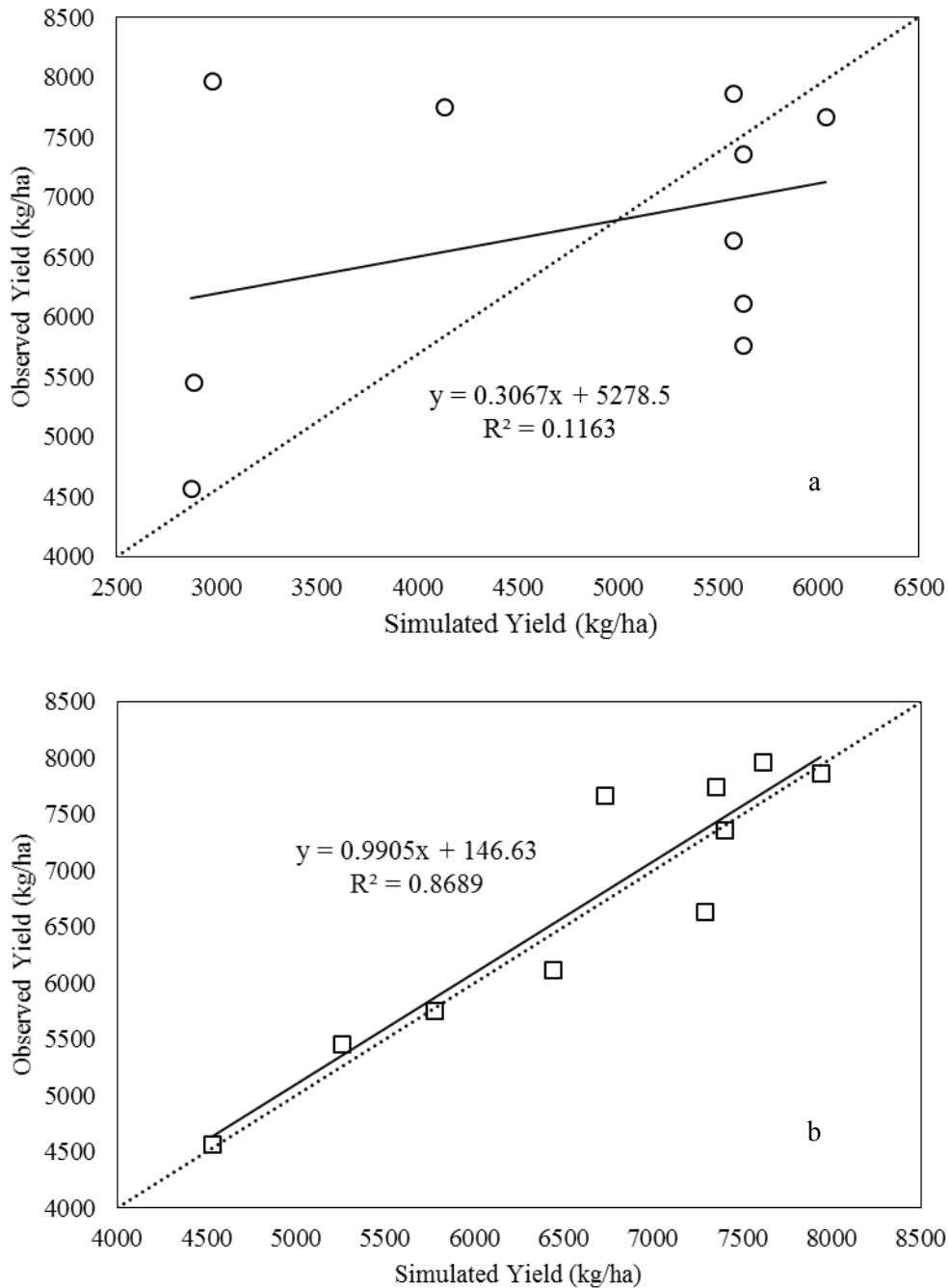
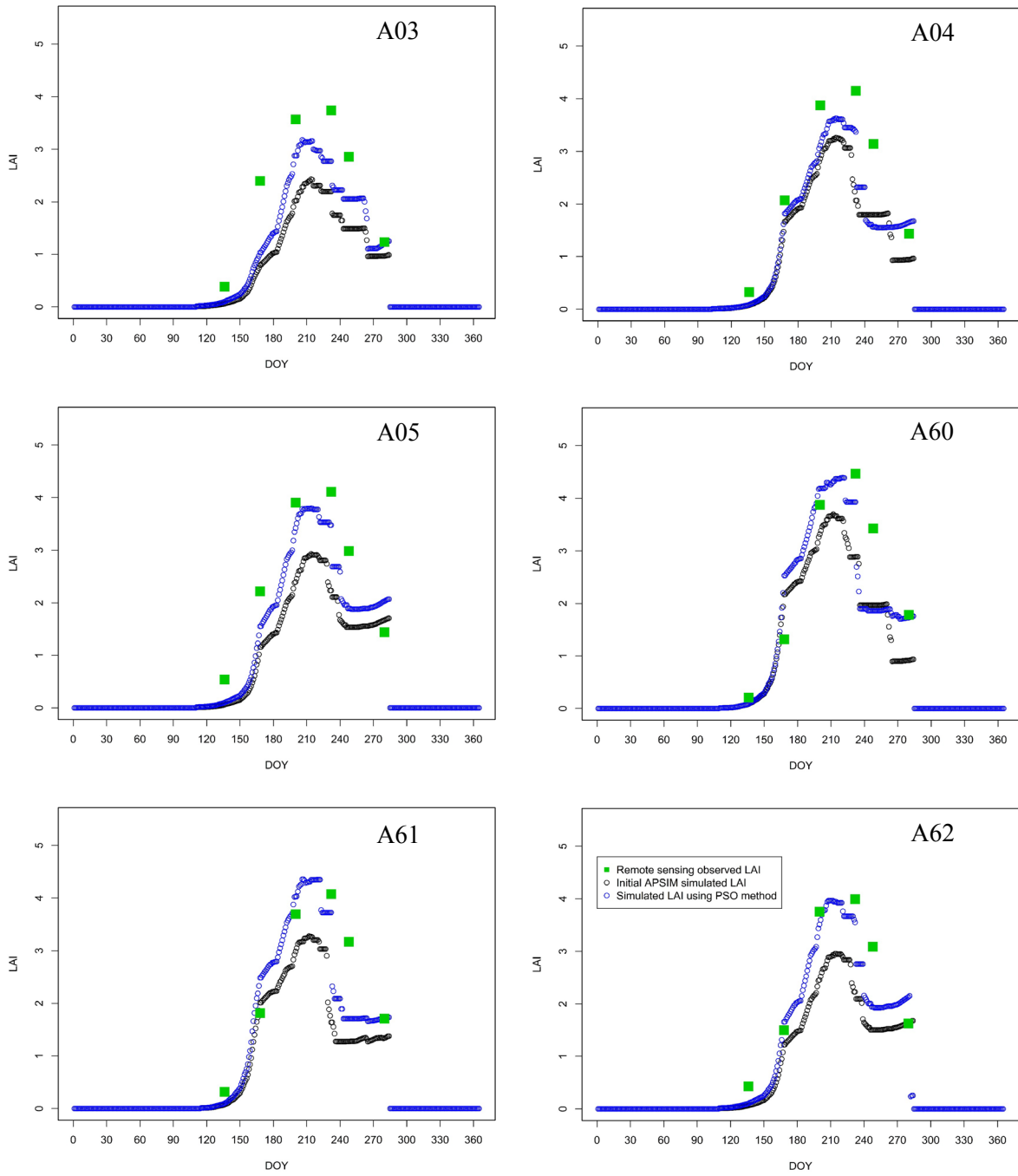


Figure 5.17 (a) the relationship between the observed and simulated yield of 10 cotton fields using the mono APSIM/OZCOT model; (b) the relationship using PSO method



*Continued*

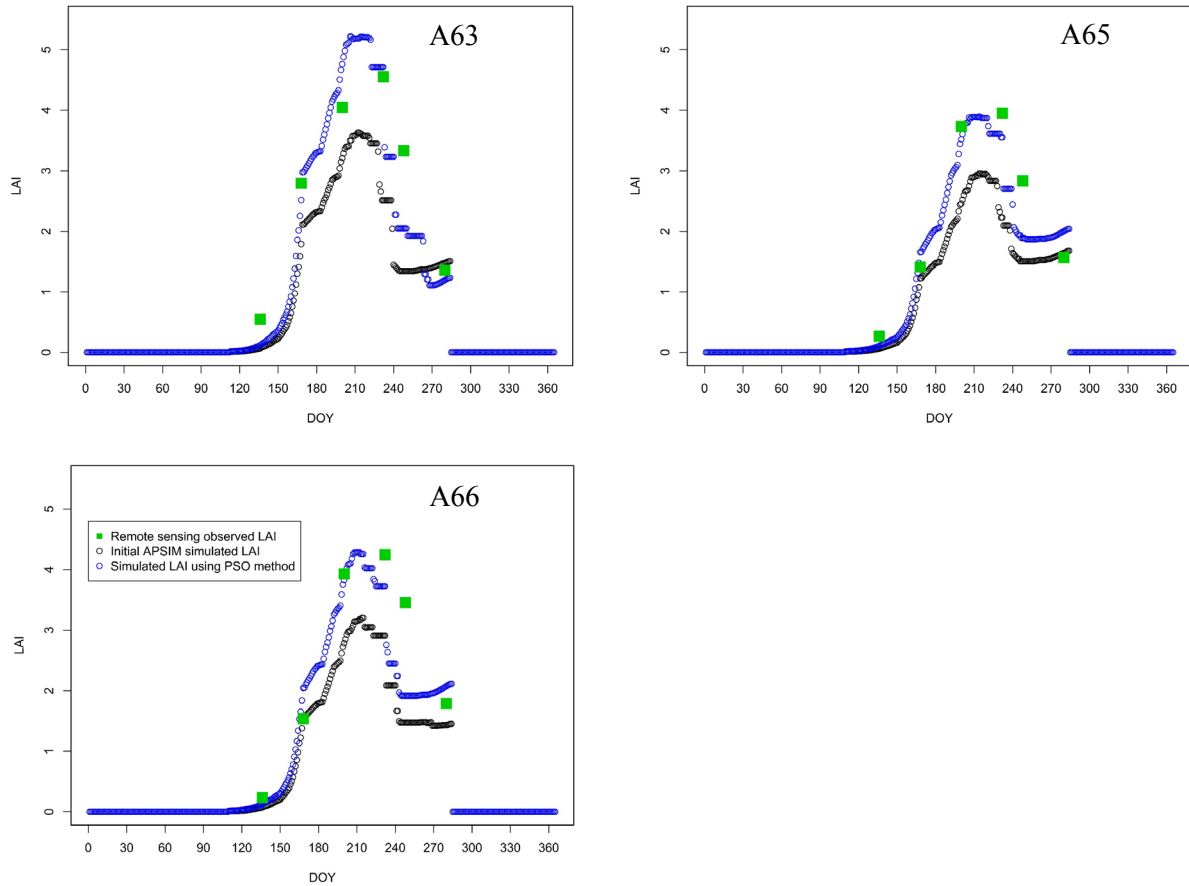


Figure 5.18 The relationship between observed and assimilated LAI using PSO method, simulated LAI using mono APSIM/OZCOT model at 9 cotton fields

## 5.4 Regional assimilation results and discussions

### *Algorithm selection on the regional assimilation*

Time consumption with 15 particles and 60 iterations was about 0.83 hours. In this paper, there are a total of 240 000 cotton cultivation pattern pixels. Therefore, application of the PSO method at pixel level would consume approximately 22.7 years ( $240\,000 \times 0.83 / (24 \times 365)$ ). The computational efficiency is the largest obstacle for the application of assimilation on a regional scale. Therefore, comparisons between the PSO and general-purpose optimization method (based on the Nelder-Mead algorithm) were analysed on a field scale based on the computational efficiency, simulated LAI curve and accuracy (RMSE). We selected nine cotton fields with in-situ yield and LAI observations covering the entire study area. The result at the Aksu station showed that the computational efficiency of the general-purpose optimization (based on the Nelder-Mead algorithm) is faster than the PSO, though the PSO method only used 15 particles and 10 iterations (**Figure 5.19**). The RMSE between the remote sensing derived LAI and simulated LAI using the general-purpose optimization method (based on the Nelder-Mead algorithm) was greater than the PSO, while their LAI curves were



similar. Then, we selected the other seven fields, which were uniformly distributed in the study area, to compare the results between the PSO and general-purpose optimization method (based on the Nelder-Mead algorithm) (**Figure 5.20**). The results revealed that two methods had similar effects (similar RMSE and LAI curves), while the computing speed of the general-purpose optimization method (based on the Nelder-Mead algorithm) was faster than the PSO method (**Table 5.7**). Thus, we can use the general-purpose optimization method (based on the Nelder-Mead algorithm) on a regional scale in the following analysis.

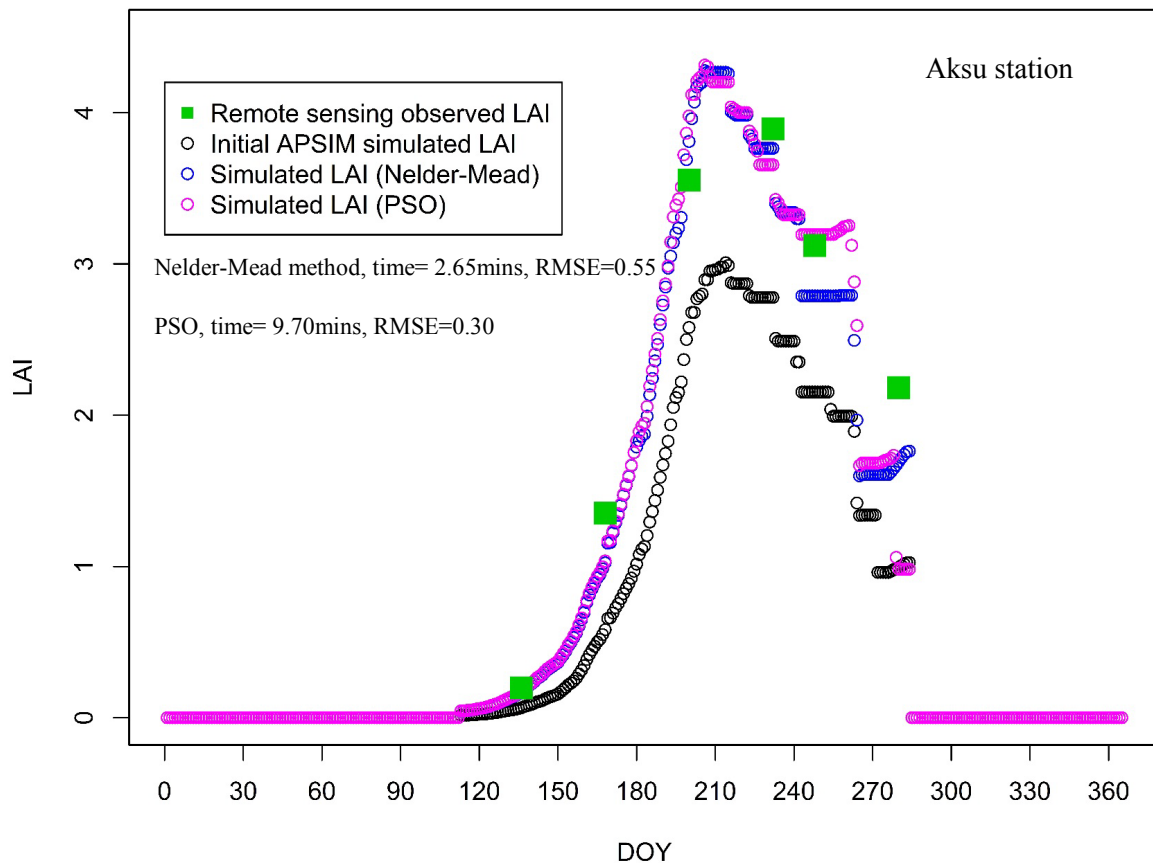


Figure 5.19 The comparison between PSO and general-purpose optimization method (based on the Nelder-Mead algorithm) at Aksu station

Table 5.7 The comparison between computational time and RMSE at various fields

	PSO		General-purpose optimization (based on Nelder-Mead algorithm)	
	Speed/Minutes	RMSE	Speed	RMSE
A63	9.35	0.59	3.29	0.73
A66	9.46	0.46	2.28	0.508
A07	9.60	0.40	5.5	0.54
A18	9.64	0.10	2.8	0.20
A25	9.36	0.27	3.85	0.27
G15	10.01	0.49	3.69	0.44
G25	9.64	0.34	2.28	0.44
G32	9.58	0.52	4.35	0.75

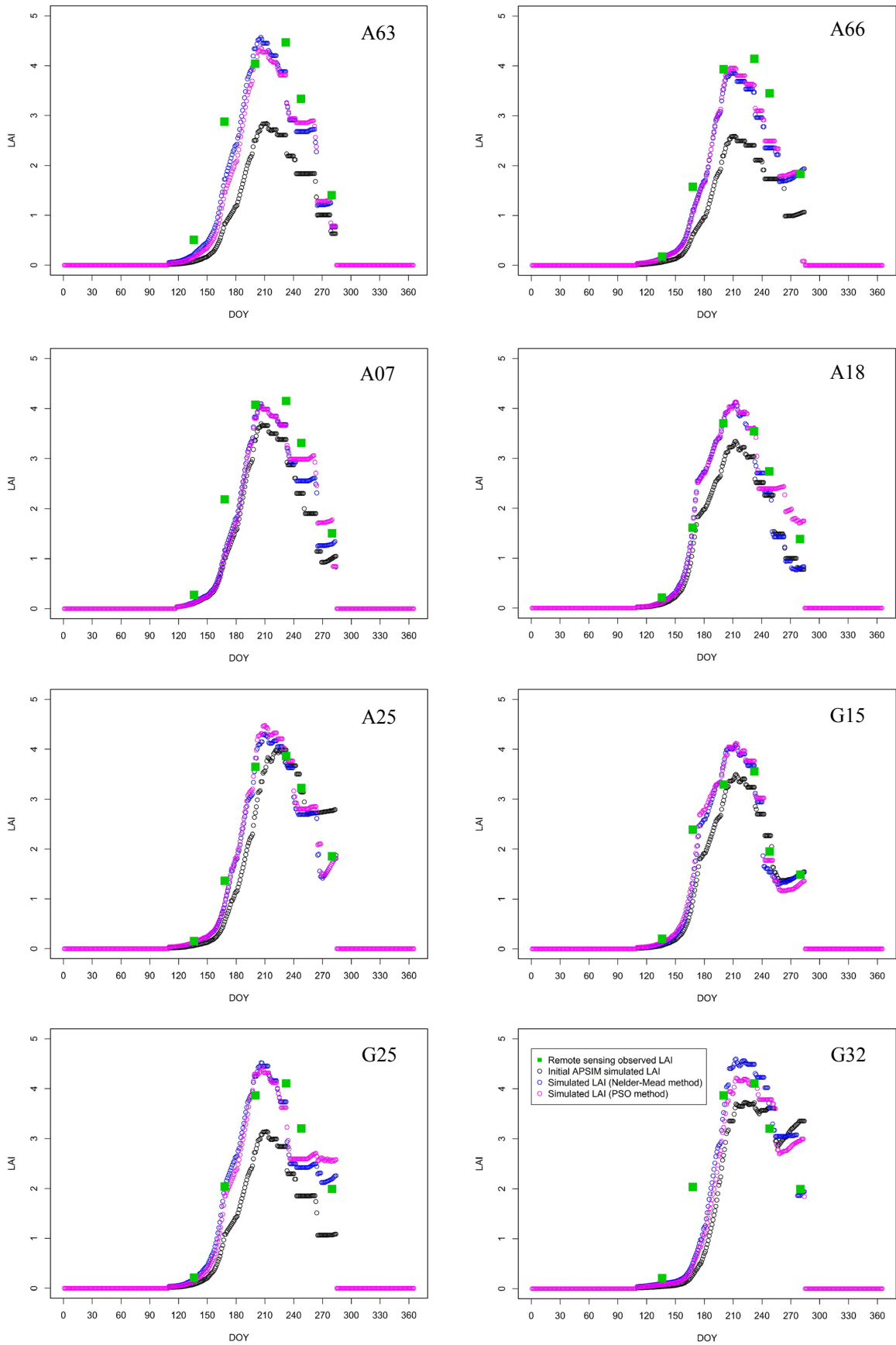


Figure 5.20 The comparison between PSO and general-purpose optimization method (based on the Nelder-Mead algorithm) at other fields

### *Regional assimilation scheme*

Although the computational efficiency of the general-purpose optimization method (based on the Nelder-Mead algorithm) is faster than the PSO algorithm, the assimilation on a regional scale based on each pixel is also a huge amount of work. Therefore, we analysed several schemes to obtain the spatial distribution of LAI and agronomic parameters. The generated grid can also divide the study area into the equivalent grids, while it breaks the boundaries of the cotton lands. Parts of the grids include various cotton fields, and it is difficult to provide a reasonable and efficient pathway for agronomic management for each cotton field. Finally, the scheme of using the cotton fields extracting from the Landsat-8 OLI images was considered the basic unit. This scheme is easier to provide scientific and convenient evidence for cotton management.

Additionally, we also divided the simulation of LAI within a growth season simulated by the APSIM/OZCOT model into three stages, namely the emergence-early stage, middle stage and late stage (**Table 5.8**; **Figure 5.21**). Then the computational efficiency dropped a lot. Meanwhile, a general-purpose optimization method (based on the Nelder-Mead algorithm) within the R package was used to replace the PSO algorithm due to its highly operational efficiency. A systematic framework was also considered when simulating the mid-late stage of LAI because LAI growth is a continuous process. In addition to assimilated parameters at different stages, the optimized parameters after assimilation at former stages were also considered. The optimized parameters from the early stage were therefore introduced in the assimilation of the mid-late stage.

Table 5.8 Descriptions of cotton LAI growth

	DOY of RS Observation	Duration
Emergence-early stage	136, 168	Mid-April -- Mid-June
Middle stage	200, 232	Mid-June -- Late August
Late stage	248, 280	After early September

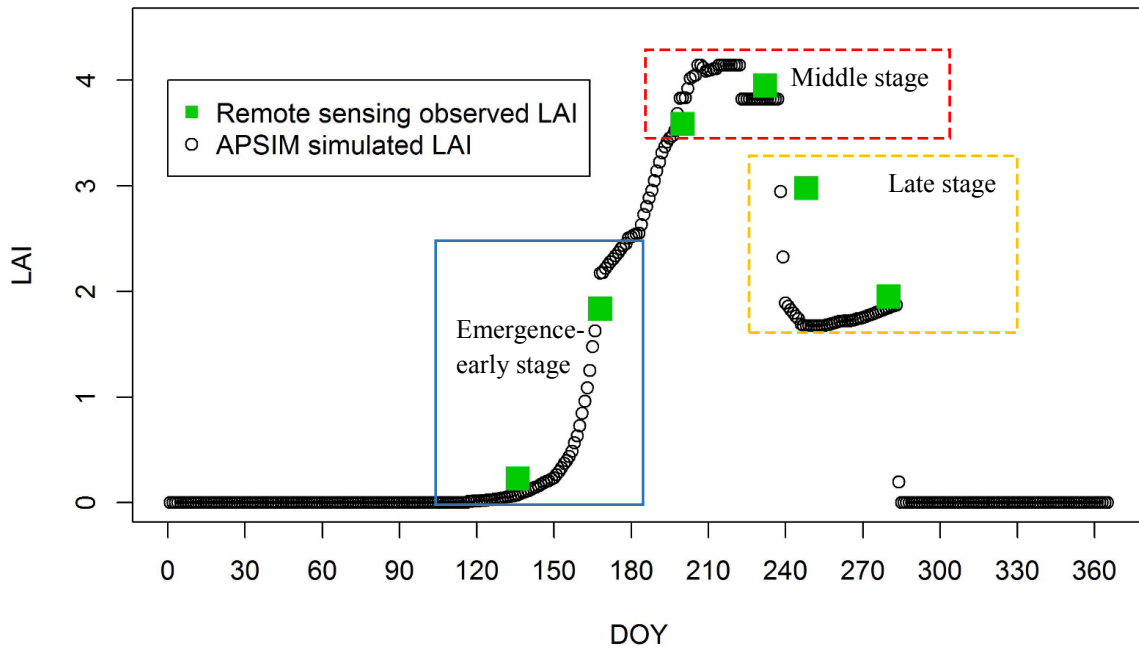


Figure 5.21 Cotton LAI development stages simulated from the APSIM/OZCOT model

### *Regional assimilation at the early stage*

Due to a small region with flat terrain in the study area and only a meteorological station, the climatic condition can be considered homogeneous. Meanwhile, we also consider the soil condition homogeneous though soil conditions spatially vary. Then APSIM/OZCOT model expects crop growth conditions by the adjustment of parameters within the model. During the early period of cotton growth, there are two remote sensing observations (DOY 136 and 168) and the major agronomic practice is the sowing density.

Regarding the early growth stage of LAI growth, the LAI is mainly controlled by the plant population when the emergence event occurs. Due to the lack of irrigation and fertilization events during this period, LAI growth is decided by the sowing density per row and row spacing. Both sowing density per row and row spacing decide the sowing density of cotton. Additionally, the sowing density is a regional parameter, varying among the different fields, which is affected by weather disasters (hail, sandstorms and drought), soil moisture, soil texture and salinity. The row spacing and plant spacing are both affected by sowing machines, which mainly control potential plant populations. However, the soil moisture, texture and salinity affected by agronomic practices and natural conditions mainly control the emergence of cotton. In addition, weather disasters are able to impact the survival rate of cotton seedling. Thus, we conclude that the sowing density is an easily dynamic parameter when upscaled in the APSIM/OZCOT model from the field to the regional level. Therefore, we selected the

sowing density per row and row spacing as two key parameters to adjust the dynamics of the LAI to fit the corresponding remote sensing observations on a regional scale.

Prior to assimilating the LAI derived from remote sensing images and the APSIM/OZCOT model, a data normalization was first implemented due to the different ranges of the two parameters. After the normalization, parameters are both assigned to the range of 0–1, under the same standard. The formula ([Aksoy and Haralick, 2001](#)) is as follows,

$$Par = \frac{x - x_{\min}}{x_{\max} - x_{\min}} \quad (5.1)$$

where *Par* is the parameter after the normalization; *x* is the initial parameter; and  $x_{\max}$  and  $x_{\min}$  are the maximal and minimal parameters before normalization.

The result shows that the row spacing varies from about 350.02 to 488.65 mm (**Figure 5.22a**) and the density per row varies from 1 to 11.99 plants/m<sup>2</sup> (**Figure 5.22b**). Moreover, the spatial distribution of the row spacing is higher in the northern study area than the southern region. Conversely, the spatial distribution of the density per row is lower in the northern region than the southern study area. The RMSE of LAI ranges from 0.06 to 0.89 and the mean RMSE is 0.22 (**Figure 5.22c**). The frequency of the RMSE is near 0.2 (**Figure 5.23**). The spatial distribution of the RMSE for assimilated results also showed that this method was feasible and robust with a higher credibility on a regional scale (**Figure 5.22c**; **Figure 5.23**). Based on these two parameters (row spacing and density per row), the sowing density of cotton was finally obtained. The result shows that the sowing density varies from about 2.4 to 34.2 plants/m<sup>2</sup> (**Figure 5.24a**). In addition, the sowing density in the northern study area is less than the southern region (**Figure 5.24a**). The sowing density was largest in the southwest region of the study area where state demonstration zones of high yield cotton fields were located, based on questionnaires.

The quality of the cotton fields is closely related to the emergence and yield of cotton while directly related to the cultivated ages of arable lands, because long-term cultivation increases the humus content in the soil ([Migdall et al., 2012](#)). Thus, the temporal and spatial dynamics of arable lands were analysed based on multi-temporal remote sensing images. **Figure 5.24(b)** shows the arable land dynamics in the study area during 2001–2013. The red, green and blue colours show the distribution of arable lands in 2001, 2008 and 2013 by employing the magnitude of the MODIS EVI ([Mader, 2013](#)). Permanent arable lands (stable arable land from 2001 to 2013) are mainly distributed in southern region. Reclamations driven by the economic

development occurred in the northern study area during 2001–2008. During 2008–2013, the reclamation also mainly appeared in the northern study area. Low sowing density was primarily located in the northern region of the study area while high sowing density was located in the southern region, illustrated by the spatial analysis distribution of plant density and arable land reclamation. This point of view is also consistent with the spatial distribution of the high-standard Farmland Construction project (**Figure 5.25**). The scope of this project is located in the southwest of study area by overlying the distribution map of this project and the Landsat OLI image at DOY 232 (**Figure 5.25a, b**). This project aimed to pursue higher yield of cotton by improving the soil fertility and irrigation facilities of arable lands.

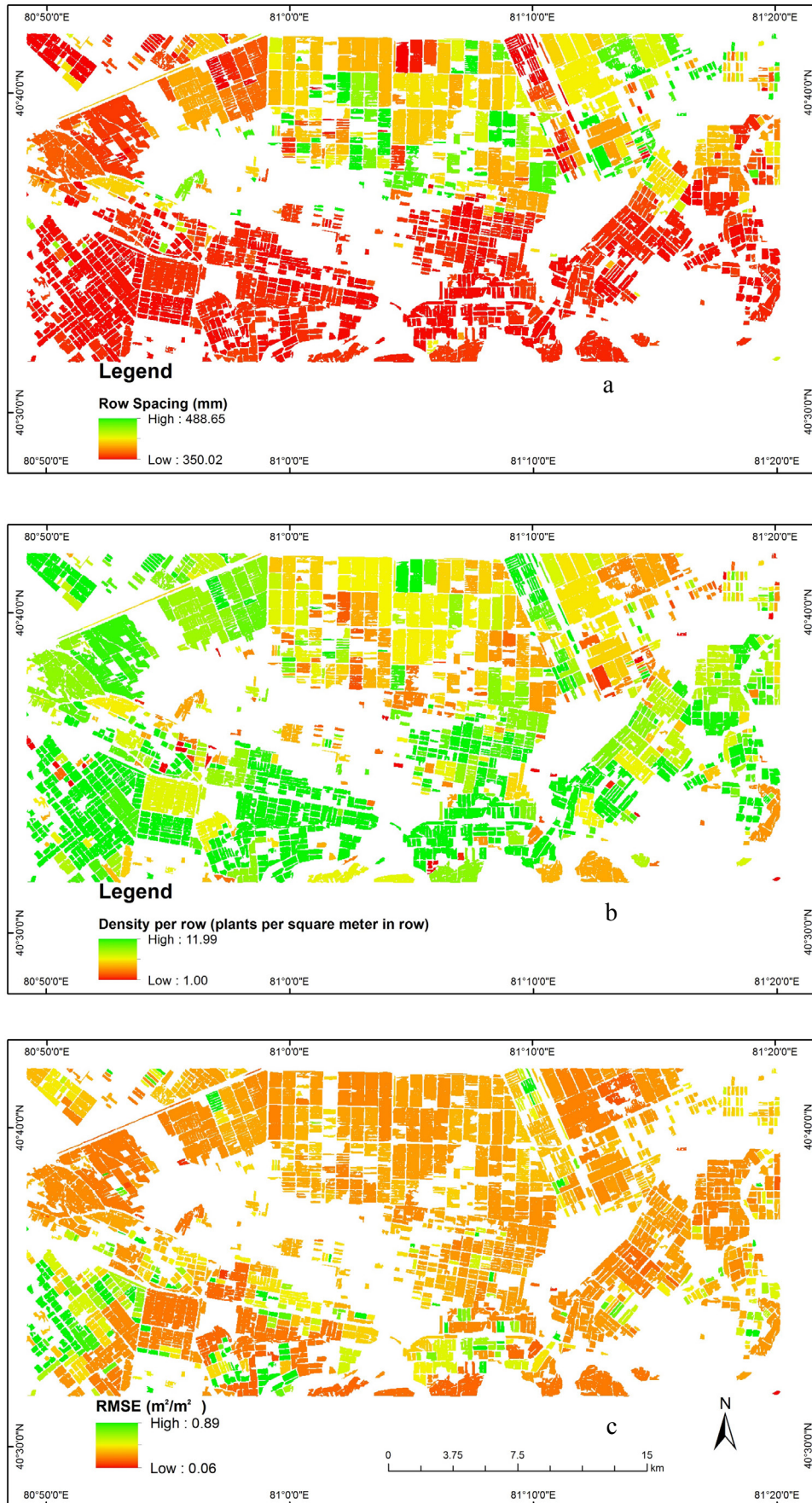


Figure 5.22 (a) Spatial distribution of row spacing; (b) Spatial distribution of density per row; (c) RMSE distribution of LAI adjusting APSIM to optimally match satellite observed LAI

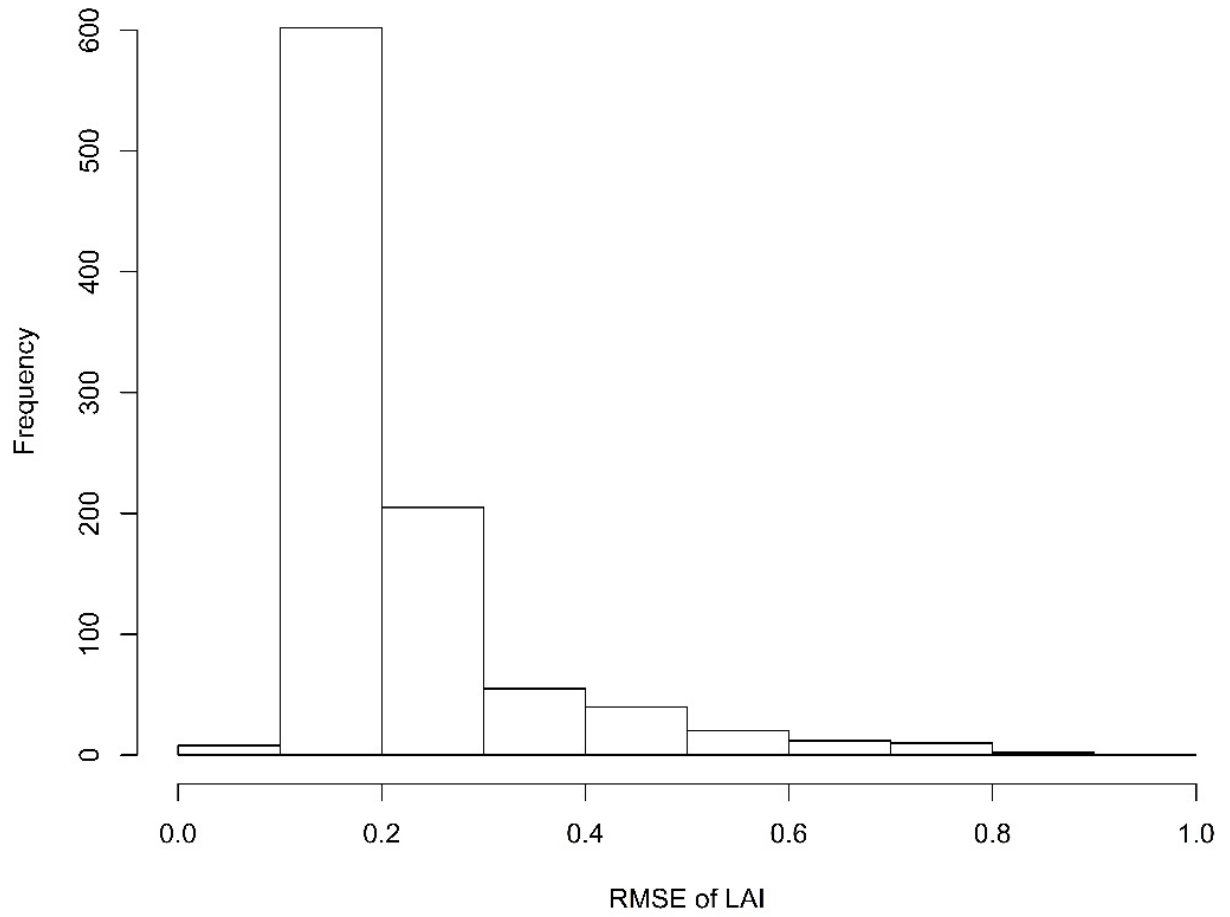


Figure 5.23 Frequency of LAI RMSE for each cotton field at early growth stage



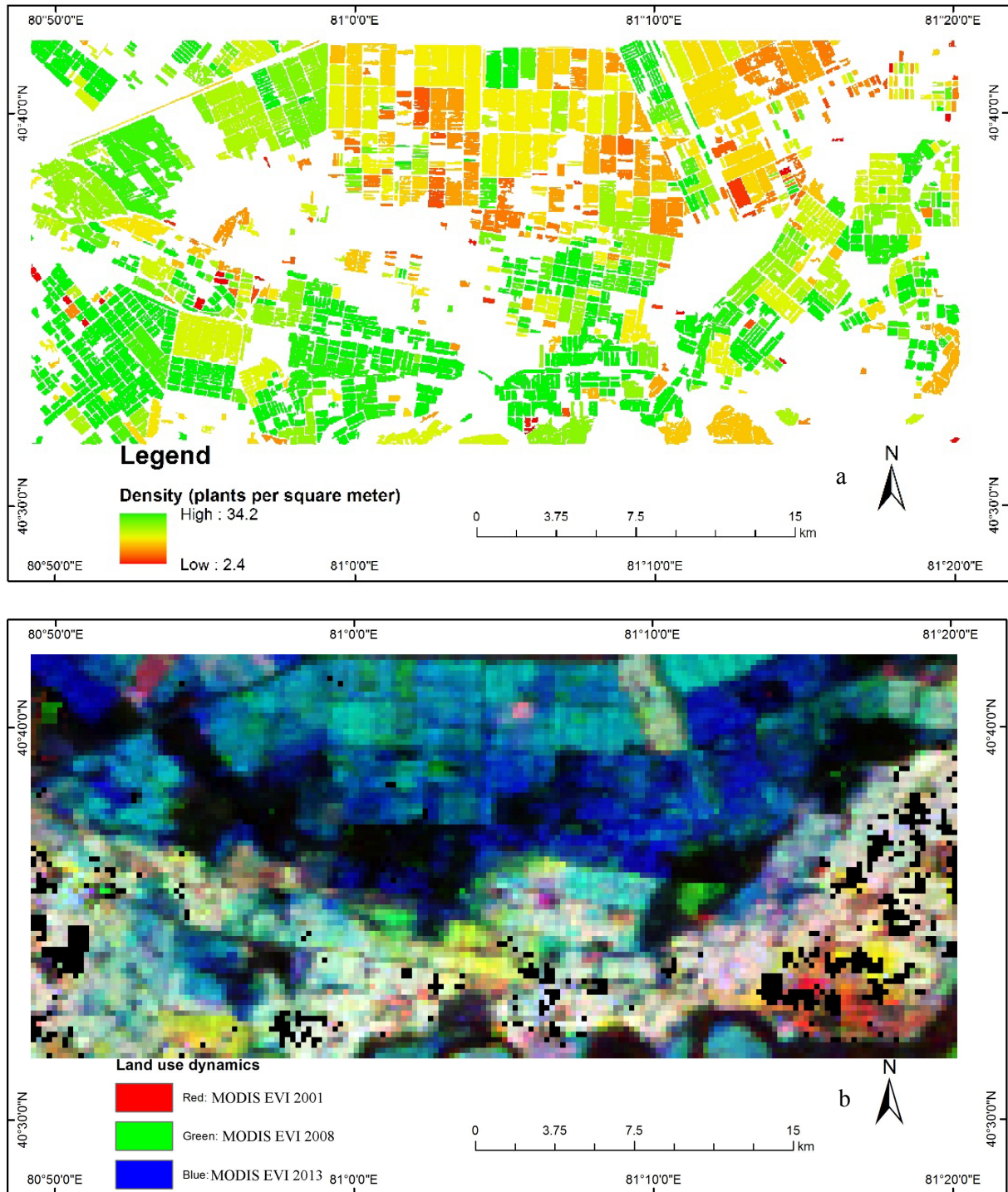
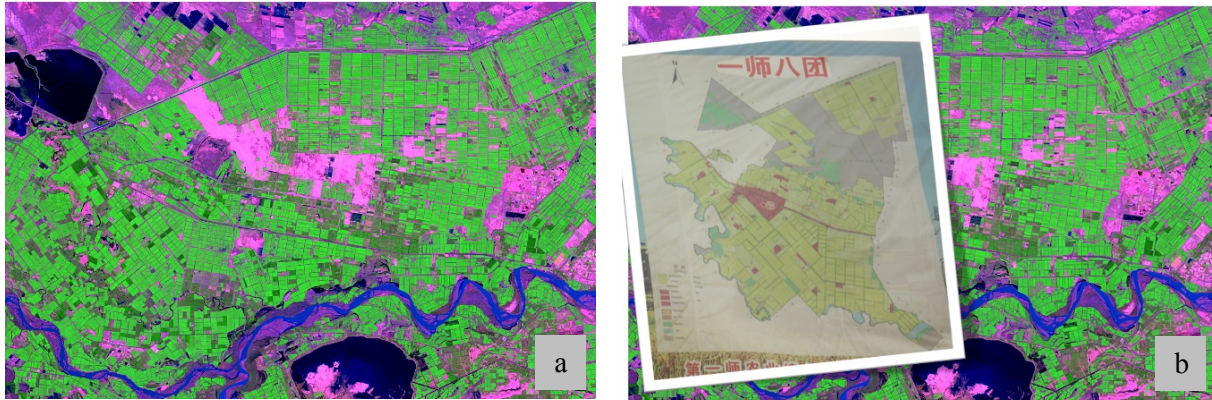


Figure 5.24 (a) Spatial distribution of sowing density by adjusting APSIM to optimally match satellite observed LAI; (b) land use dynamics based on MODIS EVI (from [Mader, 2013](#))



## Legend

### Landsat 8 OLI DOY232

#### RGB

- Red: Short Wavelength Infrared (2100-2300 nm)
- Green: Near Infrared (845-885 nm)
- Blue: Red (630-680 nm)

Figure 5.25 (a) Landsat 8 OLI image at DOY 232; (b) High-standard Farmland Construction project in the southwestern study area overlaying on the Landsat image (yellow color is farmland)

In addition to arable land dynamic analyses based on remote sensing images, we also obtained the spatial distribution of the woodland belt surrounding arable lands by the field survey and by questionnaires. Sparse woodland belt and regions lacking a woodland belt surrounded recently reclaimed arable land in the northern study area (**Figure 5.26a**). In this case, cotton plants cultivated in these recently reclaimed arable lands are easily destroyed by wind erosion at the early growth stage of cotton. During the field survey, seedlings of cotton were buried and killed by sandstorms in the northern study area, affecting the survival rate of seedlings (**Figure 5.27**). In addition, parts of recent reclamations in the northern region are located close to deserts, and as such, the soil texture is not suitable for cultivating cotton (**Figure 5.26b**). Meanwhile, deserts provide a convenient source for sandstorms, which can seriously undermine recently cultivated arable lands.



(a), Artificial windbreak in the cotton field

(b), Sand in the cotton field

(c), Soil salinity in the cotton field

Figure 5.26 Photos illustrating various factors influencing the emergence and survival rate of cotton seedling

Based on questionnaires and interviews, northern reclamations belong to private companies while southern arable lands belong to military farmland. Southern arable lands have been equipped with more perfect irrigation facilities compared to the northern region. The southwestern study area is administrated by the Group 8, 1<sup>st</sup> Agricultural Division with a national agricultural development (high standard farmland construction) project. During 2011–2013, numerous tasks were implemented to improve the quality of cotton fields, including construction of an irrigation system and canal seepage, soil improvement, windbreak updating, land levelling and agricultural technical training. The usage period of reclamation in northern region is approximately 20–30 years. To pursue higher profits and decreasing costs, these recent reclamations are generally not equipped with updated irrigation facilities. Therefore, differences in equipment and facilities of arable lands were apparent.

Meanwhile, the piped irrigation is first used to irrigate military arable land in the south of the study area prior to recently reclaimed farmlands in the north of the study area. Additionally, high soil salinity in northern cotton fields led to decreases in cotton seedling emergence. In conclusion, poor soil texture and irrigation equipment, high salinity and missing woodland belts have resulted in a low emergence rate and low survival rate of cotton seedlings at the early growth stage in the northern region (**Figure 5.26**).





Figure 5.27 Photos of (a) sandstorms; (b) cotton plants without disaster at the same day; (c) damaged cotton plants caused by sandstorms; (d) a dead cotton caused by the sandstorm

#### *Regional assimilation at the mid-late stage*

During the mid-late period of cotton growth, there are four remote sensing observations (DOY 200, 232, 248 and 280) and the major agronomic practices are fertilization and irrigation. The middle period is a stage of dramatic change in LAI due to the co-existence of vegetative and reproductive growth, greatly dominated by agronomic practices such as irrigation and fertilization. Furthermore, the effects of water and fertilizer in the early (before mid-July) and late period (after mid-July) vary considerably different functions in the dynamics of the LAI and yield formation at this stage. Early irrigation and fertilization aim to promote the vegetative growth and the early squaring event of cotton. As a result, the growth stage of cotton is consistent with climatic conditions, i.e., the boll formation stage is consistent with the stage providing best light and temperature. Irrigation and fertilization application during the early period aim to accelerate the vegetative growth for a rational canopy structure and height. A sufficient canopy height of cotton can produce fruit branches and flowers and form cotton bolls. Therefore, the irrigation and fertilization events before July aim to build a rational canopy structure and optimal phenology of cotton.

Mid-late July contains an alternating phase between the vegetative and reproductive growth periods. Therefore, increasing agronomic practices, such as irrigation and fertilization, promote rapid growth and a high yield of cotton. These measures transfer vegetative growth into reproductive growth by controlling the plant height and canopy growth of cotton. Finally, August is a prosperous reproductive growth period for cotton. Therefore, more irrigation and fertilization can prevent shedding of flowers and bolls. Sufficient irrigation and fertilization application is critical for anti-shedding caused by nitrogen and water stresses during this period. These conclusions were also confirmed by in-situ experiments (Wang et al., 2002) (Figure 5.28), which are as follows.

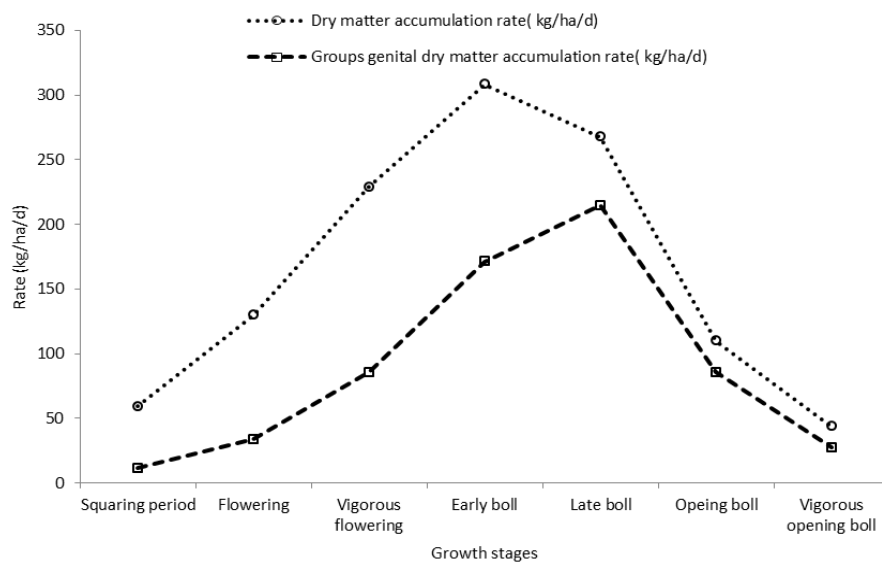


Figure 5.28 Cotton dry matter accumulation rate and its group genital dry matter accumulation rate in study area (Wang et al., 2002)

The late stage of LAI growth is a period for harvesting and leaf senescence. Generally, no irrigation and fertilization events occur. Therefore, the leaf senescence is the most critical factor influencing the LAI at the late stage, and it is decided by GDD (McMichael and Hesketh, 1982). Leaf longevity is also controlled by water. Early water stress can delay development and strengthen the life of the leaf, while late water stress can accelerate the leaf senescence (Hearn, 1994). In summary, leaf senescence is a function of GDD modified by the soil water and boll survival. Therefore, the amount of irrigations at the middle stage can affect the soil water. We mainly used the irrigation and fertilization amount as parameters to adjust the LAI at the middle stage of cotton growth. Additionally, the amount of irrigation at the middle stage can affect the LAI dynamics at the late stage of cotton growth. Therefore, we assimilated the middle and late growth stages using four remote sensing observations and two regional parameters, namely the irrigation and fertilization amount.

Similar to the simulation at the first stage, the irrigation and fertilization amount were also normalized to a range of 0–1 in order to ensure an identical standard. Then, these two parameters were used to assimilate the LAI from APSIM simulation and remote sensing inversion on a regional scale. Prior to this process, the optimal density specific to each cotton field was first introduced into the assimilation step at the mid-late stage. After the assimilation, the irrigation per time and the total fertilization amount on a regional scale were obtained by the APSIM/OZCOT model. The irrigation amount per time on a regional scale ranges from 58.14 to 89.99 mm (**Figure 5.29a**). In the mid-late period, the flood from Tarim River can relieve the shortage situation of water, especially in the northern study area. Therefore, the irrigation amount in the northern study area can also dramatically increase to maintain moisture in sandy soil. Meanwhile, the total urea fertilization mainly ranges from 500.35 to 1598.59 kg/ha (**Figure 5.29b**). The assimilated nitrogen fertilization is also close to the findings from the nearby counties in the Tarim Basin ([Wang et al., 2005](#)). On the contrary, it also confirms the accuracy of the fertilization range in the **Table 5.6**. The variations in spatial distribution of irrigation and fertilization were decided by the APSIM/OZCOT model after minimizing the gap between remote sensing retrieved LAI and model simulated LAI. The RMSE between the model simulated and remote sensing observed LAI approximately ranges from 0.07 to 1.57 m<sup>2</sup>/m<sup>2</sup> (**Figure 5.29c**). The frequency of the RSME was mainly located in the range of 0.4–0.6 m<sup>2</sup>/m<sup>2</sup> (**Figure 5.30**). Based on these four optimized parameters, the regional cotton yield was also obtained by the APSIM/OZCOT simulation. The estimated cotton yield ranged from 1489 to 8895 kg/ha (**Figure 5.31**). The spatial distribution was also consistent with the arable land reclamation. The highest cotton yield was from the southern part of study area while the northern part had the least yield.

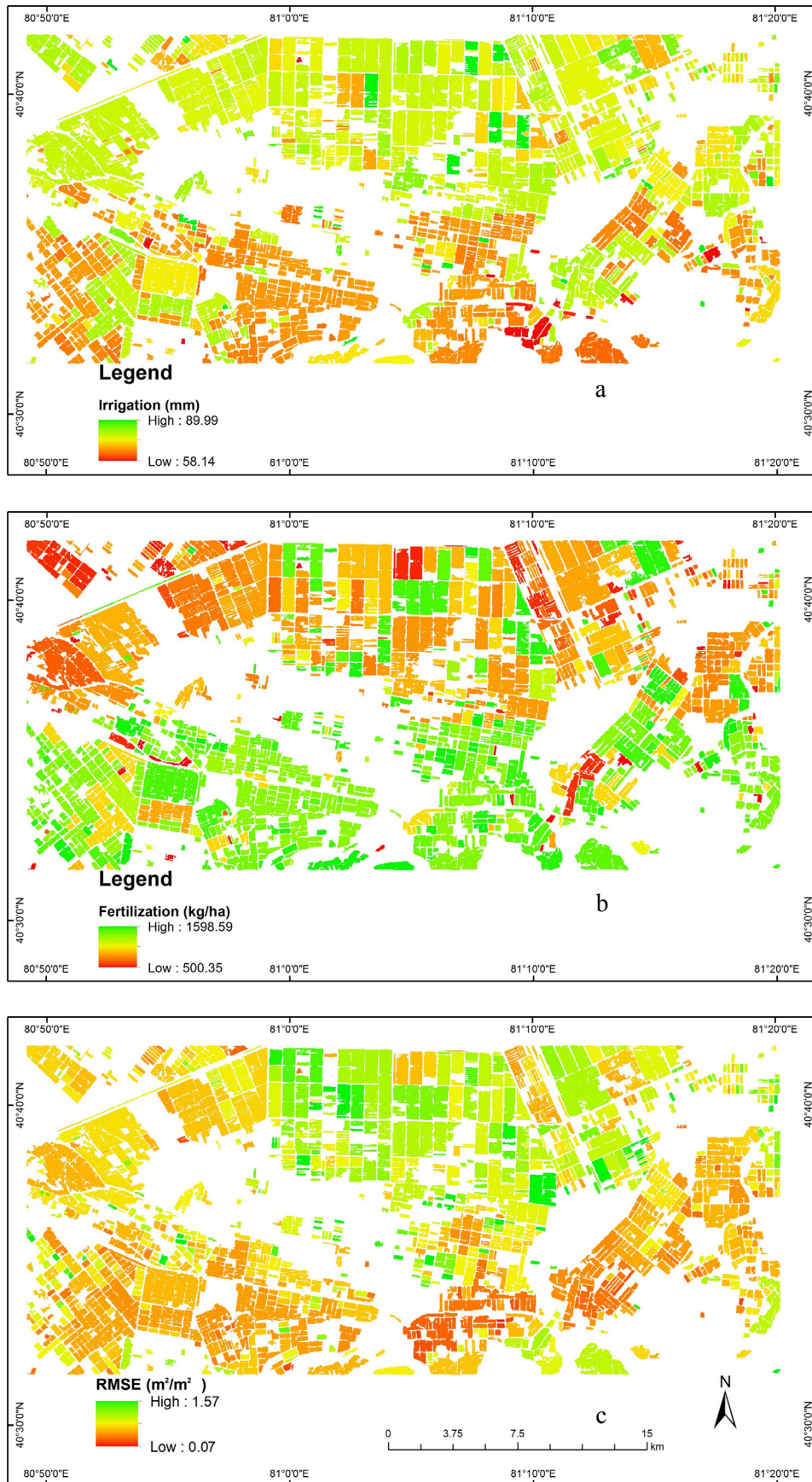


Figure 5.29 (a) Spatial distribution of irrigation per time; (b) spatial distribution of total urea fertilization; (c) the RMSE of LAI between remote sensing observations and APSIM/OZCOT simulations



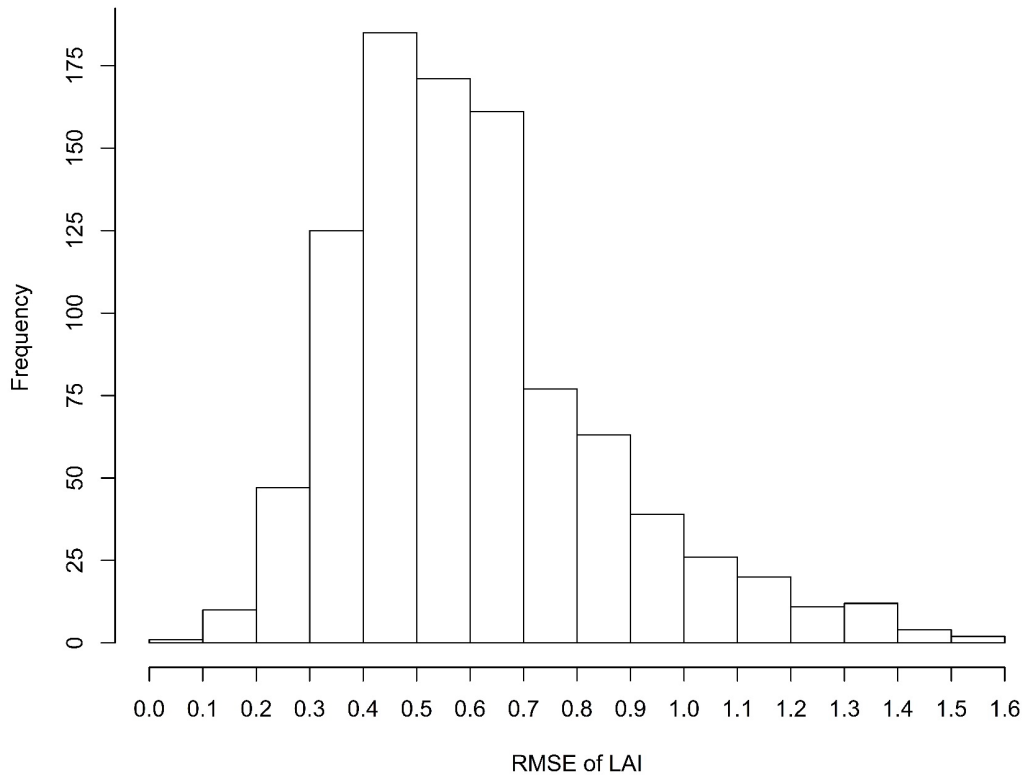


Figure 5.30 Frequency of RMSE of LAI for each cotton fields at mid-late growth stage

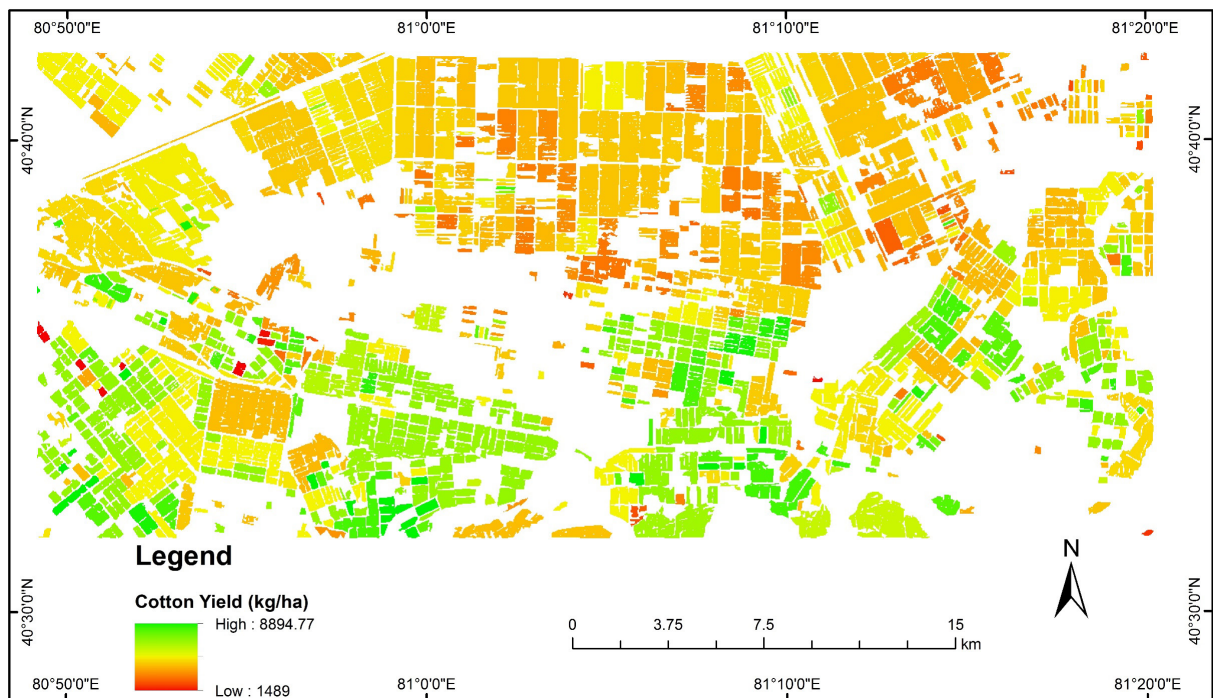


Figure 5.31 Spatial distribution of cotton yield at the end of growth season

The spatial distribution of irrigation is higher in the northern part, while it is lower in the southern part. Conversely, the spatial distribution of fertilization is lower in the northern part compared to the southern part. Meanwhile, we tested the effects of different combinations



between irrigation and fertilization on the cotton yield with in-situ observed soil profiles. Fertilization ranges from 0 to 1500 kg/ha and irrigation ranges from 10 to 100 mm. When irrigation is fixed, the yield increased with an increase in fertilization. After the maximum yield, the yield maintains a stable level and decreases a bit when urea fertilization is added (**Table 5.9**). However, the effect of irrigation on the yield under stable fertilization was complex. Additionally, we found four major combinations as follows:

- (1) Combination of high fertilization and high irrigation generally causes the maximum yield.
- (2) Combination of high fertilization and low irrigation generally causes a medium yield.
- (3) Combination of low fertilization and high irrigation generally causes the minimum yield.
- (4) Combination of low fertilization and low irrigation generally causes a low yield.

Based on these phenomena, it can be concluded that the high irrigation inhibits the growth of cotton.

Table 5.9 The response of various combination of irrigation and urea fertilization to yield (kg/ha) (taking cotton field A04 as an example)

Irrigation (mm)	Fertilization (kg/ha)												
	1500	1000	600	500	400	300	200	100	76	50	20	10	0
0	2166.8	2167.3	2152.9	2150.2	2085.7	2018.1	1883.2	1576.8	1429.1	1184.1	861.7	827.8	827.8
10	2267.6	2268.8	2269.8	2269.7	2268.4	2341	2214.7	1397.9	1231.6	1068.5	862.1	838.6	838.6
30	2270.2	2274.6	2284	2288.6	2291.4	2304.3	2224.1	1701	1518.9	1240.5	1024.8	1024.8	1024.8
40	2892.9	2881.9	2873.9	2874.7	2845.3	2740	2285	1354.3	1231.2	977.4	839.5	839.5	839.5
55	2598.2	2602	2612.4	2614.6	2617.1	2368.1	2023.5	1256.2	1135.4	861	682.5	682.5	682.5
60	2566.7	2568.4	2571.7	2589.9	2493.2	2261.7	1999.8	1376.1	1200.4	906.1	730.1	730.1	730.1
70	3211.6	3211.8	3210.5	3207.3	3118.3	2653.5	2072.7	1241.5	1111.9	889.1	740.7	740.7	740.7
80	3212.6	3212.5	3215.8	3212.4	3117.6	2569.3	1750.8	1172.7	1014.5	843.2	706.3	706.3	706.3
100	3103.6	3103.2	3099	3092.5	2561.5	2272.9	1506.8	1005.8	840.5	686.3	631.5	631.5	631.5

In conclusion, these spatial variations of irrigation and fertilization were caused by the APSIM/OZCOT model by adjusting these two parameters to minimize the difference between the remote sensing retrieved LAI and simulated LAI from the APSIM/OZCOT model. Thus, the spatial relationship between irrigation, fertilization and yield on a regional scale reveals similar results—high irrigation and low fertilization causes the low yield in the northern part while low irrigation and high fertilization causes high yield in the southern part of study area.

## 6 Conclusions

In this research, the accuracy of cotton yield estimation was improved on a regional scale by coupling time series Landsat-8 OLI remote sensing images from 2014 with the APSIM/OZCOT crop growth model. The corresponding conclusions are as follows:

(1) The sensitivity analysis was implemented to test the cultivar, soil and agronomic parameters within the APSIM/OZCOT model. These results showed that the row spacing, sowing density per row, irrigation and total fertilization amount were sensitive factors to LAI dynamics on a regional scale. A local calibration was implemented to adjust local cotton variety based on climate, soil conditions, agronomic practices and default cultivar parameters within the APSIM/OZCOT model. Then, a Chinese-specific cultivar suitable for the study area was also proposed. It is important to use the proposed Chinese specific cultivar, which is better than using the default Australian cultivar within the APSIM/OZCOT model.

(2) The accurate cotton cultivation distribution was extracted based on multi-temporal remote sensing images after a precise atmospheric correction and phenological variations of various vegetation types. This method is better than that only using single remote sensing image. Meanwhile, a series of Landsat-8 OLI images covering the entire growth period in 2014 was used to derive PVI images. The regional LAI maps were also obtained by a statistical relationship between the PVI and the observed in-situ LAI. Compared to the other vegetation indices, PVI is better to extract vegetation index by effectively minimizing the soil noise.

(3) The assimilation results on a field scale based on the PSO algorithm show that this assimilation strategy is better than the mono APSIM/OZCOT model simulation. It proved the feasibility of this assimilation strategy. Additionally, the general-purpose optimization method (based on the Nelder-Mead algorithm) had similar accuracy compared to the PSO algorithm but more rapid computational efficiency.

(4) The assimilation results on a regional scale based on the general-purpose optimization method (based on the Nelder-Mead algorithm) show that the spatial distribution of plant density appeared higher in the southern part of the study area while lower in the northern part. This spatial distribution of sowing density is consistent with arable land reclamation during 2001–2013. The northern part is the major region for recent reclamation while the southern part nearby the Tarim River is age-old reclamation. The spatial distribution of irrigation is higher in the northern part while it is lower in southern part. Conversely, the spatial distribution of fertilization is lower in the northern part compared to the southern part.

Additionally, the spatial distribution of the simulated yield also revealed a higher yield in the southern part of study area with lower cotton yield in northern part.

(5) In short, the coupling model between remote sensing and APSIM/OZCOT model proposed in this research has effectively resolved the limitation upscaling the crop growth model simulation from a field scale to a regional scale. Compared to simulated results from the mono APSIM/OZCOT model, this coupling model strategy is better on simulating the regional cotton growth process and yield. This promising approach also solves uncertainties from the stand-alone crop growth model. Model-related uncertainties can potentially be reduced by assimilating remote sensing data during the growing season of cotton. After the assimilation, the theoretically optimal time series of LAI was obtained to reduce errors.

(6) However, there are also many uncertainties with coupling of remote sensing and crop growth models. Uncertainties from remote sensing retrieved state variables, optimized algorithms, crop growth models and input parameters ([Li et al., 2017](#)) also result in uncertainties in simulated results. Because the crop growth model is a general simplification of real crop growth conditions, uncertainties induced by the model architecture ([Confalonieri et al., 2009](#)) include imperfect physical expressions of crop growth and unreasonable adjustment of model parameters. Due to these uncertainties, the simulated results usually deviate from the reality of crop conditions, resulting in low accuracy of yield prediction ([Iizumi et al., 2009](#); [Ceglar et al., 2011](#)). Additionally, numerous parameters vary over time and cannot match the temporal scale of crop growth coupling models ([Li et al., 2017](#)). Likewise, the spatial heterogeneity of soil properties, crop cultivars and meteorological data also result in uncertainties in regional crop growth models. In this research, lack of the detailed soil map with attributes on the regional scale resulted in the deviation of assimilation results. Similar to parameters in the crop growth model, uncertainties of state variables (such as the LAI) derived from remote sensing observations also lead to uncertainties in assimilation strategy. Systematic errors from the LAI-2000 equipment and personal errors both bring deviations of in situ LAI observations during the field campaigns. Moreover, lack of in situ observed LAI in June caused the data gap. Remote sensing observations and in situ LAI observations are not fully synchronous (day-to-day). These flaws thereby affected problems of the relationship between PVI and observed LAI. Then remote sensing derived LAI observations provided not enough accurate canopy states for the APSIM/OZCOT model. Additionally, the limitation of optimized algorithms ([Aote et al., 2013](#); [Shang and Mao, 2006](#)) also resulted in the uncertainties.

(7) In the future, we will extend this assimilation strategy about agronomic practices to the watershed scale and solve the pixel-based assimilation by introducing a better algorithm with high computational efficiency and accuracy. Meanwhile, multi-annual analyses of the assimilation will be implemented to make this coupling model between remote sensing and APSIM/OZCOT model more stable on simulating the cotton growth process. Thereby, simulated results with higher credibility can provide scientific evidence for decision makers. In addition to Landsat-8 OLI images, numerous remote sensing images from various sensors, such as Chinese HJ and GF/CCD, RapidEye and Sentinel-1/2 images can be used to construct a temporal curve within the cotton growth period. It makes the daily medium-resolution remote sensing images in an entire growth period of cotton. Then the dates of remote sensing observations are synchronous to in situ LAI observations during field campaigns, thereby reducing errors and uncertainties within the LAI retrieval. Since the theoretically daily remote sensing observation is not easy to obtain, multisource remote sensing images covering the major and critical growth stages (phenological events) of cotton and other crops can be considered an effective scheme. Experience during field campaigns provides a reference for designing field LAI observations by fully considering the specific phenology of cotton and other crops. During the rapid growth period of LAI, an in situ observation experiment is necessary. Additionally, a canopy height simulation will also be considered as there is no precise model simulating the canopy height within the OZCOT model. In addition to LAI, evapotranspiration and canopy height can be used as state variables to assimilate the coupling model between remote sensing and APSIM model for more robust results. The computational efficiency can be reduced due to more state variables while the stability of the assimilation can still increase.

(8) Different from similar researches (**Table 1.6**), the regional assimilation strategy in this research was treated respectively at two growth stages of cotton. This solution can reduce the interactions among the parameters within the APSIM model and clearly explain effects of these parameters on the crop growth process. Moreover, it can also reduce the local optimum by constructing a low-dimensional parameter space (Li et al., 2014). Thus, this strategy can better illustrate the mechanism of crop growth models and it can be applied for assimilations on growth processes of different crops in the future. In summary, assimilation of remote sensing images into crop growth models is a state of the art and promising approach to predict yield at the field and regional level.

## References

- Aksoy, S., and R.M. Haralick (2001). Feature normalization and likelihood-based similarity measures for image retrieval. *Pattern Recognition Letters* 22, 563-582.
- Aote, S.S., M.M. Raghuwanshi, and L. Malik (2013). A brief review on particle swarm optimization: limitations & future directions. *International Journal of Computer Science Engineering* 2, 196-200.
- Avissar, R. (1998). Which type of soil-vegetation-atmosphere transfer scheme is needed for general circulation models: a proposal for a higher-order scheme. *Journal of Hydrology* 212-213, 136-154.
- Bach, H., and W. Mauser (2003). Methods and examples for remote sensing data assimilation in land surface modeling. *IEEE Transactions on Geoscience and Remote Sensing* 41, 1629-1637.
- Baker, D.N., J.R. Lambert, and J.M. McKinion (1983). GOSSYM: A simulator of cotton crop growth and yield. South Carolina Agricultural Experiment Station Technical Bulletin No. 1089, Clemson University, Clemson, South Carolina.
- Baret, F., S. Jacquemoud, and J.F. Hanocq (1993a). About the soil line concept in remote sensing. *Advances in Space Research* 13(5), 281-284.
- Baret, F., S. Jacquemoud, and J.F. Hanocq (1993b). The soil line concept in remote sensing. *Remote Sensing Reviews* 7(1), 65-82.
- Bastiaanssen, W.G.M., and S. Ali (2003). A new crop yield forecasting model based on satellite measurements applied across the Indus Basin, Pakistan. *Agriculture, Ecosystems and Environment* 94, 321-340.
- Boogaard, H.L., C.A. van Diepen, R.P. Rötter, J.C.M.A. Cabrera, and H.H. van Laar (1998). User's guide for the WOFOST 7.1 crop growth simulation model and WOFOST control center 1.5. Technical Document 52. DLO Winand Starting Centre, Wageningen, the Netherlands, 144 p.
- Boote, K.J., M.R. Rybak, J.M.S. Scholberg, and J.W. Jones (2012). Improving the CROPGRO-Tomato model for predicting growth and yield response to temperature. *HortScience* 47(8):1038–1049.

- Bouman, B.A.M., H. van Keulen, H.H. van Laar, and R. Rabbinge (1996). The 'School of de Wit' crop growth simulation models: A pedigree and historical overview. *Agricultural Systems* 52, 171-198.
- Bouman, B.A.M., M.J. Kropff, T.P. Tuong, M.C.S Wopereis, H.F.M. ten Berge, and H.H. van Laar (2001). *ORYZA2000: Modeling lowland rice*. Los Baños (Philippines): International Rice Research Institute, and Wageningen: Wageningen University and Research Centre, 235 p.
- Bouman, B.A.M. (1992). Linking physical remote sensing models with crop growth simulation models, applied for sugar beet. *International Journal of Remote Sensing* 13(14), 2565-2581.
- Cavero, J., R.E. Plant, C. Shennan, J.R. Williams, J.R. Kiniry, and V.W. Benson (1998). Application of EPIC model to nitrogen cycling in irrigated processing tomatoes under different management systems. *Agricultural Systems* 56, 391-414.
- Ceglar, A., Z. Črepinšek, L. Kajfež-Bogataj, and T. Pogačar (2011). The simulation of phenological development in dynamic crop model: The Bayesian comparison of different methods. *Agricultural and Forest Meteorology* 151, 101-115.
- Charoenhirunyingsos, S., K. Honda, D. Kamthonkiat, and A.V.M. Ines (2011). Soil hydraulic parameters estimated from satellite information through data assimilation. *International Journal of Remote Sensing* 32, 8033-8051.
- Chen, J.S., J.X. Huang, H. Lin, and Z.Y. Pei (2010). Rice yield estimation by assimilation remote sensing into crop growth model. *Science China: Information Sciences* 40, 173-183. (in Chinese with English Abstract)
- Chiesi, M., F. Maselli, M. Bindi, L. Fibbi, L. Bonora, A. Raschi, R. Tognetti, J. Cermak, and N. Nadezhdina (2002). Calibration and application of FOREST-BGC in a Mediterranean area by the use of conventional and remote sensing data. *Ecological Modelling* 154(3), 251-262.
- Childs, S.W., J.R. Gilley, and W.E. Splinter (1977). A simplified model of corn growth under moisture stress. *Transactions of the ASAE* 20, 858-865.
- Claverie, M., V. Demarez, B. Duchemin, O. Hagolle, D. Ducrot, C. Marais-Sicre, J.F. Dejoux, M. Huc, P. Keravec, P. Béziat, R. Fieuzal, E. Ceschia, and G. Dedieu (2012). Maize and

sunflower biomass estimation in southwest France using high spatial and temporal resolution remote sensing data. *Remote Sensing of Environment* 124, 844-857.

Clevers, J.G.P.W. (1997). A simplified approach for yield prediction of sugar beet on optical remote sensing data. *Remote Sensing of Environment* 61, 221-228.

Clevers, J.G.P.W., and H.J.C. van Leeuwen (1996). Combined use of optical and microwave remote sensing data for crop growth monitoring. *Remote Sensing of Environment* 56, 42-51.

Confalonieri, R., M. Acutis, G. Bellocchi, and M. Donatelli (2009). Multi-metric evaluation of the models WARM, CropSyst, and WOFOST for rice. *Ecological Modelling* 220 (11), 1395-1410.

Crosetto, M., S. Tarantola, and A. Saltelli (2000). Sensitivity and uncertainty analysis in spatial modelling based on GIS. *Agriculture, Ecosystems and Environment* 81, 71-79.

Crosetto, M., and S. Tarantola (2001). Uncertainty and sensitivity analysis: Tools for GIS-based model implementation. *International Journal of Geographical Information Science* 15, 415-437.

Crow, W.T., W.P. Kustas, and J.H. Prueger (2008). Monitoring root-zone soil moisture through the assimilation of a thermal remote sensing-based soil moisture proxy into a water balance model. *Remote Sensing of Environment* 112, 1268-1281.

Curnel, Y., A.J.W. de Wit, G. Duveiller, and P. Defourny (2011). Potential performances of remotely sensed LAI assimilation in WOFOST model based on an OSS Experiment. *Agricultural and Forest Meteorology* 151, 1843-1855.

Curry, R.B., and L.H. Chen (1971). Dynamic simulation of plant growth. Part II. Incorporation of actual daily weather and partitioning of net photosynthate. *Transactions of the American Society of Agricultural Engineers* 14, 1170-1174.

de Wit, C.T. (1965). Photosynthesis of leaf canopies. *Agricultural Research Report No.663*. PUDOC, Wageningen, the Netherlands.

de Wit, C.T. (1970). Dynamic concepts in biology. In: *Prediction and management of photosynthetic productivity*. Center for Agricultural Publishing and Documentation (PUDOC), Wageningen, the Netherlands, 17-23.

de Wit, C.T., J. Goundriaan, H.H. van Laar, F.W.T. Penning de Vries, R. Rabbinge, H. van Keulen, W. Louwse, L. Sibma, and C. de Jonge (1978). Simulation of assimilation, respiration and transpiration of crops. Simulation Monographs, PUDOC, Wageningen, the Netherlands.

de Wit, A.J.W., and C.A. van Diepen (2007). Crop model data assimilation with the Ensemble Kalman filter for improving regional crop yield forecasts. *Agricultural and Forest Meteorology* 146, 38-56.

Delécolle, R., S.J. Maas, M. Guérif, and F. Baret (1992). Remote sensing and crop production models: present trends. *ISPRS Journal of Photogrammetry and Remote Sensing* 47, 145-161.

Dente, L., G. Satalino, F. Mattia, and M. Rinaldi (2008). Assimilation of leaf area index derived from ASAR and MERIS data into CERES-Wheat model to map wheat yield. *Remote Sensing of Environment* 112, 1395–1407.

Department of Agriculture Xinjiang Uygur Autonomous Region (DAXUAR) (2001). Cotton high density cultivation techniques about lint yield of 150 kg in Xinjiang. *Xinjiang Agricultural Science and Technology* 2, 14-16.

Doorenbos, J., and W.O. Pruitt (1977). Guidelines for predicting crop water requirements. FAO Irrigation and Drainage Paper 24, Food and Agriculture Organization of the United Nations, Rome.

Dorigo, W.A., R. Zurita-Milla, A.J.W. de Wit, J. Brazile, R. Singh, and M.E. Schaepman (2007). A review on reflective remote sensing and data assimilation techniques for enhanced agroecosystem modeling. *International Journal of Applied Earth Observation and Geoinformation* 9, 165-193.

Droogers, P., W.W. Immerzeel, and I.J. Lorite (2010). Estimating actual irrigation application by remotely sensed evapotranspiration observations. *Agricultural Water Management* 97, 1351-1359.

Eberhart, R.C., and J. Kennedy (1995). A new optimizer using particle swarm theory. *Proceedings of the Sixth International Symposium on Micro Machine and Human Science*, Nagoya, Japan, 39-43.

Eberhart, R.C., and Y.H. Shi (2001). Particle swarm optimization: developments, applications and resources. *IEEE Proceedings of Congress on Evolutionary Computation*, Seoul, 1, 81-86.



- Fan, H., X.H. Fu, Z. Zhang, and Q. Wu (2015). Phenology-based vegetation index differencing for mapping of Rubber plantations using Landsat OLI data. *Remote Sensing* 7, 6041-6058.
- Fang, H.L., S.L. Liang, and G. Hoogenboom (2011). Integration of MODIS LAI and vegetation index products with the CSM-CERES-Maize model for corn yield estimation. *International Journal of Remote Sensing* 32(4), 1039-1065.
- Fang, H.L., S.L. Liang, G. Hoogenboom, J. Teasdale, and M. Cavigelli (2008). Corn-yield estimation through assimilation of remotely sensed data into the CSM-CERES-Maize model. *International Journal of Remote Sensing* 29(10), 3011-3032.
- FAO, IIASA, ISRIC, ISSCAS, and JRC (2012). Harmonized World Soil Database Version 1.2. FAO, Rome/IIASA, Laxenburg.
- Feike, T., Y. Mamitimin, L. Li, and R. Doluschitz (2015). Development of agricultural land and water use and its driving forces along the Aksu and Tarim River, P.R. China. *Environmental Earth Science* 73, 517-531.
- Gao, X.Z. (2014). Cultivation techniques of cotton yield above 7500 kg/ha in the Alar Reclamation Region, Southern Xinjiang. *Modern Agricultural Science and Technology* 6, 43-44 (in Chinese)
- Gómez, C., J.C. White, and M.A. Wulder (2016). Optical remotely sensed time series data for land cover classification: A review. *ISPRS Journal of Photogrammetry and Remote Sensing* 116, 55-72.
- Guérif, M., and C.L. Duke (1998). Calibration of the SUCROS emergence and early growth module for sugar beet using optical remote sensing data assimilation. *European Journal of Agronomy* 9, 127-136.
- Guérif, M., and C.L. Duke (2000). Adjustment procedures of a crop model to the site specific characteristics of soil and crop using remote sensing data assimilation. *Agriculture, Ecosystems and Environment* 81, 57-69.
- Guo, J.M., Q. Wang, J.Y. Shi, T.F. Zheng, and J. Yang (2014). Incorporating remote sensing data and crop model to simulate regional winter wheat growth. *Transactions of Atmospheric Sciences* 37(2), 237-242. (in Chinese with English Abstract)

- Hamby, D.M. (1994). A review of techniques for parameter sensitivity analysis of environmental models. *Environmental Monitoring and Assessment* 32, 135-154.
- Hansen, P.M., and J.K. Schjoerring (2003). Reflectance measurement of canopy biomass and nitrogen status in wheat crops using normalized difference vegetation indices and partial least squares regression. *Remote Sensing of Environment* 86(4), 542-553.
- Hargreaves, J., B. Singh, and P. Poulton (2013). APSIM: overview of crop growth and phenology. <http://ksiconnect.icrisat.org/wp-content/uploads/2013/03/AgMIP-APSIM-crop-growth-and-phenology.pdf>
- He, L. (2015). Responses of phenology, yield and water use of winter wheat to climate change and variability on the Loess Plateau. PhD Dissertation, University of Chinese Academy of Sciences (in Chinese and English Abstract).
- Hearn, A.B. (1994). OZCOT: A simulation model for cotton crop management. *Agricultural Systems* 44, 257–299.
- Hearn, A.B., and G.D. da Roza (1985). A simple model for crop management applications for cotton (*Gossypium hirsutum* L.). *Field Crops Research* 12, 49-69.
- Hebbar, K.B., M.V. Venugopalan, M.V.R. Seshasai, K.V. Rao, B.C. Patil, A.H. Prakash, V. Kumar, K.R. Hebbar, P. Jeyakumar, K.K. Bandhopadhyay, M.R.K. Rao, B.M. Khadi, and P.K. Aggarwal (2008). Predicting cotton production using Infocrop-cotton simulation model, remote sensing and spatial agro-climatic data. *Current Science* 95, 1570-1579.
- Hill, J. (2013). Atmospheric correction processing (User Guide Version 3.0). Remote Sensing Department, University of Trier, Germany.
- Hoefsloot, P., A. Ines, J. van Dam, G. Duveiller, F. Kayitakire, and J. Hansen (2012). Combining crop model and remote sensing for yield prediction: concepts, applications and challenges for heterogeneous, smallholder environments. Reports of CCFAS-JRC Workshop at Joint Research Centre, Ispra, Italy, June13-14.
- Holzworth, D.P., N.I. Huth, P.G. de Voil, E.J. Zurcher, N.I. Herrmann, G. McLean, K. Chenu, ..., and B.A. Keating (2014). APSIM-evolution towards a new generation of agricultural systems simulation. *Environmental Modelling and Software* 62, 327-350.

- Hoogenboom, G., J.W. Jones, and K.J. Boote (1992). Modeling growth, development, and yield of grain legumes using SOYGRO, PNUTGRO and BEANGRO: a review. *Transactions of the ASAE* 35 (6), 2043-2056.
- Hoogenboom, G., J.W. White, J.W. Jones, and K.J. Boote (1994). BEANGRO, a process-oriented dry bean model with a versatile user interface. *Agronomy Journal* 86 (1), 182-190.
- Huang, J.X., S.J. Wu, X.Q. Liu, G.N. Ma, H.Y. Ma, W.B. Wu, and J.Q. Zou (2012). Regional winter wheat yield forecasting based on assimilation of remote sensing data and crop growth model with Ensemble Kalman method. *Transactions of the CASE* 28(4), 142-148. (in Chinese with English abstract)
- Huang, Y., Y. Zhu, H. Wang, X.F. Yao, W.X. Cao, D.B. Hannaway, and Y.C. Tian (2011). Predicting winter wheat growth based on integrating remote sensing and crop growth modeling techniques. *Acta Ecologica Sinica* 31(4), 1073-1084. (in Chinese with English abstract)
- Iizumi, T., M. Yokozawa, and M. Nishimori (2009). Parameter estimation and uncertainty analysis of a large-scale crop model for paddy rice: application of a Bayesian approach. *Agricultural and Forest Meteorology* 149(2), 333-348.
- Ines, A.V.M., N.N. Das, J.W. Hansen, and E.G. Njoku (2013). Assimilation of remotely sensed soil moisture and vegetation with a crop simulation model for maize yield prediction. *Remote Sensing of Environment* 138, 149–164.
- Irmak, A., and B. Kamble (2009). Evapotranspiration data assimilation with genetic algorithms and SWAP model for on-demand irrigation. *Irrigation Science* 28, 101-112.
- Jachner, S., K.G. v.d. Boogaart, and T. Petzoldt (2007). Statistical methods for the qualitative assessment of dynamic models with time delay (R Package qualV). *Journal of Statistical Software* 22(8), 1-30.
- Jarvis, A., H.I. Reuter, A. Nelson, and E. Guevara (2008). Hole-filled SRTM for the globe Version 4, available from the CGIAR-CSI SRTM 90m Database (<http://srtm.csi.cgiar.org>).
- Jiang, Z.W., Z.X. Chen, Q.B. Zhou, and J.Q. Ren (2011). Global sensitivity analysis of CERES-Wheat model parameters. *Transactions of the CSAE* 27, 236-242. (in Chinese with English abstract)

- Jiang, Z.W., Z.X. Chen, J. Chen, J.Q. Ren, Z.N. Li, and L. Sun (2014). The estimation of regional crop yield using ensemble-based four/dimensional variational data assimilation. *Remote Sensing* 6, 2664-2681.
- Jin, H.A., J.D. Wang, Y.C. Bo, G.F. Chen, and H.Z. Xue (2012). Estimation on regional maize yield based on assimilation of remote sensing data and crop growth model. *Transactions of the Chinese Society of Agricultural Engineering (Transactions of the CSAE)* 28(6), 162-173. (in Chinese with English abstract)
- Jin, M., X.N. Liu, L. Wu, and M.L. Liu (2015). An improved assimilation method with stress factors incorporated in the WOFOST model for the efficient assessment of heavy metal stress levels in rice. *International Journal of Applied Earth Observation and Geoinformation* 41, 118-129.
- Jones, C.A., and J.R. Kiniry (1986). *CERES-Maize: a simulation model of maize growth and development*. Texas A & M University Press, College Station, TX, USA.
- Jones, J.W., G. Hoogenboom, C.H. Porter, K.J. Boote, W.D. Batchelor, L.A. Hunt, P.W. Wilkens, U. Singh, A.J. Gijsman, and J.T. Ritchie (2003). The DSSAT cropping system model. *European Journal of Agronomy* 18, 235-265.
- Jones, J.W., B.A. Keating, and C.H. Porter (2001). Approaches to modular model development. *Agricultural Systems* 70, 421-443.
- Kaufman, Y.J., and L.A. Remer (1994). Detection of forests using MID-IR reflectance, an application for aerosol studies. *IEEE Transactions on Geoscience and Remote Sensing* 32, 672-683.
- Keating, B.A., P.S. Carberry, G.L. Hammer, M.E. Probert, M.J. Robertson, D. Holzworth, N.I. Huth, J.N.G. Hargreaves, H. Meinke, Z. Hochman, G. McLean, K. Verburg, V. Snow, J.P. Dimes, M. Silburn, E. Wang, S. Brown, K.L. Bristow, S. Asseng, S. Chapman, R.L. McCown, D.M. Freebairn, and C.J. Smith (2003). An overview of APSIM, a model designed for farming systems simulation. *European Journal of Agronomy* 18, 267-288.
- Kennedy, J., R.C. Eberhart, and Y. Shi (2001). *Swarm intelligence*. San Francisco: Morgan Kaufmann Publishers.
- Kennedy, J. (1997). The particle swarm: social adaptation of knowledge. *Proceedings of IEEE International Conference on Evolutionary Computation*, Indianapolis, 303-308.

- Kokaly, R.F., and R.N. Clark (1999). Spectroscopic determination of leaf biochemistry using band-depth analysis of absorption features and stepwise multiple linear regression. *Remote Sensing of Environment* 67, 267-287.
- Launay, M., and M. Guérif (2005). Assimilating remote sensing data into a crop model to improve predictive performance for spatial applications. *Agriculture, Ecosystems & Environment* 111(1), 321-339.
- Lemmon, H. (1986). COMAX: An expert system for cotton crop management. *Science* 233, 29-33.
- Li, H., Z. Chen, G. Liu, Z. Jiang, and C. Huang (2017). Improving winter wheat yield estimation from the CERES-Wheat model to assimilate leaf area index with different assimilation methods and spatio-temporal scales. *Remote Sensing* 9, 190.
- Li, Y. (2012). Study on maize yield estimation using remote sensing technology integrated with coupled WOFOST and HYDRUS models. PhD Dissertation, University of Lanzhou (in Chinese with English abstract).
- Li, R., C.J. Li, Y.Y. Dong, F. Liu, J.H. Wang, X.D. Yang, and Y.C. Pan (2011). Assimilation of remote sensing and crop model for LAI estimation based on ensemble kalman filter. *Agricultural Sciences in China* 10(10), 1595-1602.
- Li, M., W. Du, and F. Nian (2014). An adaptive particle swarm optimization algorithm based on directed weighted complex network. *Mathematical Problems in Engineering* 2014, 1-7. <http://dx.doi.org/10.1155/2014/434972>
- Li, Z.H., X.L. Jin, C.J. Zhao, J.H. Wang, X.G. Xu, G.J. Yang, C.J. Li, and J.X. Shen (2015). Estimating wheat yield and quality by coupling the DSSAT-CERES model and proximal remote sensing. *European Journal of Agronomy* 71, 53–62.
- Liu, D. (2013). Monitoring rice growth by assimilation of remote sensing and crop growth model. China University of Geosciences Dissertation (in Chinese and English Abstract).
- Liu, G.L., A. Kurban, H.M. Duan, H. Umut, A. Ablekim, and L.C. Zhang (2014a). Desert riparian forest colonization in the lower reaches of Tarim River based on remote sensing analysis. *Environmental Earth Science* 71, 4579-4589.

- Liu, G.L., G. Yin, A. Kurban, T. Aishan, and H.L. You (2016). Spatiotemporal dynamics of land cover and their impacts on potential dust sources in the Tarim Basin, NW China. *Environmental Earth Science* 75, 1477 DOI 10.1007/s12665-016-6269-y.
- Liu, J., J.R. Williams, A.J.B. Zehnder, and H. Yang (2007). GEPIC-modelling wheat yield and crop water productivity with high resolution on a global scale. *Agricultural Systems* 94, 478–493.
- Liu, J., J.M. Chen, J. Cihlar, and W.M. Park (1997). A process-based boreal ecosystem productivity simulator using remote sensing inputs. *Remote Sensing of Environment* 62(2), 158-175.
- Liu, S.S., Z.B. Zhou, X.L. Chen, and Y.D. Gan (2011b). Using RENI to study the distribution characteristics of cotton roots in different amounts of drip irrigation under film. *Cotton Science* 23, 39-43. (in Chinese with English Abstract)
- Liu, F., C.J. Li, Y.Y. Dong, X. Wang, J.H. Wang, and W.J. Huang (2011a). Monitoring crop growth based on assimilation of remote sensing data and crop simulation model. *Transactions of the CSAE* 27(10), 101-106. (in Chinese with English abstract)
- Liu, J.M., J.X. Huang, L.Y. Tian, H.Y. Ma, W. Su, W.B. Wu, R. Ramsankaran, X.D. Zhang, and D.H. Zhu (2014b). Regional winter wheat yield prediction by integrating MODIS LAI into the WOFOST model with sequential assimilation technique. *Journal of Food, Agriculture & Environment* 12 (1), 180-187.
- Loomis, R.S., and W.A. Williams (1963). Maximum crop productivity: an estimate. *Crop Science* 3, 67-72.
- Loveland, T.R., J.W. Merchant, J.F. Brown, D.O. Ohlen, B.C. Reed, P. Olson, and J. Hutchinson (1995). Seasonal land-cover regions of the United States. *Annals of the Association of American Geographers* 85, 339-355.
- Ma, Y.P., S.L. Wang, L. Zhang, Y.Y. Hou, L.W. Zhang, Y.B. He, and F.T. Wang (2008). Monitoring winter wheat growth in North China by combining a crop model and remote sensing data. *International Journal of Applied Earth Observation and Geoinformation* 10, 426–437.

- Ma, G.N., J.X. Huang, W.B. Wu, J.L. Fan, J.Q. Zou, and S.J. Wu (2013). Assimilation of MODIS-LAI into the WOFOST model for forecasting regional winter wheat yield. *Mathematical and Computer Modelling* 58, 634-643.
- Ma, Y.P., S.L. Wang, L. Zhang, and Y.Y. Hou (2005). A preliminary study on the re-initialization/re-parameterization of a crop model based on remote sensing data. *Acta Phytocologica Sinica* 29(6), 918-926. (in Chinese with English abstract)
- Maas, S.J. (1988). Use of remotely-sensed information in agricultural crop growth models. *Ecological Modeling* 41, 247-268.
- Maas, S.J. (1991). Use of remotely-sensed information in plant growth simulation models. *Advances in Agronomy* 1, 17-26.
- Maas, S.J. (1993). Parameterized model of gramineous crop growth: II. Within season simulation calibration. *Agronomy Journal* 85, 354-358.
- Maas, S.J., and N. Rajan (2010). Normalizing and converting image DC data using scatter plot matching. *Remote Sensing* 2, 1644-1661.
- Mader, S. (2013). A framework for the phenological analysis of hypertemporal remote sensing data based on polynomial spline models. PhD dissertation, University of Trier.
- Matsushita, B, and M. Tamura (2002). Integrating remotely sensed data with an ecosystem model to estimate net primary productivity in East Asia. *Remote Sensing of Environment* 81, 58-66.
- McCarthy, A.C. (2010). Improved irrigation of cotton via real-time, adaptive control of large mobile irrigation machines. PhD dissertation, University of Southern Queensland.
- McCown, R.L., G.L. Hammer, J.N.G. Hargreaves, D.P. Holzworth, and D.M. Freebairn (1996). APSIM: a novel software system for model development, model testing, and simulation in agricultural systems research. *Agricultural Systems* 50, 255-271.
- McMichael, B.L., and J.D. Hesketh (1982). Field investigation of the response of cotton to water deficits. *Field Crops Research* 5, 319-333.
- McVicar, T.R., and D.L.B. Jupp (2002). Using covariates to spatially interpolate moisture availability in the Murray-Darling Basin: a novel use of remotely sensed data. *Remote Sensing of Environment* 79, 199-212.

- Migdall, S., P. Klug, A. Denis, and H. Bach (2012). The additional value of hyperspectral data for smart farming. *Geoscience and Remote Sensing Symposium (IGARSS), 2012 IEEE International, Munich*, DOI [10.1109/IGARSS.2012.6351937](https://doi.org/10.1109/IGARSS.2012.6351937)
- Mitchell, G., R.H. Griggs, V. Benson, and J. Williams (1996). EPIC user's guide (draft) version 5300: the EPIC model environmental policy integrated climate (formerly erosion productivity impact calculator). Texas Agricultural Experiment Station, Blackland Research Center, Temple, TX.
- Mo, X.G., S.X. Liu, Z.H. Lin, Y. Xu, Y. Xiang, and T.R. McVicar (2005). Prediction of crop yield, water consumption and water use efficiency with a SVAT-crop growth model using remotely sensed data on the North China Plain. *Ecological Modelling* 183, 301-322.
- Mo, X.G., S.X. Liu, Z.H. Lin, and R.P. Guo (2009). Regional crop yield, water consumption and water use efficiency and their responses to climate change in the North China Plain. *Agriculture, Ecosystems & Environment* 134, 67-78.
- Monsi, M., and T. Saeki (2005). On the factor light in plant communities and its importance for matter production. *Annals of Botany* 95, 549-567. (A new translation into English from German: Monsi, M., and T. Saeki (1953). Über den Lichtfaktor in den Pflanzengesellschaften und seine Bedeutung für die Stoffproduktion. *Japanese Journal of Botany* 14, 22-52.)
- Morari, F., E. Lugato, and M. Borin (2004). An integrated non-point source model-GIS system for selecting criteria of best management practices in the Po Valley, North Italy. *Agriculture, Ecosystems & Environment* 102(3), 247-262.
- Moulin, S., A. Fischer, G. Dedieu, and R. Delécolle (1995). Temporal variations in satellite reflectances at field and regional scales compared with values simulated by lining crop growth and SAIL models. *Remote Sensing of Environment* 54, 261-272.
- Muslim, M., S.A. Romshoo, and A.Q. Rather (2015). Paddy crop yield estimation in Kashmir Himalayan rice bowl using remote sensing and simulation model. *Environmental Monitoring and Assessment* 187, 316 DOI [10.1007/s10661-015-4564-9](https://doi.org/10.1007/s10661-015-4564-9)
- Nash, J. C. (1990). *Compact numerical methods for computers: linear algebra and function minimization (Second Edition)*. Bristol: Institute of Physics Publications.
- Nearing, G.S., W.T. Crow, K.R. Thorp, M.S. Moran, R.H. Reichle, and H.V. Gupta (2012). Assimilating remote sensing observations of leaf area index and soil moisture for wheat yield



- estimates: An observing system simulation experiment. *Water Resources Research* 48, W05525, doi: 10.1029/2011WR011420
- Nelder, J.A., and R. Mead (1965). A simplex algorithm for function minimization. *Computer Journal* 7, 308–313.
- Nouvellon, Y., M.S. Moran, D. Lo Seen, R. Bryant, S. Rambal, W. Ni, A. Bégué, A. Chehbouni, W.E. Emmerich, P. Heilman, and J.G. Qi (2001). Coupling a grassland ecosystem model with Landsat imagery for a 10-year simulation of carbon and water budgets. *Remote Sensing of Environment* 78, 131-149.
- Otter-Nacke, S., J.T. Ritchie, D. Godwin, and U. Singh (1991). A user's guide to CERES Barley V2.10. International Fertilizer Development Center, Muscle Shoals, Alabama, USA.
- Peddle, D.R., F.G. Hall, and E.F. LeDrew (1999). Spectral mixture analysis and geometric-optical reflectance modeling of boreal forest biophysical structure. *Remote Sensing of Environment* 67, 288-297.
- Peng, G.X., L. Deng, W.H. Cui, T. Ming, and W. Shen (2009). Remote sensing monitoring of tobacco field based on phenological characteristics and time series image: a case study of Chengjiang County, Yunnan Province, China. *China Geography Science* 19, 186-193.
- Penning de Vries, F.W.T., H.H. van Laar, and L.J.M. Basstanie (1982). Simulation of plant growth and crop production. *Simulation Monographs*, PUDOC, Wageningen, the Netherlands.
- Qin, Q., L. You, Y. Zhao, S. Zhao, and Y. Yao (2012). Soil line automatic identification algorithm based on two-dimensional feature space. *Transactions of the CSAE* 28(3), 167-171. (in Chinese with English abstract)
- Reddy, V.R., and D.N. Baker (1988). Estimation of parameters for the cotton simulation model GOSSYM: cultivar differences. *Agricultural Systems* 26, 111-122.
- Rembold, F., and F. Maselli (2006). Estimation of inter-annual crop area variation by the application of spectral angle mapping to low resolution multitemporal NDVI images. *Photogrammetric Engineering and Remote Sensing* 72, 55-62.
- Ren, J.Q., Z.X. Chen, H.J. Tang, Q.B. Zhou, and J. Qin (2011). Regional crop yield simulation based on crop growth model and remote sensing data. *Transactions of the CSAE* 27(8), 257-264. (in Chinese with English abstract)

- Richardson, A.J., and C.L. Wiegand (1977). Distinguishing vegetation from soil background information. *Photogrammetric Engineering and Remote Sensing* 43(12), 1541-1552.
- Ritchie, J.T., and S. Otter (1985). Description and performance of CERES-Wheat: A user-oriented wheat yield model. In *ARS Wheat Yield Project*, pp. 159-175. ARS-38. National Technology Information Service, Springfield, VA.
- Ritchie, J.T., E.C. Alocijia, and G. Uehara (1986). IBSNAT/CERES rice model. *Agrotechnology Transfer* 3, 1-5.
- Roerink, G.J., M. Menenti, and W. Verhoef (2000). Reconstructing cloud free NDVI composites using Fourier analysis of time series. *International Journal of Remote Sensing* 21, 1911–1917.
- Saltelli, A., S. Tarantola, and K.P.S Chan (1999). A quantitative model independent method for global sensitivity analysis of model output. *Technometrics* 41, 39-56.
- Saltelli, A., and I.M. Sobol' (1995). About the use of rank transformation in sensitivity analysis of model output. *Reliability Engineering and System Safety* 50, 225-239.
- Sehgal, V.K., C.V.S. Sastri, N. Kalra, and V.K. Dadhwal (2005). Farm-level yield mapping for precision crop management by linking remote sensing inputs and a crop simulation model. *Journal of the Indian Society of Remote Sensing* 33 (1), 131-136.
- Shang, S.H., and X.M. Mao (2006) Application of a simulation based optimization model for winter wheat irrigation scheduling in North China. *Agricultural Water Management* 85, 314-322.
- Shen, S.H., S.B. Yang, B.B Li, B.X. Tan, Z.Y. Li, and T. Le Toan (2009). A scheme for regional rice yield estimation using ENVISAT ASAR data. *Science China Earth Sciences* 52, 1183-1194.
- Spitters, C.J.T., H. van Keulen, and D.W.G. van Kraalingen (1989). A simple and universal crop growth simulator: SUCROS87. Pages 147-181 in Rabbinge R, Ward SA, van Laar HH (Eds.). *Simulation and systems management in crop protection*. Simulation Monographs, PUDOC, Wageningen, the Netherlands.
- Stapleton, H.N., and R.P. Meyers (1971). Modeling subsystems for cotton plant simulation. *Transactions of the ASAE* 14, 950-953.

- Stenberg, P., M. Rautiainen, T. Manninen, P. Voipio, and H. Smolander (2004). Reduced simple ratio better than NDVI for estimating LAI in Finnish pine and spruce stands. *Silva Fennica* 38, 3-14.
- Stoner, E.R., and M.F. Baumgardner (1981). Characteristic variations in reflectance of surface soils. *Soil Science Society of America Journal* 45(6), 1161-1165.
- Sun, L.L., Y.P. Ma, Y.S. Jing, Y.D. Zou, and K.Y. Xing (2013). Assimilation of observations with crop growth model based on the constrained analysis of parameters. *Journal of Applied Meteorological Science* 24, 287-296. (in Chinese with English Abstract)
- Supit, I. (1997). Predicting national wheat yields using a crop simulation and trend models. *Agricultural and Forestry Meteorology* 88, 199-214.
- Tan, G., and R. Shibasaki (2003). Global estimation of crop productivity and the impacts of global warming by GIS and EPIC integration. *Ecological Modelling* 168, 357-370.
- Tan, Z., X.N. Liu, X.Q. Zhang, and L. Wu (2011). Simulation of dynamics of crop biomass by assimilation SAR data into crop growth model. *Chinese Agricultural Science Bulletin* 27(27), 161-167. (in Chinese with English abstract)
- Thorp, K.R., S. Ale, M.P. Bange, E.M. Barnes, G. Hoogenboom, R.J. Lascano, A.C. McCarthy, S. Nair, J.O. Paz, N. Rajan, K.R. Reddy, G.W. Wall, and J.W. White (2014). Development and application of process-based simulation models for cotton production: a review of past, present, and future direction. *Journal of Cotton Science* 18, 10-47.
- Thorp, K.R., D.J. Hunsaker, and A.N. French (2010). Assimilating leaf area index estimates from remote sensing into the simulations of a cropping systems model. *Transactions of the ASABE* 53(1), 251-262.
- Tong, C.L., W.J. Zhang, Y. Tang, and H.Q. Wang (2005). Estimation of daily solar radiation in China. *Chinese Journal of Agrometeorology* 26(3), 165-169. (in Chinese with English Abstract)
- Uehara, G., and G.Y. Tsuji (1991). Progress in crop modelling in the IBDNAT Project. In: Muchow, R.C., J.A. Bellamy (Eds.), *Climatic risk in crop production: models and management in the semi-arid tropics and subtropic*. CAB International, Wallingford, 143-156.
- Van Keulen, H. (1975). *Simulation of water use and herbage growth in arid regions*. Simulation Monographs, PUDOC, Wageningen, the Netherlands.

Van Keulen, H., and J. Wolf (Eds) (1986). Modeling of agricultural production: weather, soil and crops. Simulation Monographs, PUDOC, Wageningen, the Netherlands.

Vazifedoust, M., J.C. van Dam, W.G.M. Bastiaanssen, and R.A. Feddes (2009). Assimilation of satellite data into agro-hydrological models to improve crop yield forecasts. *International Journal of Remote Sensing* 30, 2523-2545.

Wang, K.R., S.K. Li, G.J. Song, G. Chen, and S.Z. Cao (2002). Studies on cultivated physiological indices for high-yielding cotton in Xinjiang. *Scientia Agricultura Sinica* 35, 638-644. (in Chinese with English Abstract)

Wang, J. (2010). A cultivation technique of XLZ 37 for high yield. *Rural Science and Technology* 9: 5. Available at <http://mall.cnki.net/magazine/article/NCKJ201009003.htm>

Wang, H., Y. Zhu, W.L. Li, W.X. Cao, and Y.C. Tian (2014). Integrating remotely sensed leaf area index and leaf nitrogen accumulation with RiceGrow model based on particle swarm optimization algorithm for rice grain yield assessment. *Journal of Applied Remote Sensing* 8, DOI: 10.1117/1.JRS.8.083674

Wang, H., Y. Zhu, M.L. Ma, W.L. Li, K.J. Gu, W.X. Cao, and Y.C. Tian (2012). Coupling remotely sensed information with a rice growth model by combining updating and assimilation strategies. *Acta Ecologica Sinica* 32(14), 4505-4515. (in Chinese and English Abstract)

Wang, P., X. Chen, C. Tian, Q. Tang, and F. Zhang (2005). Actuality and evaluation of fertilization in cotton fields in South Xinjiang. *Arid Zone Research* 22, 264-269. (in Chinese with English Abstract)

Wang, P.J., R. Sun, J.H. Zhang, Y.Y. Zhou, D.H. Xie, and Q.J. Zhu (2011). Yield estimation of winter wheat in the North China Plain using the remote-sensing–photosynthesis–yield estimation for crops (RS-P-YEC) model. *International Journal of Remote Sensing* 32(21), 6335-6348.

Wang, J. (2013). Estimating near future regional corn growth by integrating of multi-source observations into a crop growth model. PhD Dissertation, University of Chinese Academy of Sciences (in Chinese and English Abstract).

- Wardlow, B.D., S.L. Egbert, and J.H. Kastens (2007). Analysis of time-series MODIS 250m vegetation index data for crop classification in the U.S. Central Great Plains. *Remote Sensing of Environment* 108, 290-310.
- Wardlow, B.D., and S.L. Egbert (2008). Large-area crop mapping using time-series MODIS 250m NDVI data: An assessment for the U. S. Central Great Plains. *Remote Sensing of Environment* 112, 1096-1116.
- Watson, D.J. (1947). Comparative physiological studies in the growth of field crops: I. Variation in net assimilation rate and leaf area between species and varieties, and within and between years. *Annals of Botany* 11, 41–76.
- Weiss, M., D. Troufleau, F. Baret, H. Chauki, L. Prévot, A. Olioso, N. Bruguier, and N. Brisson (2001). Coupling canopy functioning and radiative transfer models for remote sensing data assimilation. *Agricultural and Forest Meteorology* 108: 113–128.
- Wiegand, C.L, A.J. Richardson, and E.T. Kanemasu (1979). Leaf area index estimates for wheat from Landsat and their implications for evapotranspiration and crop modeling. *Agronomy Journal* 71, 336-342.
- Wilkerson, G.G., J.W. Jones, K.J. Boote, K.T. Ingram, and J.W. Mishoe (1983). Modeling soybean growth for crop management. *Transactions of the ASAE* 26, 63-73.
- Wu, D.R., Q. Yu, C.H. Lu, and H. Hengsdijk (2006). Quantifying production potentials of winter wheat in the North China Plain. *European Journal of Agronomy* 24(3), 226-235.
- Wu, J., F.S. Yu, Z.X. Chen, and J. Chen (2009). Global sensitivity analysis of growth simulation parameters of winter wheat based on EPIC model. *Transactions of the CSAE* 25, 136-142. (in Chinese with English abstract)
- Wu, L., X.N. Liu, B.T. Zhou, L.F. Li, and Z. Tan (2012). Spatial-time continuous changes simulation of crop growth parameters with multi-source remote sensing data and crop growth model. *Journal of Remote Sensing* 16(6), 1173–1191.
- Wu, L., X.N. Liu, P. Wang, B.T. Zhou, M.L. Liu, and X.Q. Li (2013). The assimilation of spectral sensing and the WOFOST model for the dynamic simulation of cadmium accumulation in rice stress. *International Journal of Applied Earth Observation and Geoinformation* 25, 66-75.

- Wu, S.J. (2012). Study on winter wheat yield prediction based on assimilating remote sensing data and crop growth model. Master thesis, Central South University China (in Chinese and English Abstract).
- Xing, Y.J., D.S. Liu, and P.X. Wang (2009). Advances of the coupling application of remote sensing information and crop growth model. *Advances in Earth Science* 24(4), 444-451. (in Chinese with English Abstract)
- Xiong, W., L. Holman, D. Conway, E. Lin, and Y. Li (2008). A crop model cross calibration for use in regional climate impacts studies. *Ecological Modelling* 213, 365-380.
- Xu, W., H. Jiang, and J. Huang (2011). Regional crop yield assessment by combination of a crop growth model and phenology information derived from MODIS. *Sensor Letters* 9, 981–989.
- Yan, Y., Q.H. Liu, Q. Liu, J. Li, and L.F. Chen (2006). Methodology of winter wheat yield prediction based on assimilation of remote sensing data with crop growth model. *Journal of Remote Sensing* 10(5), 804-811.
- Yang, F., J.L. Sun, H.L. Fang, Z.F. Yao, J.H. Zhang, Y.Q. Zhu, K.S. Song, Z.M. Wang, and M.G. Hu (2012). Comparison of different methods for corn LAI estimation over northeastern China. *International Journal of Applied Earth Observation and Geoinformation* 18, 462-471.
- Yang, Y.M., Y.H. Yang, S.M. Han, I. Macadam, and D.L. Liu (2014). Prediction of cotton yield and water demand under climate change and future adaptation measures. *Agricultural Water Management* 144, 42-53.
- Yun, J.I. (2003). Predicting regional rice production in South Korea using spatial data and crop-growth modeling. *Agricultural Systems* 77(1), 23-38.
- Zhang, J.X., and W. Su (2012). Sensitivity analysis of CERES-Wheat model parameters based on EFAST method. *Journal of China Agricultural University* 17, 149-154. (in Chinese with English abstract)
- Zhang, L., S.L. Wang, Y.B. He, Y.P. Ma, L.W. Zhuang, and Y.Y. Hou (2007). Winter wheat growth simulation under water stress by remote sensing in North China. *Acta Agronomica Sinica* 33(3), 401- 410. (in Chinese with English abstract)

Zhao, Y.X., S.N. Chen, and S.H. Shen (2013). Assimilating remote sensing information with crop model using Ensemble Kalman Filter for improving LAI monitoring and yield estimation. *Ecological Modelling* 270, 30-42.

Zhao, G., B.A. Bryan, and X.D. Song (2014). Sensitivity and uncertainty analysis of the APSIM-wheat model: interactions between cultivar, environmental, and management parameters. *Ecological Modelling* 279, 1-11.

Zhao, C.Y., and S.J. Hu (2010). Datasets of observation and analysis of ecosystem in China (agro-ecosystem volume). Beijing: China Agriculture Press.

Zhao, R.F., P.H. Jiang, N.J. Chen, P.J. Shi, J.H. Pan, and H.L. Zhao (2012). Land use/cover change and its eco-environment effect in the main stream of Tarim River. *Scientia Geographica Sinica* 32, 244-250. (in Chinese with English Abstract)

Zhao, Y.X., J. Qin, and X.J. Zhou (2005). Study on combinations of remote sensing and cotton model to retrieve initial inputs and parameters. *Cotton Science* 17(5), 280-284. (in Chinese with English Abstract)

Zhu, Y.L., Y. Zhu, Y. Huang, X. Yao, L.L. Liu, W.X. Cao, and Y.C. Tian (2010). Assimilation technique of remote sensing information and rice growth model based on particle swarm optimization. *Journal of Remote Sensing* 14(6), 1226-1240.

Zhu, X.H., Y.S. Zhao, and X.M. Feng (2013). A methodology for estimating leaf area index by assimilating remote sensing data into crop model based on temporal and spatial knowledge. *Chinese Geographical Science* 23(5), 550-561.

Zuo, D.K., Y.X. Wang, and J.S. Chen (1963). Characteristics of the distribution of total radiation in China. *Acta Meteorologica Sinica* 33, 78-96. (in Chinese with English Abstract)

## Appendix

The appendix is about sensitivity analysis, PSO and General-purpose Optimization method using R script. If you will use these scripts in the future work, please cite this dissertation.

### Appendix 1 PSO R script

```
##### read remote sensing LAI from a text file#####
setwd ("D:\\OZCOT_LAI_RS\\")
data<-read.table("D:\\OZCOT_LAI_RS\\LAI_per_Field_all.txt",header =TRUE, sep="")
for (i in 1:36){
  A=data[i,1]
  B=data[i,2]
  Z=data[i,3]
  C=data[i,4]
  E=data[i,5]
  G=data[i,6]
}
#####Constant Day of Year (DOY) #####
Ai = 136; # DOY 136
Bj = 168; # DOY 168
Zq = 200; # DOY 200
Cp = 232; # DOY 232
El = 248; # DOY 248
Gm = 280; # DOY 280
#####The code about extracting biomass, although this part is not used in this paper#####
#####The biomass can be also extracted from APSIM.out file using sink and scan commands, similarly
#####the density and the other parameters and result can be used this method. These two methods can be
#####used as a reference for similar researches #####
getbiomass <- function(fname) {
  gettoken <- function(con, tok) {
    pos <- 1
    repeat {
      ch <- readChar(con,1)
      if (identical(ch, character(0))) return(FALSE)
      if (ch==substr(tok,pos,pos)) {
        pos <- pos+1
        if (pos==(nchar(tok)+1)) return(TRUE)
      } else {
        pos <- 1
      }
    }
  }
}
```



```

con <- file(fname, "rt")
if (gettoken(con, "total above ground biomass (kg/ha) ==") == FALSE) {
  close(con)
  warning(paste("File", fname, "doesn't seem to be an APSIM file!"))
  return(numeric(0))
}
tmp <- scan(con, double(), 1, quiet = TRUE)
close(con)
return(tmp)
}

#####Descriptions about using R to run APSIM model #####
#The R script about running APSIM model is provided by Liang He (Institute of Geographic Sciences and
#Natural Resources Research, Chinese Academy of Sciences, Beijing, 100101, China) (He, 2015), and
#modified by Guilin Liu (Trier University, Environmental Remote Sensing & Geoinformatics, D-54286 Trier,
#Germany).
#####
APSIM<-function(x){
library(XML) # Loading the XML packages in R
library(stringr)
doc <- xmlParse("Cotton_Alar_simulation.sim") #reading the xml file (*.sim document)
r <- xmlRoot(doc) # getting the top-level node of *.sim xml file
#####set the start date and end date of simulation#####
xmlValue(r[[3]][["initdata"]][["start_date"]])<-"01/01/2014" #beginning of year in simulation
xmlValue(r[[3]][["initdata"]][["end_date"]])<-"31/12/2014" #end of year in simulation
##### Agronomic parameters #####
xmlValue(r[[5]][[6]][["initdata"]][["ui"]][["row_spacing"]])<-x[1] # the row space of cotton
xmlValue(r[[5]][[6]][["initdata"]][["ui"]][["density"]])<-x[2] # the density per row of cotton
xmlValue(r[[5]][[15]][["initdata"]][["ui"]][["amount"]])<-x[3] # irrigation
xmlValue(r[[5]][[16]][["initdata"]][["ui"]][["FertAmt"]])<-x[4] # fertilization
#####setting the sowing date#####
xmlValue(r[[5]][[6]][["initdata"]][["ui"]][["date1"]])<- "10-apr" # sowing date
xmlValue(r[[5]][[6]][["initdata"]][["ui"]][["date2"]])<- "10-apr" # sowing date
#####update the output data#####
xmlValue(r[[5]][[2]][["initdata"]][["outputfile"]])<-"Cotton_Alar_simulation.out"
#### save the modified xml document ####
saveXML(newXMLDoc(r),file="Cotton_Alar_simulation_temp.sim", encoding=getEncoding(doc))
shell("Cotton_Alar_simulation_temp.sim") #run the external exe in R
SUM<-read.table(paste0("Cotton_Alar_simulation.out"),skip=4,
               col.names=c("day_of_year","lai","yield","height","dm"))
lai<-SUM$lai
yield_max<-SUM$yield

```

```

dm<-SUM$dm
biomass<-getbiomass("Cotton_Alar_simulation.sum")
return(list(lai,yield_max,dm,biomass))
}
##### ##### cost function ##### #####
FITNESSSUM<-function(x,A,B,Z,C,E,G,Ai,Bj,Zq,Cp,El,Gm){
  result<-APSIM(x)
  lai<-result[[1]]
  Fit=sqrt(((A-lai[Ai])*(A-lai[Ai])+(B-lai[Bj])*(B-lai[Bj])+(Z-lai[Zq])*(Z-lai[Zq])+(C-lai[Cp])*(C-lai[Cp])
    +(E-lai[El])*(E-lai[El])+(G-lai[Gm])*(G-lai[Gm]))/6)
  return(Fit)
}
##### ##### PSO program ##### #####
#MATLAB scripts provided by Zhenhai Li (Beijing Research Center for Information Technology in Agriculture,
#Beijing Academy of Agriculture and Forestry Sciences and National Engineering Research Center for
#Information Technology in Agriculture, Beijing, 100101, China and Institute of Agricultural Remote Sensing
#and Information Application, Zhejiang University, Hangzhou 310029, China) and Da Liu (China University of
#Geosciences) (Liu, 2013), modified by Guilin Liu (Trier University, Environmental Remote Sensing &
#Geoinformatics, D-54286 Trier, Germany).
PSOSUM<-function(A,B,Z,C,E,G,Ai,Bj,Zq,Cp,El,Gm){
  x=matrix(0,nrow=N,ncol=D)
  v=matrix(0,nrow=N,ncol=D)
  p=matrix(0,N,1)
  y=matrix(0,nrow=N,ncol=D)
  pg=matrix(0,nrow=1,ncol=D)
  Pbest=matrix(0,nrow=M,ncol=1)
  Xmin=array(1,D)
  Xmax=array(1,D)
  Vmin=array(1,D)
  Vmax=array(1,D)
#####using a default value of D =4 (number of parameters) #####
  Xmin[1]=350;Xmax[1]=550
  Xmin[2]=1;Xmax[2]=12
  Xmin[3]=50;Xmax[3]=90
  Xmin[4]=500;Xmax[4]=1600
  Vmin[1]=-Xmin[1]/10;Vmax[1]=Xmax[1]/10;
  Vmin[2]=-Xmin[2]/10;Vmax[2]=Xmax[2]/10;
  Vmin[3]=-Xmin[3]/10;Vmax[3]=Xmax[3]/10;
  Vmin[4]=-Xmin[4]/10;Vmax[4]=Xmax[4]/10;
#####initilization#####
  for (i in 1:N){

```

```

for (j in 1:D){
  x[i,j]=Xmin[j]+runif(1,0,1)*(Xmax[j]-Xmin[j])
  v[i,j]=Vmin[j]+runif(1,0,1)*(Vmax[j]-Vmin[j])
}
}
for (k in 1:N){
  p[k]=FITNESSSUM(x[k,],A,B,Z,C,E,G,Ai,Bj,Zq,Cp,El,Gm)
  y[k,]= x[k,]
}
pg = x[N,]
tmin = FITNESSSUM(pg,A,B,Z,C,E,G,Ai,Bj,Zq,Cp,El,Gm)
for ( l in 1:(N-1)){
  t1=FITNESSSUM(x[l,],A,B,Z,C,E,G,Ai,Bj,Zq,Cp,El,Gm)
  if (t1<tmin){
    tmin = t1;
    pg = x[l,]
  }
}
pg_ini = pg;
#####iteration begins#####
for (m in 1:M){
  for (n in 1:N){
    v[n,]=w*v[n,]+c1*runif(1,0,1)*(y[n,]-x[n,])+c2*runif(1,0,1)*(pg-x[n,])
    for (dim in 1:D){
      if (v[n,dim]>Vmax[dim]){
        v[n,dim]=Vmax[dim]
      }else{
        if (v[n,dim]<Vmin[dim]){
          v[n,dim]=Vmin[dim]
        }
      }
    }
  }

  x[n,]=x[n,]+v[n,]
  for (dim in 1:D){
    if (x[n,dim]>Xmax[dim]){
      x[n,dim]=Xmax[dim]
    }else{
      if (x[n,dim]<Xmin[dim]){
        x[n,dim]=Xmin[dim]
      }
    }
  }
}

```

```

    }
  }
  print(x[n,])
  pnow=FITNESSSUM(x[n,],A,B,Z,C,E,G,Ai,Bj,Zq,Cp,El,Gm)

  if (pnow<p[n]){
    p[n]=pnow;
    y[n,]=x[n,];
  }
  pbest_m= FITNESSSUM(pg,A,B,Z,C,E,G,Ai,Bj,Zq,Cp,El,Gm)
  if (p[n]<pbest_m){
    pg=y[n,]
  }
}
Pbest[m]=FITNESSSUM(pg,A,B,Z,C,E,G,Ai,Bj,Zq,Cp,El,Gm)
}
print(pg)
xm=t(pg)
fv=FITNESSSUM(pg,A,B,Z,C,E,G,Ai,Bj,Zq,Cp,El,Gm)
gui=APSIM(pg)
lai_best=gui[[1]]
yield_max=gui[[2]]
dm=gui[[3]]
biomass=gui[[4]]
return(list(xm,fv,pg_ini,Pbest,lai_best,yield_max,dm,biomass))
}

#####main function and plot#####
strt<-Sys.time()
##### Constants in the PSO code#####
c1 = 2.0; #learning factor
c2 = 2.0; #learning factor
M = 60; #M is the iteration
D = 4; #D is the number of independent variables, it is better to use a small value by dividing growth stages
N = 15; #N is the number of particles
w = 0.4; #Weight
##### read txt#####
setwd("D:\\OZCOT_LAI_RS\\")
data<-read.table("D:\\OZCOT_LAI_RS\\LAI_per_Field_all.txt",header =TRUE, sep="")
parameters<-matrix(0,nrow=D,ncol=37)
RMSE_result<-matrix(nrow=M,ncol=37)
lai_result<-matrix(nrow=365,ncol=37)

```

```

yield_max<-matrix(nrow=365,ncol=37)
dm<-matrix(nrow=365,ncol=37)
biomass<-matrix(nrow=365,ncol=37)
  for (i in 1:36){
A=data[i,1]
B=data[i,2]
Z=data[i,3]
C=data[i,4]
E=data[i,5]
G=data[i,6]
xm = PSOSUM(A,B,Z,C,E,G,Ai,Bj,Zq,Cp,El,Gm)
VV<-xm[[1]]
parameters[,i]<-VV
RMSE_result[,i]<-xm[[4]]
lai_result[,i]<-xm[[5]]
yield_max[,i]<-xm[[6]]
dm[,i]<-xm[[7]]
biomass[,i]<-xm[[8]]
}
#####Constant#####
Ai = 136; # DOY 136
Bj = 168; # DOY 168
Zq = 200; # DOY 200
Cp = 232; # DOY 232
El = 248; # DOY 248
Gm = 280; # DOY 280
doy=array (1,365)
for (i in 1:365){
  doym[i]=i
}
#####xm = PSOSUM(A,B,Z,C,E,G,Ai,Bj,Zq,Cp,El,Gm)
lais <- APSIM(unlist(xm[1]))
lais=unlist(xm[5])
doy_obs<-list(Ai,Bj,Zq,Cp,El,Gm)
lai_obs<-list(A,B,Z,C,E,G)
plot(doy,lais)
points(doy_obs,lai_obs,col=2)
#####Save as result#####
write.table(parameters,file="D:\\OZCOT_LAI_RS\\parameters.txt",row.names=F,col.names=F,sep=",")
write.table(RMSE_result,file="D:\\OZCOT_LAI_RS\\RMSE.txt",row.names=F,col.names=F,sep=",")
write.table(lai_result,file="D:\\OZCOT_LAI_RS\\lai_result.txt",row.names=F,col.names=F,sep=",")

```

```
write.table(yield_max,file="D:\\OZCOT_LAI_RS\\yield_max.txt",row.names=F,col.names=F,sep=",")
write.table(dm,file="D:\\OZCOT_LAI_RS\\biomass.txt",row.names=F,col.names=F,sep=",")
write.table(biomass,file="D:\\OZCOT_LAI_RS\\dm.txt",row.names=F,col.names=F,sep=",")
print(Sys.time()-strt)
```

## Appendix 2 Sensitivity analysis R script

```
##### Descriptions about Sensitivity analysis R script#####
#The sensitivity analysis algorithm with R script was used in this research based on detailed descriptions of
#this algorithm from https://cran.r-project.org/web/packages/sensitivity/sensitivity.pdf. The R script is
#provided by Liang He (Institute of Geographic Sciences and Natural Resources Research, Chinese
#Academy of Sciences, Beijing, 100101, China) (He, 2015), and modified by Guilin Liu (Trier University,
#Environmental Remote Sensing & Geoinformatics, D-54286 Trier, Germany).
#####

library(XML) # Loading the XML packages
library(sensitivity)
library(stringr)
source("Cot_APSIM2014_A02.R")
#####ready for saving sensitivity data#####

no_parameter<-13;
first_order_yield<-matrix(0,nrow=1,ncol=no_parameter)
total_order_yield<-matrix(0,nrow=1,ncol=no_parameter)
first_order_lai<-matrix(0,nrow=1,ncol=no_parameter)
total_order_lai<-matrix(0,nrow=1,ncol=no_parameter)
first_order_height<-matrix(0,nrow=1,ncol=no_parameter)
total_order_height<-matrix(0,nrow=1,ncol=no_parameter)

#start time
strt<-Sys.time()

##### sensitivity analysis #####

n<-100
loop<-n*no_parameter
yield_sa<- fast99(model = NULL, factors=c("flai",
                                         "dlds_max",
                                         "RLAI",
                                         "DDISQ",
                                         "ACOTYL",
                                         "fbur",
                                         "popcon",
                                         "fcutout",
                                         "sqcon",
                                         "row_spacing",
                                         "density",
                                         "amount",
```

```

"FertAmt"),

n = n,q ="qunif", q.arg = list("flai"=list(min=0.1,max=1.0),
                                "dlds_max"=list(min=0.009,max=0.15),
                                "RLAI"=list(min=0.001,max=0.03),
                                "DDISQ"=list(min=400,max=500),
                                "ACOTYL"=list(min=0.1,max=1000.0),
                                "fburr"=list(min=0.8,max=5.0),
                                "popcon"=list(min=0.1,max=1.0),
                                "fcutout"=list(min=0.1,max=1.0),
                                "sqcon"=list(min=0.01448,max=0.02844),
                                "row_spacing"=list(min=400,max=600),
                                "density"=list(min=15,max=35),
                                "amount"=list(min=10,max=300),
                                "FertAmt"=list(min=60,max=1000))

)
y<-c()
lai<-c()
height<-c()
for (i in 1:loop){
  result<- APSIM(yield_sa$X[i,])
  y[i]<-result[1]
  lai[i]<-result[2]
  height[i]<-result[3]
  print(i)
}
#####for yield#####
tell(yield_sa, as.numeric(y))
print(yield_sa)
first_order_1<-yield_sa$D1/yield_sa$V
total_order_1<-1-yield_sa$Dt/yield_sa$V
first_order_yield[1,]<-first_order_1
total_order_yield[1,]<-total_order_1
#####for LAI#####
tell(yield_sa, as.numeric(lai))
first_order_1<-yield_sa$D1/yield_sa$V
total_order_1<-1-yield_sa$Dt/yield_sa$V
first_order_lai[1,]<-first_order_1

```



```

total_order_lai[1,]<-total_order_1
#####for height#####
tell(yield_sa, as.numeric(height))
first_order_1<-yield_sa$D1/yield_sa$V
total_order_1<-1-yield_sa$Dt/yield_sa$V
first_order_height[1,]<-first_order_1
total_order_height[1,]<-total_order_1
#####for sensitivity save#####
write.table(first_order_yield,file=('firstorder_yield_A.txt'),row.names=FALSE,col.names=FALSE)
write.table(total_order_yield,file=('totalorder_yield_A.txt'),row.names=FALSE,col.names=FALSE)
write.table(first_order_lai,file=('firstorder_lai_A.txt'),row.names=FALSE,col.names=FALSE)
write.table(total_order_lai,file=('totalorder_lai_A.txt'),row.names=FALSE,col.names=FALSE)
write.table(first_order_height,file=('firstorder_height_A.txt'),row.names=FALSE,col.names=FALSE)
write.table(total_order_height,file=('totalorder_height_A.txt'),row.names=FALSE,col.names=FALSE)
#####save the simulation results#####
write.table(y,file=('efast_yield_A.txt'),row.names=FALSE,col.names=FALSE)
write.table(lai,file=('efast_lai_A.txt'),row.names=FALSE,col.names=FALSE)
write.table(height,file=('efast_height_A.txt'),row.names=FALSE,col.names=FALSE)
print(Sys.time()-strt)

```

### Appendix 3 General-purpose optimization algorithm in R script

#The R script about running APSIM model is provided by Liang He (Institute of Geographic Sciences and  
#Natural Resources Research, Chinese Academy of Sciences, Beijing, 100101, China) (He, 2015), and  
#modified by Guilin Liu (Trier University, Environmental Remote Sensing & Geoinformatics, D-54286 Trier,  
#Germany).

```

APSIM<-function(x){
  library(XML)
  library(stringr)
  doc <- xmlParse("Alar Cotton_ID_A3.sim")
  r <- xmlRoot(doc)
  ## ##set the start date and end date of simulation ## ## ## ##
  xmlValue(r[[3]][["initdata"]][["start_date"]])<-"01/01/2014"
  xmlValue(r[[3]][["initdata"]][["end_date"]])<-"31/12/2014"
  ##### Agronomic parameters #####
  xmlValue(r[[5]][[6]][["initdata"]][["ui"]][["row_spacing"]])<-x[1]
  xmlValue(r[[5]][[6]][["initdata"]][["ui"]][["density"]])<-x[2]
  #####set the sowing date#####
  xmlValue(r[[5]][[6]][["initdata"]][["ui"]][["date1"]])<-"10-apr"
  xmlValue(r[[5]][[6]][["initdata"]][["ui"]][["date2"]])<-"10-apr"
  #####update the output data#####
  xmlValue(r[[5]][[2]][["initdata"]][["outputfile"]])<-"Alar Cotton_ID_A3.out"
  ##save the modified xml document
  saveXML(newXMLDoc(r),file="Alar Cotton_ID_A3_temp.sim", encoding=getEncoding(doc))
  shell("Alar Cotton_ID_A3_temp.sim")
  SUM<-read.table(paste0("Alar Cotton_ID_A3.out"),skip=4,
                 col.names=c("day_of_year","lai","yield"))
  lai<-SUM$lai
  yield_max<-SUM$yield
  return(list(lai,yield_max))
}
par=runif(2)
fn<-function (par,min.x, max.x,A,B,Ai,Bj){
  min.x<-c(350,1)
  max.x<-c(550,12)
  if (any(par<0)||any(par>1)) return (9999)
  x<-par*(max.x-min.x)+min.x
  result<-APSIM(x)
  lai<-result[[1]]

```

```

Fit=sqrt(((A-lai[Ai])*(A-lai[Ai])+(B-lai[Bj])*(B-lai[Bj]))/2)
return(Fit)
}
#####Constant#####
Ai = 136; # DOY 136
Bj = 168; # DOY 168
data<-read.table("D:\\Early_simulation_density\\LAI_954Polygons_all.txt",header =TRUE, sep="")
parameters<-matrix(0,nrow=2,ncol=477)
RMSE_result<-matrix(0,nrow=1,ncol=477)

#####Descriptions about Nelder-Mead method in R#####
#The general-purpose optimization based on Nelder–Mead method was coded by Guilin Liu
#and Dr. Sebastian Mader (Trier University, Environmental Remote Sensing &
#Geoinformatics, D-54286 Trier, Germany), based on the detail description from
#https://stat.ethz.ch/R-manual/R-devel/library/stats/html/optim.html
#####

for (i in 1:477){
  A=data[i,1]
  B=data[i,2]
  xm<-optim(par,fn,gr=NULL,min.x, max.x,A,B,Ai,Bj,method=c("Nelder-Mead"))
  VV<-xm[[1]]
  WW<-xm[[2]]
  parameters[i]<-VV
  RMSE_result[i]<-WW
}
#####Save as result#####
write.table(parameters,file="D:\\Early_simulation_density\\parameters.txt",row.names=F,col.names=F,sep=",")
write.table(RMSE_result,file="D:\\Early_simulation_density\\RMSE.txt",row.names=F,col.names=F,sep=",")

```

## Declaration

I hereby declare that I am the sole author of my dissertation and that no other sources or learning aids, other than those listed, have been used. Furthermore, I declare that I have acknowledged the work of others by providing detailed references of said work.

I also declare that my dissertation has not been prepared for another examination or assignment, either wholly or excerpts thereof.

Trier, 07.12.2017

Place, date

*Guolin Liu*  
刘格林

Signature

# Curriculum Vitae

## Personal Data

Guilin Liu  
Pluwiger Straße 10  
54295 Trier, Germany

Date of Birth: 15 January, 1985

Place of Birth: Qingzhou City, Shandong Province, P.R. China

Nationality: Chinese

## School Education

09/1993–07/1997 Primary school in the Qingzhou City, Shandong Province, P.R. China

09/1997–07/2000 Junior High School, in the Qingzhou City, Shandong Province, P.R. China

09/2000–06/2004 Senior High School, in the Qingzhou City, Shandong Province, P.R. China

## Higher Education

**09/2004–07/2008** Bachelor Studies of Land Resources of Management at the Shandong Agricultural University, P.R. China

**09/2008–07/2009** Master Studies (Courses) of Remote Sensing and Geographic Information Systems at the Graduate University of Chinese Academy of Sciences (Now it is called University of Chinese Academy of Sciences), P.R. China

**09/2009–07/2011** Master Studies (Thesis) of Remote Sensing and Geographic Information Systems at the Xinjiang Institute of Ecology and Geography, Chinese Academy of Sciences, P.R. China

**08/2011–12/2012** Registered as a PhD candidate at the Nanjing Institute of Geography and Limnology, Chinese Academy of Sciences, P.R. China and participated in several projects as an assistant

**Since 01/2013** Doctoral studies at the Faculty of Regional and Environmental Sciences, University of Trier, Germany

## Working Experience

**01/2013–02/2016** Research assistant at the Department of Environmental Remote Sensing and Geoinformatics, University of Trier

Project: Sustainable Management of River Oases along the Tarim River (SuMaRio, <http://www.sumario.de/>)